CLIMATIC AND VEGETATIVE DRIVERS OF SOIL GENESIS, SOIL PROPERTIES, AND SOIL DISTRIBUTION IN SANKURU PROVINCE, CENTRAL DEMOCRATIC REPUBLIC OF CONGO (DRC)

A DISSERTATION
SUBMITTED TO THE FACULTY OF THE UNIVERSITY OF MINNESOTA
BY

Esakakondo Alphonse Lohese

IN PARTIAL FULFILLMENT OF THE REQUIREMENTS
FOR THE DEGREE OF
DOCTOR OF PHILOSOPHY

Adviser: Dr. Nicolas A Jelinski

August, 2021

Acknowledgements

I would like to thank individuals and organisms who contributed to the fulfilment of this **historic** academic achievement (it is not common for a minority senior citizen to engage in such a high level of academic education in soil science).

I am first of all grateful to Dr. Carl Rosen, SWAC Department Head, Drs. David Mulla and Dylan Millet, directors of the graduate studies in the same department, for accepting my student application and enabling various funding opportunities for my benefit. I am also grateful to Interdisciplinary Center for Global Change (ICGC) for its global food security fellowship and Annie's Homegrown for its sustainable agriculture scholarship.

I have a deep gratitude to the University Notre Dame of Tshumbe for our partnership during the field work phase of this research in Sankuru. I wish to express my profound indebtedness to the smallholders in Sankuru who spent long, challenging days with me in the field under the rain and heat.

My special thanks go to my adviser, Dr. Nic Jelinski, for his unrelinquished full support, a relationship that transcended academic scope, and the privilege of his friendship. My deep appreciation goes also to all the members of my dissertation committee for their expertise and encouragement; Dr. Jay Bell, Dr. Brandy Toner, Dr. Paul Porter, and particularly to Dr. Andrew Margenot.

Many thanks to the Jelinski lab group members for their lab work effectiveness and friendship, similarly to the SWAC department staff and faculty/staff at the UMN Institute for Rock Magnetism. May Bob and Marcy Grant find here the expression of my deep gratitude for their faithful multi-decade friendship as well as the Normans for their hospitality.

Dedication

To the Smallholders in Sankuru Province.

To Temati, my wife.

Abstract

Much of what is known regarding soil properties in the Democratic Republic of Congo (DRC) is based on broad estimates from studies covering only 15% of the vast country's territory, about a 1⁄4 of the USA. Understanding how soil types and soil properties vary across the landscape and change with major vegetation types across climatic zones is a critical foundation that must be established in order to ensure the lasting success of future effort to improve land use, soil health, and food security. In this study, soil investigations were undertaken on a transect across the forest-savanna ecotone in Sankuru province, central DRC. Soils across the transect were generally sandy, acidic, kaolinitic, and low carbon soils, but significant differences in soil properties and soil classification existed between climate zones and vegetation types. Soils formed under savanna vegetation were characterized by thick, dark colored topsoils (umbric epipedons) and classified as Inceptisols regardless of climate zone, while soils formed under forest vegetation had thin, light-colored topsoils (ochric epipedons) and were more diverse, classifying as Entisols, Inceptisols, Ultisols, and Oxisols. Analysis of soil magnetic properties and the $\delta^{13}C$ ratio of soil organic matter revealed that while climatic differences are recorded in iron oxide assemblages, it is likely that forest was much more expansive in the mid-late Holocene and covered modern-day savanna sites across the transect. Finally, soil phosphorus stocks vary significantly across the transect and is highest under savanna vegetation in wetter climate zones. These phosphorus (P) stocks exist largely in association with iron and aluminum oxy-hydroxides, but are non-occluded, which may allow P to become available to crops under innovative agronomic management. These results suggest that by focusing crop production in savanna areas in the Am and Af climate zones, and applying locally available amendments that may boost soil pH and CEC could increase crop productivity and food security in central DRC.

Table of Contents

List of Tables

List of Figures

CHAPTER 1

Soil properties and classification across a climate and vegetation gradient in Sankuru Province, central Democratic Republic of Congo (DRC)

1.1. Introduction

Forest-grassland transition zones are globally important ecotones (regions of transition between two biological communities) where shifting vegetative boundaries impact biodiversity (Cuni-Sanchez et al., 2016), ecosystem carbon and nutrient storage (Furley, 1997, Lloyd et al., 2008, Gibbon et al., 2010), soil productivity, and soil diversity (Bockheim and Schliemann, 2014). Critical pedological transformations often occur at these major ecotone boundaries and are aligned with abrupt climatic and vegetative transitions (Schaetzl, 2002, Munroe, 2012, Bockheim and Schliemann, 2014). The major ecotone that occurs across the humid tropical regions of South America, Africa, and southeast Asia is the boundary between equatorial forest and tropical savanna (grassland) (Murphy and Bowman, 2012). Globally, this ecotone is largely aligned with the transition between the Köppen-Geiger climate zone Af (equatorial forest), Am (tropical monsoon) and Aw (tropical savanna) classifications (Peel et al., 2007), and the transition between equatorial forest and tropical savanna vegetation can be quite abrupt in many regions, with forest and savanna acting as alternative stable ecological states (Oliveras and Malhi, 2016).

The major ecological drivers of the tropical forest-savanna ecotone are climate, fire, grazing, and edaphic factors (Gray and Bond, 2015, Mills et al., 2006). The purely climatic (precipitation-based) threshold for the equatorial forest-tropical savanna boundary is estimated to be 1500 mm yr^{-1} (Morely, 2000), but savanna often occurs in regions that experience greater amounts of precipitation and should support forest vegetation (Bond, 2010, Lehmann et al., 2011). Fire disturbance therefore plays a role in determining this boundary at both global and regional scales, and some authors have argued that fire, not climate, is the primary determinant of the distribution of this ecotone (Bond et al., 2004). It is also likely that anthropogenic fire regimes have played a major role in determining the current boundaries for this ecotone across the world, for at least the past few millennia (Veenendaal et al., 2018). Stable plant communities and soil properties themselves may play a role in maintaining this abrupt boundary by directly or indirectly driving water availability and patterns of disturbance, which on field scales can control seasonal soil moisture and water balance across ecotones (Marfo et al., 2019).

Critical pedogenic thresholds in soil pH, nutrient status, and mineral weathering, and soil morphology have been shown to occur between ~ 900-2500 mm precipitation,

depending on local soil forming factors (Vitousek and Chadwick, 2013). This climatic boundary overlaps with the major global boundaries between Af, Am, and Aw and the equatorial forest-tropical savanna vegetation transition zones (Kottek et al., 2006). In addition to climatic drivers of soil variability across this ecotone, soil heterogeneity across forest-grassland transitions in the tropics is significantly influenced by the stability of the vegetative boundary (i.e., the vegetation memory is "imprinted" on the soil) (Favier et al., 2004).

The literature on pedological thresholds across forest-savanna or forest-grassland vegetative transitions has largely been driven by temperate perspectives in the United States and Europe, which have found that soils developed under forest vegetation exhibit greater clay increases in the subsurface, lower pH values, leaching of carbonates, and lower SOC stocks than their grassland counterparts (Severson and Arneman, 1973, Anderson, 1987, Bronger, 1991). Most of this literature from temperate regions has focused on high base status soils under moderate to weak weathering regimes, formed in loamy to fine parent materials (Bekele et al., 2006, Bekele and Hudnall, 2006, Munroe, 2012). The literature on pedological transitions across forest-savanna boundaries in tropical climates is much more mixed. Many studies report higher soil organic carbon (SOC), pH, and soil phosphorus (P) under forest, which may be due in part to relatively shallow depths of soil sampling (often less than 30 cm deep) in many tropical studies, which are often ecologically focused (Markham and Babbedge, 1979, Dunham, 1991, Isichei and Muoghalu, 1992, Belsky et al., 1993, Silva et al., 2013).

The African forest-savanna ecotone is the most extensive in the tropics and subtropics (Murphy and Bowman, 2012). Two major regions of equatorial forest-tropical savanna ecotone occur on the African continent; the linear equatorial forest – savanna transition in west Africa, and the concentric equatorial forest – savanna transition that encircles the central Congo basin (Aleman et al., 2020). There is reason to believe that soil properties across the equatorial forest-savanna transition zone may differ substantially in central Africa, where rainfall is higher and less seasonal, the landscape is significantly modified by the Congo River and its tributaries, and has experienced more stable vegetation dynamics throughout the Holocene than outlying regions (Hessler et al., 2010). Sankuru Province in central Democratic Republic of Congo (DRC) encompasses one of

the steepest climatic gradients from equatorial forest to tropical savanna in central Africa, and contains the critical transition zone on the African continent between the humid Congo basin and the drier regions to the south (Murphy and Bowman, 2012). Moreover, the vast majority of central and south-central DRC is underlain by a large sand sheet which makes these soils in this region unique and difficult to manage for agricultural production (Hartemink et al., 2007).

Despite its location in a vegetatively and pedologically important transition zone, central Africa and DRC in particular has received much less attention than regions with similar climatic gradients in more developed tropical and subtropical regions such as Hawaii, West Africa, China, and South America (Issaka et al., 1996, Long et al., 2011, de L. Dantas et al., 2013, Vitousek and Chadwick, 2013). Soil data in central DRC is particularly sparse and DRC continues to be one of the least data-dense countries in the world in terms of soil information (Leenars et al., 2014). Much of what is estimated regarding soil properties in DRC comes from only a handful of widely spaced studies and broad estimates (Batjes, 2008, Baert et al., 2013). Since 1960, soil investigations evolved sporadically under private agricultural business in DRC (Baert et al.,2013). As of today, only about 250 soil profiles have been investigated since 1945 (Batjes, 2008), equivalent to about one profile per 10,000 km2 (or one per 3,862 sq miles) in the country. Due to the lack of soil investigations in DRC, preliminary soil maps in the area do not represent true soil variability on the ground. Currently, the best available predictions (Hengl et al., 2015) show the most probable soil classes as Oxisols and Ultisols in the study area, despite the fact that significantly more diverse soil types have been discovered in preliminary investigations (Leenars et al., 2014).

Understanding how soil properties, soil morphology, and classification vary across the equatorial forest – tropical savanna boundary in central Africa is a critical foundation that must be established in order to ensure the lasting success of future efforts to improve land use, soil health, and food security in central DRC. Therefore, the objectives of this research were to attempt to test the hypothesized impact of climatic and vegetative factors on soil properties, morphology, and classification across a combined bio-climo-sequence (the “Sankuru transect”) in central DRC.

1.2. Materials and Methods

1.2.1. Study Area, Geology, Soil Parent Materials, and Vegetation

Field work was completed in two phases from August 2015 to January 2016 and June to August 2017 in Sankuru Province, central DRC (Figure 1.1), across a transect along a steep (≈250km) climate gradient from Af in the north, through Am to Aw in the south (Figure 1.1). The area is occupied by Tetela tribe whose staple crops remain rice (*Oryza sativa indica* sp), cassava (*Manihot utilissima*), maize (*Zea mays*), Millet (*Pennisetum glaucum*), and peanut (*Arachis hypogea*). Mean annual precipitation (MAP) in the study area varies between 1613 mm/year in the south of the transect (near Lubefu) and 1742 mm in the north near Ekomakoko (Fick and Hijmans, 2017, Figure 1.1). Importantly, although MAP varies by only ~130mm across the transect, the seasonality of precipitation is strikingly different from south to north (Herrmann and Mohr, 2011, Munzimi et al., 2015). In Af, there is no seasonality to the precipitation regime, while Am is characterized by a single, biomodal wet season (longer wet season, bimodal), and sites in the Aw experience a shorter, unimodal wet season (Herrmann and Mohr, 2011, Munzimi et al., 2015). Additionally, this transect lies across the Udic-Ustic soil moisture regime (SMR) transition zone in central DRC, with sites in the Af and Am under a Udic SMR and sites in the Aw in an Ustic SMR (Soil Survey Staff, 2007, Soil Survey Staff, 2014b). Along this gradient, six site clusters were established in Lomela (under Af) at Mukumari (2.92°S; 23.48°E) and Ekomakoko (2.70°S, 24.16°E), in Katako-Kombe (under Am) at Kiete (3.62°S, 24.57°E) and Ovungu (3.82°S, 24.39°E), and in Lubefu (under Aw) at Tshumbe (4.15°S; 24.59°E), Eshima Ngandungandu/Maluanyi (4.88°S, 24.56°E (Figure 1.1). The choice of these site clusters was driven by the steep climatic and vegetation gradient, accessibility, and lack of local soil data.

Sankuru Province is enmeshed in the Congo River Basin (CRB) geology which is part of the unconsolidated Kalahari Group (KG) sediments (Linol et al., 2015). Parent materials for Sankuru soils derive from the sand sheets of the Salonga and Yangambi deposits (Beernaert, 1999), which are underlain by consolidated and unconsolidated materials of the Kalahari Group that covers most of southern DRC (Linol et al., 2015). Lithostratigraphy of the KG sediments reveals a variable thickness between 50 to 250 m in the CRB and sub-formation successions of eolian sand, lacustrine sediments and alluvium

with limestone and sandstone duricrusts, and basal gravel (Linol et al., 2015). In Sankuru, the KG sediments overlie unconsolidated cretaceous red-beds 300-1000 m thick located above the Precambrian basement formations (Linol et al., 2015). The dominant surficial material in our study area appears to be best correlated with the Salonga formation, a Cenozoic era (perhaps Pleistocene epoch) sand sheet covering much of lower plateau surrounding the central Basin (Beernaert, 1999). The Salonga formation has also been synonymously termed the "Plateau sands" and is likely of early- (on the outer, upper plateau steps of the Congo basin) to late-Pleistocene (on the lower, inner plateau steps) age (Beernaert, 1999, Senut et al., 2009). The origins of this sand sheet appear to be complex, and it has previously been characterized as of mixed fluvial and eolian origins (Beernaert, 1999, Baert et al., 2009, Senut et al., 2009, Baert et al., 2013, Guillocheau et al., 2015).

Vegetation in Sankuru province is split between forest in the north and savanna in the south and southeast, consistent with the climate gradient from Af to Aw (Figure 1.1). The tropical rainforest in the north is also synonymously termed equatorial forest or broadleaf evergreen forest (Sanchez, 1976) with at least a two-strata canopy, highly diversified tree species, and few to no herbaceous species on the floor. Savanna vegetation is of the "tall grass-low tree" type, a mixed of Hyparrhenia sp., Imperata sp. and other grasses, and low, scattered trees. The precipitation range across this transect (1613 to 1740 mm/yr) is in the range where alternation between stable states of forest and savanna is predicted on the African continent (Hirota et al., 2011). On a local scale in equatorial forest, isolated savanna vegetation can occur within a matrix of forest (Markham and Babbedge, 1979, Lehmann et al., 2011). These isolated savannas may be driven by interactions among edaphic and disturbance factors such as fire, and provide an opportunity to separately evaluate the impacts of both climate and vegetation on soil properties across this ecotone (Bowman and Perry, 2017).

1.2.2. Morphological Description, Soil Sampling, and Soil Classification

A total of 130 horizons in 26 profiles from 26 pit-excavations (2 m × 2 m × 2 m deep) were examined across the transect (Figure 1.1) and triplicate samples were collected from each genetic horizon using the soil core method for bulk density measurement: a sliding hammer carefully drives a metallic cylinder sampler (96 cm^3) into the soil to

minimize structure disturbance of the mineral soil samples, which is imperative for accurate soil bulk density evaluation. Samples were weighed immediately in the field then bagged before air-drying. The samples were oven-dried for 24 h at 105˚C, weighed, and sieved to separate the fine earth (< 2 mm) from coarse fragments (> 2 mm). The fine earth fraction (< 2 mm) was utilized for chemical and physical characterizations. As it is inappropriate to use the ring method on organic materials, surface organic horizon bulk densities were collected using a serrated knife to cut blocks of 262 cm3 (2 in x 2 in x 4 in) from the pit surface before excavation. Soil morphology was described in the field, and morphological properties including soil color, structure, texture, and visual differences in volume estimates of coarse fragments were utilized to define genetic horizons (Schoeneberger et al., 2012). A simplified soil darkness index (VC) was calculated for each genetic horizon by multiplying the value by the chroma,

$$VC = V * C \qquad (1),$$

where V is the Munsell value and C is the Munsell chroma. This index was chosen instead of an integrative whole-pedon index such as profile darkness index (Thompson et al., 1997) in order to examine differences in soil darkness by depth. This simplified darkness index results in low values of VC index for darker soil colors and high values of VC for lighter soil colors.

Soils were classified to the family level following U.S. Soil Taxonomy (Soil Survey Staff, 2014b). Soil diversity at the order and suborder levels within climate zone and vegetation groupings was determined using Simpson's index of diversity (Morris et al., 2014),

$$D_s = 1 - \left(\frac{\sum n(n-1)}{N(N-1)}\right) \qquad (2),$$

where D_s is Simpson's diversity index, n is the total number of entities of a particular taxonomic class, and N is the total number of observations. This index ranges from 0 to 1 and increases with increasing taxonomic diversity.

1.2.3. Soil Physical Characterization

Soil texture analysis was performed using both the pipette and hydrometer methods (Soil Survey Staff, 2014a). A solution of 5% sodium hexametaphosphate (SHMP) was used to disperse soil aggregates and maintain the dispersion in aqueous solution as sodium

saturates the exchange complex and raises particle zeta potential (Blake and Hartge, 1986). No pretreatment for organic matter, carbonate, or iron oxide removal was deemed necessary due to very low organic carbon content (0.9 % on average) (Jackson, 1956), lack of carbonate, and sandy soil textures (Table 1.1). Soil can remain dispersible while retaining some free iron oxides (Jackson 1956). Briefly, 50g of soil was dispersed overnight (12 h) in 5% of SHMP on a reciprocating shaker at 38 cycles per minute. The dispersed slurry was quantitatively wet sieved through a 50 μm sieve into a 1L sedimentation column to separate sand particles from finer size fractions (silts and clays). The sand fraction was oven-dried and subsequentially dry-sieved through a sieve stack of 1mm, 500 μm, 250 μm, 100 μm sieves in order to separate very coarse-, coarse-, medium-, fine-, and very fine-sand on a sieve shaker. In the sedimentation column, the slurry of clay and silt was diluted to 1L using deionized water. A Lowy 25 ml pipette was used to remove aliquots from an initially fully dispersed and stirred sample at pre-determined times and sampling depths. The < 20 μm fraction was determined by removing an aliquot from 10cm depth at a pre-determined time (Soil Survey Staff, 2014a). Because the temperature in the laboratory was kept nearly constant at +/- 22°C, the sampling time typically used for the < 20 μm fraction was 4 min and 25 s (Soil Survey Staff, 2014a). Determination of the < 2 μm fraction was completed by removing an aliquot from the solution at 5h from a pre-determined depth. Again, because laboratory temperature was kept nearly constant, this sampling depth was typically 6.79 cm (Soil Survey Staff, 2014a). Each aliquot was pipetted into an aluminum weighing tin, which was oven dried along with a 25 ml aliquot of blank SHMP concentration of the same solution as the dispersant. Once oven dried, tins were quantitatively weighed, the blank mass was subtracted from the sample mass, and masses were scaled to the 1L of solution and the original oven dry mass of the soil sample to calculate particle size distributions. Mineral particle fractions (sand subfractions, silt, and clay) are reported as percentages of the oven-dried fine-earth soil mineral particles (< 2 mm).

1.2.4. Soil Chemical Characterization

Total soil carbon (TC, g 100g-1) and nitrogen (TN, g 100g-1) were determined by dry combustion at 800 ºC using a LECO 2000 CN analyzer (LECO Corporation, 2003).

Soil pH for mineral samples was determined in 1:1 slurry of 5 g of air-dried soil and 5 ml of water (pH_{H2O}) followed by additional 5 ml of 0.01M $CaCl_2$ (pH_{CaCl2}) (Soil Survey Staff, 2014a). Labile phosphorus was evaluated using the Bray-P1 method, which simulates the buffering process by using HCl and NH_4F at low concentrations to maintain the dissolution of Aluminum (Al) and enable the release of P into the solution for measurement. CEC was determined by ammonium acetate (NH_4OAc) extraction buffered at pH 7, and exchangeable Aluminum (Al_{ex}) was determined using a 1M KCl extractant (Soil Survey Staff, 2014a).

Total elemental concentrations of Al, Ca, Fe, K, and Si were quantified by X-Ray Fluorescence (XRF), using an Olympus Delta P4000EX portable XRF (p-XRF) instrument (Olympus, Inc) which is equipped with a silicon drift detector (SDD), that has a resolution better than 155 eV in practice. During analysis, the instrument was mounted in an Innov-X System Stand for stability and operated remotely through a computer console. We operated the instrument in the "mining" mode, which uses the fundamental parameters (FP) approach to correct the measured X-rays for a variety of physical phenomena (e.g., absorption and fluorescence, attenuation from incoherent scattering and the photoelectric effect, differences in characteristic X-ray intensities). Measuring the elements of interest used three proprietary, built-in X-ray filters (main – tube voltage of 40kV, tube current of 50 μA; low -20 kV and 100 μA; and light 6 kV and 200 μA). Our analytical times were 20 s for both the "main" and "low" X-ray filters and 80 s for the "light" mode. Consequently, the total analytical time was 120 s for each individual measurement.

In addition to measurements of total iron (Fe_t) and total aluminum (Al_t), extractable "free" or pedogenic Fe and Al were extracted by selective dissolution using Dithionite-Citrate solution (Jackson et al., 1986, Soil Survey Staff, 2014a). Briefly, 0.4 g of sodium dithionite (a reducing agent) and 25 ml of 0.57 M sodium citrate is added to 0.75 g of < 2 mm soil material and shaken overnight. The solution is subsequently centrifuged and an aliquot is removed for analysis of Fe and Al by ICP-OES (Soil Survey Staff, 2014a). The dithionite-citrate selective extraction is thought to predominantly extract non-crystalline, amorphous, and organically-complexed Fe and Al, but is a poor extractor of crystalline Fe and Al (Wada, 1989). It is thus a reasonable measure of the total pedogenic Fe and Al oxy-hydroxides in the soil. A subset of these pedogenic Fe and Al oxy-hydroxides, amorphous

"active" Fe and Al (Fe_o and Al_o), were selectively extracted with 0.2 M ammonium oxalate buffered to pH 3.0 in a mechanical vacuum extractor under darkness over a period of 12 hours (Soil Survey Staff, 2014a).

1.2.5. Clay Mineralogy

For selected soil horizons across the study area (n = 14), we used previously obtained silt and clay isolates (remaining from particle size measurements) as starting materials to obtain pure clay (< 2 μm) isolates for subsequent mineralogical analyses. First, we removed soil organic matter using a household solution of bleach (sodium hypochlorite, NaOCl) titrated to pH 9.5 with hydrochloric acid (HCl), which we heated between 70–90 °C for 1 h (Soil Survey Staff, 2014a). After cooling, we centrifuged the samples at > 3500 rpm for at least 10 min – or until the supernatant became clear – before decanting. We repeated these oxidizing treatments until samples no longer bubbled when heated; this typically required 1–2 repetitions for subsoils and 3–5 repetitions for surface horizons. Following organic matter removal, we extracted poorly crystalline/hydrous Fe and Al oxides using a standard citrate-dithionite method (Soil Survey Staff, 2014a). We repeated citrate-dithionite treatments until the extracting solution was visibly clear following overnight (12–16 hour) shaking. After completing the selective extractions, we separated the remaining silt and clay materials by size (above and below 2 μm) using standard sedimentation methods assuming a room temperature of 25 °C and particle settling behavior according to Stoke's Law.

When >1 g of clays had been obtained for each sample, we divided the isolate from each horizon in half and saturated the clay splits with either 0.5 M $MgCl_2$ or 1.0 M KCl (Jackson and Barak, 2005). We repeated the Mg– or K–saturation step (i.e., thorough vortexing in Mg– or K–rich salt solution, followed by centrifuging and decanting) at least two times before washing each sample 2–3 times with a 50:50 solution of ethanol:water to remove excess salts and chloride ions, followed by 1–2 additional rinses in nanopure H_2O (18.2 MΩ) to remove any traces of ethanol. Then we pipetted 400–500 μL of the Mg– or K–saturated clay slurries onto glass slides (three slides for K–, two for Mg– per horizon) and allowed the samples to dry slowly under minimal airflow. Once dried, we heated the extra K–saturated slides at 350 °C or 550 °C for 1 h in a muffle furnace.

We mounted the oriented clay slides and assessed mineralogy of the clay-sized (< 2 μm) soil fraction using a Rigaku MiniFlex X-ray diffractometer fitted with a 2.2 kW, 60 kV Cobalt X-ray source in the Department of Earth and Environmental Sciences at the University of Minnesota–Twin Cities. We x-rayed pure Mg– and K–saturated samples from 5º to 65º 2θ (Co–Kα radiation, λ= 1.78899 Å) using 0.02–degree steps and a dwell time of 0.60 degrees min-1 (2 seconds per step). We x-rayed the other K–heated samples (i.e., K–350 ºC) from 10º to 27º 2 θ utilizing the same step sizes and dwell times. We then exported all of our spectra into Jade 10 (Materials Data Inc.) and converted from Co to Cu–Kα (λ = 1.54059 Å) wavelength to facilitate comparisons with previous studies and reference databases. When necessary, we made additional baseline corrections in Jade before conducting semi-quantitative phase identifications using a full pattern summation approach, which iteratively matches sample spectra against reference powder diffraction files (PDF) sourced from the PDF-4 Minerals 2020 database (International Centre for Diffraction Data, 2020). Lastly, we exported the baseline corrected and Cu-converted spectra from Jade as ASCII text files for final normalizations (by treatment type), spectral visualizations (by profile), and terminal graphic production in R (R Core Team 2019).

1.2.6. Statistical Analysis

All statistical analyses were performed in R (version 3.3.1, R Core Team, 2019). We utilized Kendall's tau-b (τ_b) non-parametric rank correlation coefficient (with Holm's correction for multiple comparisons) to examine the relationship between measured soil properties across all samples because (1) we did not assume linear relationships between variables and (2) several variables had a significant number of tied values. Post-hoc analyses for significant differences in response variables between groups after ANOVA analyses were conducted using Tukey's Honest Significant Difference (HSD) in group means. Unless otherwise mentioned in manuscript text or figure captions, all reported uncertainties represent a single standard deviation around the mean.

Because our dataset represents a mixture of sites sampled by genetic horizon, we chose to utilize Land Degradation Surveillance Framework (LDSF) (Vågen et al., 2013) standardized depth increment (0–20 cm, 20–50 cm, and 50–100 cm (combining the 50–80 cm and 80–100 cm LDSF standardized depth increments into one 50–100 cm increment)

weighted averages to compare soil properties by depth between sites. We calculated the weighted averages of all available soil properties by depth increment for each sampling site using the "slab" function in the AQP package in R (Beaudette et al., 2013, R Core Team, 2019). These standardized depth-increment weighted averages were utilized to examine the relationships between soil properties and site-level characteristics such as land use, landscape position, vegetation, and climate using ANOVA. The effects of climate and vegetation on soil physical and chemical properties were evaluated using both ANOVA (for categorical variables vegetation and Köppen climate zone) and regression models (for the continuous co-variates mean annual precipitation (MAP) and latitude).

1.3. Results

1.3.1. Soil Property Distributions and Relationships Between Soil Properties

The distribution statistics for all measured soil properties are shown in Table 1.1. Very fine sand, medium sand, coarse sand, pH, total P, Fe_o, Al_d, and Al_t were the most symmetrically distributed variables, while the distributions of most other soil properties were skewed to the left (many observations at lower values) and heavy tailed (few observations at much higher values). Among all samples, SOC and pH were significantly correlated to more soil properties (10 and 11 other properties, respectively) than any other measured variables (Table 1.2). Total nitrogen (TN) was also significantly correlated to the same 10 variables as SOC, however due to strong collinearity with SOC ($\tau_b = 0.74$), the high correlation of TN with the other variables is a consequence of its relationship with SOC.

SOC was significantly negatively correlated with depth, clay content, pH, bulk density, Al_t, Fe_t, CBD-Fe (Fe_d), and CBD-Al (Al_d); and significantly positively correlated to TN and Al_{ex}. Fe_t was strongly correlated with ($\tau b = 0.51$) and linearly related to clay content ($Fe = 0.143*Clay + 0.385$, $R^2 = 0.773$, $p < 0.0001$), while total Si was moderately correlated with ($\tau_b = 0.481$) and linearly related to total sand content ($Si = 0.453*Sand – 7.379$, $R^2 = 0.526$, $p < 0.001$). Soil pH was most strongly correlated with Al_o ($\tau_b = 0.58$) and Al_{ex} ($\tau_b = -0.47$) (Table 1.2). pH was significantly negatively correlated with depth, clay content, TN, Al_{ex}, Fe_t, and Fe_d; and significantly positively correlated with bulk density, Al_t, Al_o, Fe_o, and Al_d (Table 1.2).

Across all measured samples, CEC and base saturation were extremely low (Table 1.1). The highest CEC value recorded among all measured samples (n = 40) was 5.52 $cmol_c$ kg^{-1}, and base saturation never exceeded 10% in samples analyzed, with many values below the limit of detection. CEC was positively correlated with ($p < 0.001$, $\tau b = 0.49$) and linearly related to SOC ($p < 0.001$, $R^2 = 0.62$, Figure 1.2a), while bulk density was negatively correlated, and non-linearly related to SOC (Figure 1.2b). Exchangeable aluminum was non-linearly related to soil pH across all samples and increased significantly with decreasing pH (Figure 1.2c).

Clay-sized (< 2 μm) fractions of all analyzed soil samples were dominated (>> 50%) by kaolinite (Table 1.4). The predominance of kaolin-group minerals was visibly evident from diagnostic peaks at ~7.15 Å and ~3.58 Å, which were ubiquitous across all of the samples (Supplementary Figures 1.S1, 1.S2 and 1.S3; Moore and Reynolds, 1997). In some samples, kaolinite was the only clay mineral present in detectable quantities (Table 1.4; Supplementary Figure 1.S1). More commonly, kaolinite was present as the dominant phase (>>50%), coexisting with minor (5% ≤ x < 50%) and/or accessory (< 5%) amounts of crystalline Al–hydroxides (gibbsite, α–Al(OH)3) and primary minerals (i.e., quartz) (Supplementary Figures 1.S2, 1.S3). Gibbsite was captured in most (>70 %) full pattern fitting analyses (Table 1.4) and could also be identified qualitatively by peaks at ~ 4.85 Å and/or 4.37 Å that collapsed when heated to 350 °C (Moore and Reynolds, 1997, Jackson and Barak, 2005, Supplementary Figures 1.S2, 1.S3). Sub-micron quartz (~3.34 Å peak) was present in trace (< 5 %) quantities of ~30% of the soils (Table 1.4; Supplementary Figure 1.S3). Clay-sized (< 2 μm) primary minerals (i.e., quartz) were only detected in soils where gibbsite was also present as a minor or accessory/trace phase (Table 1.4). No smectite–, vermiculite–, chlorite–, or mica–group minerals were observed in any profiles.

1.3.2. Particle size distributions with depth and latitude

Across all samples, total sand percentages were high (87.9 ± 6.7 %). Sands were well sorted and dominated by fine sands (fS) (46.3 ± 5.6%) and medium sands (mS) (27.0 ± 6.3 %) (Table 1.1). Very fine sands (vfs) (10.1 ± 3.6%), coarse sands (CoS) (4.1 ± 1.8%) and very coarse sands (VCoS) (0.4 ± 0.4 %) formed more minor components of the sand

fraction (Table 1.1). Clay percentages were low across all samples (7.8 ± 6.5 %), followed closely by silt sized particles (4.1 ± 3.1%). Soil texture classes in the study area were predominantly sands or fine sands (63%, n = 95) and loamy sands or loamy fine sands (20%, n = 30), with few fine sandy loams or sandy loams (9%, n = 14) and sandy clay loams (9%, n =14). Finer texture classes were more likely to occur in Af and Am. All sandy clay loams (n = 14) only occurred in Af under forest vegetation, while sandy loams and fine sandy loams occurred under forest vegetation in Af and Am. Soils in Aw and Am showed little texture variability with depth, while several of the pedons in Af showed significant relative increases in clay in the subsurface.

Although dominant sand particle size classes in the sand, loamy sand and sandy loam texture classes vary between fine and medium, the difference in proportion of fine sand and medium sand particles in most cases was borderline (< ±5%) between criteria for sand texture subclasses. Sands of all sizes were dominated by quartz grains, and were typically comprised of less than 1% of other mineral grains. Family particle size classes across all investigated pedons were predominantly sandy (n = 22), with few pedons classified as coarse loamy (n = 1), and fine-loamy (n = 3). Percentages of coarse, medium, fine, and very fine sand fractions varied significantly in all cases with latitude in particle size control section weighted averages (Figure 1.3). Both fine ($p < 0.001$, $R^2 = 0.39$) and very fine ($p < 0.0001$, $R^2 = 0.59$) sand fractions increased with increasing latitude, moving south across the bio-climosequence, while coarse ($p < 0.01$, $R^2 = 0.30$) and medium ($p < 0.01$, $R^2 = 0.32$) sand proportions decreased with increasing latitude (Figure 1.3). Very coarse sands, silt and clay particles percentages in the particle size control section did not demonstrate any significant variations with latitude ($p > 0.05$).

1.3.3. Impact of Climate on Soil Characteristics

Analysis of soil properties by mean annual precipitation (MAP) as a continuous variable and Köppen climate zone as a categorical variable revealed that climate had the greatest impact on concentrations of Fe_t, total Si (Si_t), and pedogenic Fe across the entire soil profile depth. Fe_t concentrations increase with increasing MAP ($R^2 = 0.172$, $p = 0.020$) in the subsoil, but not in surface soils (0-20 cm) (Figure 1.4a). When using climate zone as a categorical variable, Fe_t concentrations were highest in soils of the Af throughout all

depth increments except for the 10-20 cm depth increment (Table 1.5). Increases in Fe_t concentrations in some pedons were quite abrupt in the Af relative to concentrations in the Am and Aw. Total iron concentrations by weight in Af ranged from 1.73 to 2.62%, while in Am the range was 0.9 to 1.19% and 0.88 to 1.13% for Aw. Si_t concentrations in surface (0-20cm) and deep (180-200cm) soils decreased significantly with increasing MAP (Figure 1.4c). This effect was more significant for deep soil horizons than for surface horizons (Figure 1.4c), and both surface and deep horizons demonstrated a more continuous trend in concentration decrease of Si across the climatic gradient than Fe, which exhibited a dramatic increase in concentration in the Af climate zone.

Fe_d was strongly correlated to Fe_t across all samples ($\tau_b = 0.93$), following a similar trend to Fe_t and generally decreasing from Af to Aw across all depths (Table 1.5). However, unlike Fe_t, the differences between categorical climate zones for Fe_d were statistically significant only in the top 3 standardized depth increments (0-10cm, 10-20cm, 20-50cm) (Table 1.5). Similar to Fe_t, when considering MAP as a continuous variable, surface concentrations of Fe_d were not linearly related to MAP ($p > 0.05$). Fe_o concentrations were significantly higher in soils of Af than Fe_o concentrations in Am and Aw for all depth increments. Fe_o concentrations in the surface (0-20cm) were significantly linearly related with MAP ($y = 10.349x - 15739$, $p = 0.0015$, $R^2 = 0.332$), but deep Fe_o concentrations (180-200cm) were not ($p > 0.05$). Fe_o was not correlated to either Fe_d or Fe_t, and the ratio of amorphous to pedogenic iron (Fe_o/Fe_d) or pedogenic iron to total iron (Fe_d/Fe_t) did not differ significantly by climate zone between any depth increments, nor was it related to MAP. Additionally, Fe_d/Fe_t ratios showed little variability with depth, averaging 0.38 ± 0.09 and 0.36 ± 0.06 in topsoils (0-20cm) and subsoils (180-200cm) respectively, while Fe_o/Fe_d ratios were more variable (0.50 ± 0.36 and 0.51 ± 0.31 in topsoils and subsoils, respectively).

In contrast to Fe and Si, which showed variation by climate zone across many depth increments, Al did not show major variations with climate (Figure 1.4b, Table 1.5). By categorical climate zones, Al_t concentrations differed only in the 50-100cm depth increments, where concentrations were highest in Af, intermediate in Am, and lowest in Aw (Table 1.5). Both Al_d and Al_o differed significantly between climate zones only in the

0-10, 50-100 and 100-200cm depth increments. No metrics of Al (Al_t, Al_d, Al_o) were significantly linearly related to MAP in all cases.

Significant differences in pH by climate zone were limited to only a few depth increments. pH differed between climate zones in the top 50 cm (ANOVA, $p < 0.02$) (Table 1.5). Specifically, average pH in the 0-10 cm, 10-20 cm, and 20-50 cm depth increments was lower in equatorial forest (3.9, 4.0, and 4.1, respectively) than tropical savanna (4.3, 4.4, and 4.4, respectively) ($p < 0.05$, Tukey's HSD, Table 1.5). However, average pH in the 0-10 cm, 10-20 cm depth increments did not differ between Am and either Af or Aw ($p > 0.05$, Tukey's HSD, Table 1.5). From increasing depth from 50 cm to 200 cm, pH increased by approximately 0.4 to 0.5 units in all investigated soils, but did not vary between climate zones ($p > 0.05$, Tukey's HSD, Table 1.5). Both surface (0-20cm) and deep soil (180-200cm) pH values decreased linearly with increasing MAP ($p = 0.002$ and 0.048, respectively, Figure 1.4d).

SOC and soil color (as quantified by VC index) were significantly different between climate zones only in the subsoil (50-100 cm for SOC and 20-50 and 50-100 cm increments for VC index (Table 1.5)). SOC in the 50-100 cm depth increment was significantly higher in soils of Am and Aw (0.65 ± 0.4 and 0.44 ± 0.2, respectively) relative to soils in the Af climate zone (0.28 ± 0.1, Table 1.5). SOC was not related to MAP for either surface or deep soils ($p > 0.13$ in both cases). Soil darkness as quantified by VC index was significantly lower (darker) in Am and Aw soils in the 20-50cm depth increment (6.36 ± 2.94 and 7.44 ± 4.04, respectively) than in soils of the Af climate zone in the same increment (13.41 ± 5.02) $p < 0.02$, Tukey's HSD). In the 50-100 cm depth increment, Aw and Af soils were significantly different (12.16 ± 7.10 and 21.23 ± 5.34, respectively), while Am soils were intermediate in darkness (15.93 ± 8.50) and not different from either Aw or Af ($p > 0.26$ in both cases).

Across all profiles, SOC stocks in the top 1 m ranged from 4.29 kg C m^{-2} to 23.64 kg C m^{-2} and averaged 7.89 ± 3.82 kg C m^{-2} (Table 1.6). 2 m SOC stocks ranged from 6.45 to 33.8 1 kg C m^{-2} and averaged 12.56 ± 5.5 kg C m^{-2}. Numerically, SOC stocks to both 1m and 2m depth were highest in the Am climate zone (10.1 ± 5.7, Table 1.6), but these differences were not statistically significant ($p > 0.05$). Stocks of Fe_t and pedogenic iron Fe_d to both 1 m and 2 m were more than double in Af soils compared to Am and Aw ($p <$

0.05), while stocks of Fe_o differed significantly only between Af and Aw (Table 1.6). 2-m stocks of Al_t were greater in Af soils than Aw soils, while 2-m stocks of Al_d and Al_o were highest in the Am climate zone (Table 1.6). There was no effect on Al_{ex} ($p = 0.23$), clay content ($p = 0.16$), and available phosphorus (Bray-1) ($p = 0.13$) across categorical climatic zones (Af, Am, Aw) and all depth increments (Table 1.5).

1.3.4. Impact of Vegetation on Soil Characteristics

In contrast to differences between climate zones or along the continuous MAP gradient, differences in soil properties by vegetation type were primarily related to pH, clay content, available P, and soil color (Table 1.7). Soil pH was significantly higher under savanna than under forest across all depth increments by an average of 0.4 ± 0.1 pH units (Table 1.7, Figure 1.5). Depth trends of pH in both forest and savanna followed similar patterns, increasing from the surface to the deep soil, and converged with depth (Table 1.7). Average pH values in the top 20 cm of soil were significantly higher under savanna vegetation relative to forest vegetation regardless of climate zone (Figure 1.5). This same pattern held but became less significant with depth as pH values converged with depth (Table 1.7).

Between vegetation types, differences in Fe and Al metrics were much more limited than for climate zones. Both Fe_t and Al_t concentrations were significantly higher under forest relative to savanna in deeper depth increments (100-200 cm for Al_t and 50-100 and 100-200 cm for Fe_t) (Table 1.7). Fe_d, Fe_o, and SOC concentrations did not differ by vegetation type, and Al_d and Al_o concentrations differed only in the 0-10 cm depth increments, where savanna had higher average values than forest vegetation. Al_{ex}, which was not significantly different between climate zones, did differ significantly between vegetation types in the 50-100 and 100-200 cm depth increments. There were no significant differences in Fe_t, Fe_d, Fe_o, Al_t, Al_d, and Al_o stocks to 1 m or 2 m between vegetation type (Table 1.6).

Clay contents differed significantly between vegetation types in the surface and subsoils. Forest soils had significantly higher clay percentages in the 0-10, 10-20 and 50-100 cm depth increments than savanna soils. Clay content noticeably increased within the first 20 cm and at 50-100 cm in the forest (Table 1.7): 9.9 %, 9.9 %, and 11.7 % at 0-10

cm, 10-20 cm, and 50-100 cm, respectively, $p < 0.03$, Tukey's HSD). The variability in clay content overall, however was much higher in forest sites than savanna sites (Table 1.7).

Substantial labile inorganic P (Bray-1P) concentrations occurred in savanna relative to forest, but those concentrations were significantly higher only within the top 20 cm (59 mg kg^{-1} (0-10 cm) and 56 mg kg^{-1} (10-20 cm) in savanna versus 19 mg kg^{-1} (0-10 cm) and 18 mg kg^{-1} (10-20 cm) in forest ($p < 0.03$, Tukey's HSD, Table 1.7). Soil color, as indicated by VC index, was darker under savanna than forest in the 20-50 cm depth increment (VC index values of 7 and 12, respectively, $p < 0.02$, Tukey's HSD) (Table 1.7).

1.3.5. Soil Classification and Diagnostic Features

A total of 5 unique soil orders (Entisols (15%), Inceptisols (62%), Spodosols (4%), Ultisols (15%) and Oxisols (4%)), 9 suborders, and 10 soil Great Groups (US Soil Taxonomy) were identified across the study transect (Table 1.8). Most of the taxonomic diversity occurred at the suborder level (Table 1.8). Inceptisols (62% of all profiles) predominated in Aw and Am; Ultisols, and a single Oxisol and Spodosol profile (23% of all investigated profiles) were located primarily in Af; and Entisols (15% of all investigated profiles) were also identified in Af zone. Soil diversity at the order level (as quantified by Simpson's index, Equation 2) was highest in Af and under forest vegetation (0.8 and 0.81, respectively) than under the Am and Aw (0.25 and 0, respectively) and savanna vegetation (0.14) (Table 1.9). At the suborder level, soil diversity was also highest in the Af (0.82) relative to the Am (0.46) and Aw (0) (Table 1.9).

The presence of diagnostic horizons differed significantly across the transect. Umbric epipedons were by far the most common in the Aw and Am (present in 87% of investigated profiles in Am and Aw), while ochric epipedons were most common in the Af (82% of all investigated profiles in Af). Kandic and Oxic subsurface diagnostic horizons were present in 36% of all of the profiles investigated in the Af climate zone, 13% of the profiles in the Am climate zone, and were not present in the Aw. A single soil profile with a spodic horizon was identified in the Af. Representative soil individuals and vegetation across the transect are shown in Figure 1.6.

1.4. Discussion

1.4.1. Soil Genesis and Soil Diversity Across the Equatorial Forest-Savanna Ecotone in Sankuru Province, Central DRC

Soils across the Sankuru transect are formed on sandy parent materials, which, based on the well sorted particle size distribution of fine (46% ± 5%) medium (27 ± 6%) and very fine sands (10 ± 4%), appear to be largely eolian in nature. Nevertheless, there is some evidence of variability in both the geographic sources and transport mechanism of these sands. This large sand sheet, although recognized to the south and west (Hartemink and Huting, 2005) of Sankuru province, is poorly characterized in both composition and extent in central DRC (Hengl et al., 2017). The variations of sand particle sizes by latitude (Figure 1.3) appear to indicate a northerly source for the sands in Sankuru Province, because medium and coarse sands increase going north, whereas fine and very fine sands increase going south (Figure 1.3). These findings are also consistent with a regional deep time model in the Congo basin which posits the Jurassic-Cretaceous northeastern eolian sand origin (Linol et al., 2015). However, some soils in the northern equatorial forest zone have significant relative clay increases in the subsurface and a greater range in particle sizes that cannot be explained by eolian deposition alone. Therefore, it may be that the northern region of the study transect consists of reworked fluvial and eolian materials. Linol et al. (2015) also suggested that there is evidence for Oligo-Miocene fluvial excavation and erosion of the unconsolidated sandstone in Congo basin, while the southern zones are largely influenced by eolian deposition from a northern source. This material was likely moved and deposited during periods of aridity in the Congo Basin that were aligned with Pleistocene glacial cycles (Cohen et al., 2007). It is likely therefore that the sheet of sands that form the parent material for Sankuru soils (the Salonga formation, dominated by fine and medium sands, Guillocheau et al., 2015) are of early to late Pleistocene age. Although the Congo Basin experienced drier periods in the Holocene (Maley et al., 2018), and those periods were characterized by the fragmentation and retreat of forest to refugia and expansion of savanna (Mahli et al., 2013), it is unlikely that the climate was dry and unvegetated enough to mobilize large amounts of sediments from unvegetated areas to generate such a large sand sheet throughout the southern Congo Basin. Furthermore, the upper terrace regions of the Congo Basin (where Sankuru province is located) are highly

dissected landscapes (Flügel et al., 2015), which would have taken much longer than a few millennia to develop, even in the equatorial zone of intense rainfall, and there is no direct geomorphic or surface evidence of relict dune morphology in the study area.

Overlain on the stage set by the sandy soil parent materials in Sankuru province are additional soil formation processes that have been largely influenced by vegetation and climate. Across the entire transect soils are highly weathered, with kaolinite, gibbsite and quartz as the major mineral assemblages in the clay fraction, pH values below 5.5, and extremely low CEC and base saturation. Base cation depletion and kaolinitization have been prevalent processes across the transect, and indeed many Ca and other base cations were below the limit of detection by pXRF. This is likely due to 1) sandy, quartz dominated soil materials, with low CEC, in a high rainfall environment, and 2) pre-weathering of materials in the sand sheet (potentially in the Congo Basin) prior to transport (either eolian or fluvial). These properties are broadly comparable to soils formed in the Bateke sands (a marine fluvio-lacustrine formation) in Nigeria under equatorial forest vegetation; which are characterized by a clay enriched subsoil, low CEC, pH, OC, and base saturation, siliceous or kaolinitic mineralogy, and spodic characteristics in isolated pedons (Lekwa and Whiteside, 1986). Acidification appeared to be strongest with increasing MAP across the transect, as many soils in Af were within the pH range where hydrolysis of Al and potentially even Fe becomes the dominant proton buffering system (Chadwick and Chorover, 2001). The degree of latosolization/ferrallitization (residual accumulation of Fe oxy-hydroxides) (Schaetzl and Thompson, 2014), desilication, and lessivage (illuvial clay accumulation in the subsoil) increased with MAP, while humification and melanization (the formation humic materials from raw organic matter and subsequent darkening of mineral topsoils) decreased with increasing MAP.

Thus, soil formation appears to have occurred under stable savanna vegetation through the development of a dark colored, thick A horizons (umbric epipedons), and minimal subsoil development, regardless of climate zone. In contrast, soils underlying forest vegetation are more likely to exhibit clay illuviation and increases in the subsoil, sometimes with thin O or A horizons, and evidence of incipient or mature E horizon formation (Figure 1.6). Therefore, soils under savanna vegetation are more likely to be classified as Inceptisols (if they have an umbric epipedon) or Entisols (if they have an

ochric epipedon), while soils under forest vegetation are more likely to be classified as Ultisols, Oxisols, or Spodosols (Table 1.8).

Previous studies across environmental transition zones have hypothesized that pedodiversity would be highest in the transition zone or ecotone (Bockheim and Schliemann, 2014), but failed to show that this taxonomic class diversity is borne out at a landscape scale. Similarly, although we had expected soil taxonomic diversity to be highest near the modern-day ecotone boundary in Am, we instead found that soil taxonomic diversity was highest in Af at the soil order and suborder levels.

1.4.2. Climatic Influences on Soil Properties Across the Ecotone.

Soil iron concentrations and stocks, and topsoil soil pH were the properties that appeared to be most influenced by the climatic gradient across the study area. Free Fe (in crystalline and noncrystalline forms) is important for its potential role in controlling chemical and physical soil characteristics such as pH, SOC retention, CEC, specific surface area, phosphorous retention, and aggregation (Jackson et al. 1986, Bruand, 2005, Blanchart et al., 2005, Bortoluzzi et al., 2015, Coward et al., 2017). Accumulation of iron and aluminum oxyhydroxides throughout the profile is driven by soil mineral weathering and clay illuviation (Jackson, 1986, Schaetzl & Anderson, 2005), which are the dominant pedogenic processes in the equatorial forest zone in Sankuru province. Specifically, our data shows that total iron (Fe_t) and pedogenic iron (including crystalline and non-crystalline, Fe_d and Fe_o) concentrations and stocks were highest in soils of the Af climate zone and generally increased along the climate gradient with increasing MAP. Total iron concentrations in the soils of our study transect (1.51 ± 1.1%) were generally lower than those reported in finer textured soils of other tropical sites in non-sandy soils, where Fe_t concentrations may be as high as 5-20% (Long et al., 2011, Vitousek and Chadwick, 2013, da Silva et al., 2016, Huang et al., 2016Taboada et al., 2019).

There is conflicting evidence in the literature regarding whether or not Fe_o/Fe_d and Fe_d/Fe_t ratios are generally indicative of intensified weathering. Previous studies have shown similar increases in total and pedogenic iron concentrations with time and weathering intensity across climosequences of similar magnitude (Birkeland et al., 1991, Bortoluzzi et al., 2015). In fine-textured soils in southern Brazil, Fe_t, Fe_d, and Fe_o

concentrations all increased significantly along a mean annual precipitation gradient from 1688 to 1792 mm yr^{-1} (Bortoluzzi et al., 2015), while along a climosequence from 500 to 1800mm yr^{-1} in northeastern Brazil in soils formed on granite residuum, Fe_t, Fe_d and Fe_o increased significantly in the most humid sites (da Silva et al., 2016). Some studies have reported no significant changes in Fe_d/Fe_t ratios with increased precipitation/weathering (Long et al., 2011), while others have reported non-linear (Aiku and Singer, 1990, Long et al., 2016) trends associated with increased Fe_d/Fe_t ratios and increased rainfall or weathering. We found no significant differences in Fe_d/Fe_t or Fe_o/Fe_d ratios across the Sankuru climosequence at any depth, however the precipitation gradient along the Sankuru climosequence (1613 to 1742 mm yr^{-1}) is within the range of non-linear changes observed in these ratios in tropical soils on basalt residuum (Long et al., 2016).

The Fe_d/Fe_t ratios reported in this study are generally higher than those reported in other temperate and tropical studies (McFadden and Hendricks, 1985, Mahaney et al., 2016, Huang et al., 2016), while conversely, the Fe_o/Fe_d ratios in our study were generally similar or lower than those reported in other studies (Blume and Schwertmann, 1969, Bera et al., 2005, Portes et al., 2016). These results make sense in the context of the soil parent materials and properties across the Sankuru transect. Soils are low in total iron because they are sandy and quartz dominated, with total iron concentrations increasing significantly in the Af climate zone. However, a significant proportion of the total iron (~ 40%), generally greater than that reported in other studies, is largely pedogenic. The low proportion of Fe_o/Fe_d in the soils of our study area can be explained by either 1) much of the iron is crystalline instead of non-crystalline as the intense weathering and aerobic environments may favor crystallinity or 2) the prevalence of Fe oxyhydroxide species such as magnetite or maghemite which are differentially soluble in citrate dithionite and ammonium oxalate extractants (Rennert et al., 2019).

Both surface and subsoil pH systematically decreased along the transect, along the MAP gradient, and across discrete climate zones (Figure 1.4, Figure 1.5). Decreases in soil pH with increasing MAP or effective precipitation are commonly observed across a wide range of climates and soil parent materials, particularly in the range of 1000 to 2000 mm yr^{-1}, which is the MAP range in which the Sankuru transect occurs (Vitousek and Chadwick, 2013, Long et al., 2016, Slessarev et al., 2016). Surface (0-10 cm) SOC

concentrations, although numerically higher in the Af climate zone, did not differ significantly between categorical climate zones or along the MAP gradient. Deep SOC concentrations and stocks also did not differ significantly along the climosequence.

1.4.3. Vegetative Influences on Soil Properties Across the Ecotone.

Vegetation appeared to have a much broader impact on soil properties than climate across the investigated ecotone transect. Specifically, soils under forest vegetation have 1) lower pH in the surface and subsurface, 2) a higher probability of an increase in clay in the subsurface, 3) lower available P, and 4) lighter color in the subsurface, relative to soils formed under savanna vegetation, regardless of climate zone. These observations are consistent with previous work in temperate regions, which has shown that vegetation can drive major, abrupt changes in soil properties that are larger in magnitude across ecotone boundaries than climatic effects alone (Anderson, 1987). The effects of forest vs grassland vegetation in temperate ecotones includes 1) higher available soil moisture throughout the year and increased leaching (which results in clay illuviation, nutrient leaching and acidification relative to nearby grassland soils) (Pettapiece, 1969); 2) thickening of A horizons and the lack of O horizons or litter layers in grassland soils (St. Arnaud and Whiteside, 1964) including increased overall carbon storage and carbon stocks in grassland soils (Anderson, 1987), and 3) increased weathering, nutrient losses, and decreased biocycling of elements such as Ca, Mg, K, and P in forest soils (St. Arnaud, 1986).

These trends also generally hold in tropical regions (Issaka et al., 1996, Sugihara et al., 2015), although there is conflicting information in the literature on soil properties across tropical forest-savanna ecotones that may largely be an artifact of sampling depth and a conflict between a pedological and ecological perspectives. Many studies from the tropical forest-savanna ecotone, unlike their temperate counterparts, have come from an ecological perspective which typically focus on shallow sampling increments and surface soils (i.e., Bond, 2010, Silva et al., 2013). This has led to some apparent contradictions in patterns of properties of soils and observed trends which can appear to be opposite of those derived from pedological studies in temperate regions. For example, on a transect in the Gran Sabana highlands in southern Venezuela characterized by sandy soils dominated by kaolinite, gibbsite, and Fe-oxides, surface savanna soils were found to be lower in P than

adjacent forest soils (Dezzeo et al., 2004). In a study of forest and savanna soils in Cameroon, the authors found higher SOC in the top depth increments of forested sites (Sugihara et al., 2014). In a study in Gabon which sampled forest and adjacent grassland surface soils, pH and available P were higher in grassland than in forest, but soil carbon concentrations were lower under grassland (Cuni-Sanchez et al., 2016). Another study (looking at only the top 5cm) on sandy soils in Australia found little to no differences in pH, and higher SOC and available P in forest compared to savanna (Bowman, 1992). When viewed from a pedological perspective, these apparent contradictions may be reconciled by considering that the thin O and A horizons in forest soils are the primary repository of SOC and nutrients in those systems. If only shallow surface samples are taken, forest soils may appear to be higher in SOC and nutrients (and potentially P) than savanna soils (Furley and Ratter, 1990, Staal and Flores, 2015). However, when deeper soil layers are taken into account across the Sankuru transect, it becomes clear that differences in SOC are equivocal, while available P and pH are significantly higher under savanna vegetation.

1.4.4. Implications for Soil Use and Agronomic Management

Generally, the soils across the equatorial forest to savanna ecotone in Sankuru Province, DRC are sandy, acidic, low carbon, and have only low to moderate available P. This combination of factors presents many challenges to agronomic management, and sandy soils of the tropics are some of the more difficult soils to manage for crop production (Hartemink and Huting, 2005). Nevertheless, the diversity of soil properties and pedogenetic pathways within the Sankuru transect suggest several management strategies that may be effective for increasing agronomic productivity in these soils. First, the Sankuru climosequence also includes an implied seasonality gradient. Soils in the south are subjected to increased rainfall seasonality, with a distinct dry season associated with water stress (Munzimi et al., 2015), while soils in the north have more rainfall, less distinct seasonality and are less likely to be water limited throughout the year. However, northern soils are also likely to be more difficult to manage for carbon and residue retention, as mineralization rates are much higher without a distinct dry season and under higher annual average temperatures in the equatorial forest zone. Soils under savanna vegetation in the Af climate zone are distinct and appear to be a major opportunity for agronomic

management, with relatively high available P and pH and a lower potential for drought stress. Interestingly, while some authors have reported waterlogged conditions or low nutrient conditions associated with isolated soils under savanna vegetation in the equatorial forest zone (Mills et al., 2006), the savanna soils in the Af climate zone on the Sankuru transect were well drained, aerobic soils with enhanced fertility parameters and may be easily adapted to agricultural management.

Any sustainable increases in organic carbon concentrations are likely to have a large impact on soil chemical properties and water and nutrient retention. In tropical sandy soils, organic carbon is the critical property controlling cation exchange capacity (Figure 1.2a; Hartemink and Huting, 2005), and additionally, even though the absolute concentrations may be low, soil organic carbon plays an outsized role in buffering acidification processes in tropical sandy soils (Fujii et al., 2017). Our analysis suggests that for every 1% increase in carbon levels in Sankuru soils, CEC may be improved by ~1.5 $cmol_c\ kg^{-1}$ (Figure 1.2a), which would be very significant in these soils given that the range in CEC is extremely low ($1.48 \pm 1.05\ cmol_c\ kg^{-1}$). The organic carbon levels in these soils are much lower than those reported in other tropical sandy soils (Hartemink and Huting, 2005, Mujuru et al., 2013, Fujii et al., 2017), which could indicate additional carbon carrying capacity in these soils under adaptive management schemes. However, in reality, even a 1% increase in OM may be difficult to achieve due to intensive mineralization processes, particularly in the Af climate zone (Shirato et al., 2005).

Management systems that increase residue retention are critical to building soil organic matter in the long term in soils with intensive mineralization (Blanchart et al., 2005, Mujuru et al., 2013). Although shifting cultivation strategies associated with slash and burn agriculture can be effective under long return intervals, more frequent burning and residue removal can deplete soil organic matter via mineralization and export nutrients by crop harvest (Bell and Seng, 2007). There are many challenges with external organic matter inputs to these soils, including logistical and cultural adoption challenges.

Therefore, one of the most effective local amendments could be high carbon biochar, which could both increase water holding capacity, increase carbon storage and CEC, and increase pH (Jeffery et al., 2017). Conversely, N-rich, low cellulose residues derived from natural vegetation (such as Dipterocarp sp. residues) have been shown to

increase SOC even in tropical sandy soils (Puttaso et al., 2011), which suggests that increasing afforestation, decreasing shifting agriculture burning times, and confining high intensity agriculture to more naturally fertile soils such as those under savannas in the Af climate zone may assist in raising overall SOC and nutrient and water holding capacity, and productivity in soils across the Sankuru transect (Armolaitis et al., 2013).

1.5. Conclusion

This work fills a critical gap in knowledge of the environmental drivers of soil variability across the equatorial forest-tropical savanna ecotone of central DRC, which remain understudied, but occur in one of the most critical pedological transition zones in the world. The soils across the study area are extremely sandy, low organic matter, very acidic and have low to moderate available P. Despite their occurrence in a region previously mapped as dominantly Oxisols, we described five soil orders (Entisols, Inceptisols, Ultisols, Oxisols, and Spodosols), 9 soil suborders, and 10 great groups across the study area. Vegetation is perhaps the most important driver of soil properties across the Sankuru transect, with soils under savanna being higher in available P, pH, and lower in clay than soils under forest. However, climate also played a role in driving variability through increased Fe accumulation and desilication in the wetter northern region of the transect. Soil diversity varied significantly across the ecotone boundary and climate zones, with soils in the Aw and Am Köppen zones and under savanna demonstrating much less pedologic diversity relative to soils under forest vegetation and in the Af Köppen zone, which had significantly greater diversity in properties and taxonomic classification. This information can be used to provide improved pathways to soil management and productivity in the sandy soils of central DRC. The most fruitful paths forward may include intensifying cultivation on the most fertile soils, a renewed focus on the sustainable management and accumulation of organic carbon, and the use of locally produced soil amendments such as biochar.

Table 1.1. *Descriptive statistics of the distribution of soil properties and site variables for all samples across the climatic transect in Sankuru Province, DRC. Note that this includes all samples from the study, regardless of depth or origin.*

Property	N	Range (min-max)	Mean	Median	25th Percentile	75th Percentile	CV (%)	Skewness	Kurtosis
Clay (%)	149	0.4 – 32.3	7.8	5.6	3.6	9.2	0.84	1.63	5.28
Silt (%)	148	0.4 – 27.8	4.1	3.8	2.6	5.1	0.75	3.70	26.34
Total Sand (%)	151	59.2 – 98.2	87.9	90.1	87.0	91.9	0.08	-1.73	6.13
VCoS (%)	151	0 – 2.1	0.4	0.2	0.1	0.6	1.15	1.43	4.90
CoS (%)	151	0.9 – 8.9	4.2	3.5	2.9	5.4	0.43	0.65	2.49
mS (%)	151	15.2 – 42.5	27.0	26.3	22.0	32.5	0.23	0.21	2.06
fS (%)	151	25.3 – 57.2	46.3	46.3	43.1	50.1	0.12	-0.55	4.30
vfS (%)	151	1.9 – 18.8	10.1	10.0	8.0	12.3	0.35	0.17	2.68
pH	133	3.4 – 5.5	4.4	4.4	4.1	4.8	0.10	0.16	2.46
SOC (g $100g^{-1}$)	149	0.1 – 26.3	0.9	0.5	0.3	0.7	2.85	8.15	73.80
TN (g $100g^{-1}$)	149	0.01 – 2.04	0.07	0.02	0.02	0.05	3.10	7.95	70.12
Bd (g cm^{-3})	124	0.9 – 1.50	1.33	1.35	1.29	1.39	0.08	-1.74	7.32
Bray P (mg/kg)	124	1.5 – 133.6	32.5	20.9	6.1	51.8	0.97	1.15	3.60
Total P (mg/kg)	146	41.8 – 675.3	210.8	184.3	90.9	298.3	0.64	0.91	3.41
Ex Al ($cmol_c$ kg^{-1})	147	0 – 3.77	0.77	0.64	0.41	1.06	0.68	2.21	11.77
Al_o (mg/kg)	146	127 – 16,876	2,270	1,470	812	2,721	1.13	3.42	18.01
Fe_o (mg/kg)	146	92 – 5,330	2,200	2,012	1,278	2,959	0.52	0.47	2.60
Al_d (mg/kg)	146	229 – 3,848	1,541	1,467	1,068	1,989	0.45	0.49	3.37
Fe_d (mg/kg)	146	157 – 20,588	5,851	4,272	3,266	7,027	0.73	1.58	4.85
XRF Al (%)	149	0.51 – 10.77	4.94	4.67	3.48	6.09	0.42	0.40	2.73
XRF Fe (%)	154	0.12 – 5.20	1.51	1.10	0.87	1.77	0.73	1.66	5.26
XRF K (mg/kg)	112	177 – 806	327	296	235	373	0.40	1.35	4.65
CEC NH_4OAc ($cmol_c$ kg^{-1})	40	0.33 – 5.52	1.48	1.28	0.88	1.60	0.71	2.00	7.70
Sum Ex Bases ($cmol_c$ kg^{-1})	18	0.01 – 0.08	0.03	0.03	0.02	0.03	0.55	1.92	6.43
Base Sat (%)	18	1.6 – 10.0	3.9	2.7	2.3	5.5	0.6	1.2	3.5

***Table 1.2**. Correlations between soil organic carbon (SOC), pH, and other properties (Kendall's tau-b, τ_b) across all samples.*

Property	Depth (cm)	Clay (%)	TN	pH	BD	Bray P	Total P	Al_{ex}	Al_t	Fe_t	Al_o	Fe_o	Al_d	Fe_d
SOC (g $100g^{-1}$)	-0.39***	-0.13*	0.74***	-0.23***	-0.51***	0.11	0.05	0.35***	-0.33***	-0.31***	-0.05	-0.14	-0.15**	-0.31***
pH (H_2O)	-0.36***	-0.29***	-0.30***		0.17**	0.06	-0.02	-0.47***	0.18**	-0.22***	0.58***	0.20***	0.32***	-0.25***

*Number of asterisks indicate significance levels: * < 0.05 – 0.01, ** < 0.01 – 0.001, *** < 0.0001*

TN = total nitrogen, BD = bulk density, Al_{ex} = exchangeable aluminum, Al_t = total aluminum, Fe_t = total iron, Al_o = ammonium oxalate extractable aluminum, Fe_o = ammonium oxalate extractable iron, Al_d = citrate-dithionite extractable aluminum, Fe_d = ammonium oxalate extractable iron.

Table 1.3. *Correlations between citrate-dithionite extractable iron and aluminum (Fe_d and Al_d) and ammonium oxalate extractable iron and aluminum (Fe_o and Al_o) and total iron and aluminum (Fe_t and Al_t), exchangeable aluminum (Al_{ex}), Bray P, and Total P (Kendall's tau-b, τ_b) across all samples.*

Property	Depth (cm)	Al_t	Fe_t	Al_{ex}	Bray P	Total P	Al_d (mg/kg)	Fe_d (mg/kg)
Al_d	-0.20**	0.44***	0.14*	-0.11*	0.07	0.20**	1	0.11*
Fe_d	-0.02	0.32***	0.79***	0.12*	-0.0006	0.20**	-0.11*	1
Al_o	-0.25***	0.22***	-0.23***	-0.22***	0.24***	0.18**	0.51***	-0.27***
Fe_o	-0.10	0.06	0.16**	-0.14*	0.34***	0.32***	0.14*	0.14*

*Number of asterisks indicate significance levels: * < 0.05 – 0.01, ** < 0.01 – 0.001, *** < 0.0001*

Table 1.4. *Clay (< 2 μm sized) mineralogy of selected DRC soil horizons (xxx = dominant/major phase; xx = minor phase; x = accessory/trace phase)*

Profile	*Horizon*	*Kaolin-group*	*Al–(hydr)oxides*	*Prim. minerals (Quartz)*
Sample	# Code	1:1 clay	*(Gibbsite)* [$Al(OH)_3$]	[SiO_2]
LM 1-6	2	xxx[a]		
KK 2-4	4	xxx	x[b]	
LM 3-3	5	xxx		
EM 3-BTM	6	xxx	x	
LM 4-4	7	xxx	x	x
LM 1-BTM	8	xxx		
LM 4-BTM	9	xxx	x	
KO 4-BTM	10	xxx		
KK 3-6	11	xxx	x	x
LE 5-4	12	xxx	x	
LE 5-BTM	13	xxx	x	
EM 2-BTM	14	xxx	xx[c]	x
TU 1-7	15	xxx	x	
KO 4-4	17	xxx	x	x

[a] *Dominant/major phase: xxx ≥ 50% of the mineral assemblage*
[b] *Accessory/trace phase: x < 5% of the mineral assemblage*
[c] *Minor mineral phase: 5% ≤ xx < 50% of the mineral assemblage*

Table 1.5. *Average and standard deviation of soil properties by depth increment between Köppen climate zones.*

	Af					Am					Aw				
	0-10	10-20	20-50	50-100	100-200	0-10	10-20	20-50	50-100	100-200	0-10	10-20	20-50	50-100	100-200
SOC (g 100 g^{-1})	2.48 ± 4.2 -	0.76 ±0.1 -	0.49 ±0.1 -	0.28 ±0.1 A	0.26 ±0.06 -	1.10 ±0.8 -	1.11 ±0.8 -	0.85 ±0.6 -	0.65 ±0.4 B	0.44 ±0.2 -	0.69 ±0.1 -	0.64 ±0.1 -	0.55 ±0.2 -	0.44 ±0.2 B	0.33 ±0.2 -
pH	3.89 ±0.3 A	3.95 ±0.2 A	4.08 ±0.2 A	4.37 ±0.3 -	4.5 ±0.4 -	4.08 ±0.3 AB	4.16 ±0.2 AB	4.35 ±0.2 B	4.65 ±0.4 -	4.93 ±0.4 -	4.31 ±0.1 B	4.36 ±0.1 B	4.44 ±0.1 B	4.55 ±0.3 -	4.88 ±0.3 -
Al_t (%)	3.13 ±1.7 -	3.73 ±2.4 -	5.09 ±2.6 -	6.20 ±2.4 A	6.78 ±2.2 -	3.67 ±0.9 -	3.90 ±0.8 -	3.99 ±1.1 -	4.95 ±1.6 AB	6.56 ±1.3 -	2.65 ±0.7 -	2.81 ±0.9 -	3.34 ±1.3 -	3.66 ±1.2 B	4.71 ±1.2 -
Fe_t (%)	1.73 ±0.9 A	1.82 ±1.3 -	2.25 ±1.5 A	2.54 ±1.5 A	2.62 ±1.5 A	0.90 ±0.5 B	0.95 ±0.5 -	0.97 ±0.6 B	1.03 ±0.6 B	1.19 ±0.6 B	0.88 ±0.2 B	0.90 ±0.2 -	0.99 ±0.2 AB	1.02 ±0.3 B	1.13 ±0.3 B
Al_d (mg/kg)	791.78 ±624 -	726.4 ±569 A	843.55 ±535 -	1363.81 ±879 A	1642.0 ±1129 A	1415.49 ±772 -	1914.80 ±1588 B	2066.3 ±1661 -	3314.32 ±1741 B	5735.37 ±4645 B	1108.19 ±298 -	1105.80 ±266 AB	1225.26 ±485 -	1272.60 ±510 AB	2388.15 ±1598 AB
Fe_d (mg/kg)	2208.2 ±917 A	2111 ±884 A	2485.20 ±1025 A	2978.22 ±1509 -	2796.7 ±1476 -	1617.91 ±837 AB	1844.63 ±636 AB	2015.79 ±600 AB	2641.09 ±961 -	2622.96 ±829 -	996.5 ±462 B	1002.54 ±459 B	1077.39 ±510 -	1313.59 ±644 -	1837.77 ±758 -
Al_o (mg/kg)	1030.6 ±599 -	1023.99 ±594 B	1259.82 ±614 -	1655.14 ±579 B	1817.8 ±515 B	1120.15 ±577 -	1396.52 ±848 A	1448.2 ±724 -	1991.18 ±644 A	2216.18 ±399 A	1077.52 ±187 -	1150.43 ±213 AB	1181.48 ±212 -	1173.62 ±186 B	1324.24 ±306 AB
Fe_o (mg/kg)	7354.9 ±4350 A	7339.2 ±4909 A	8972.8 ±5370 A	9982.8 ±5326 A	10336 ±5283 A	3065.9 ±2208 B	3269.9 ±2003 B	33800 ±1983 B	3879.7 ±2391 B	4207 ±2818 B	3743.1 ±806 AB	3592.1 ±594 AB	3725.8 ±740 B	3997.3 ±843 B	4324.4 ±1075 B
Al_{ex}, ($cmol_c$ kg^{-1})	1.16 ±0.7 -	0.96 ±0.4 -	0.92 ±0.3 -	0.78 ±0.3 -	0.68 ±0.3 -	1.36 ±0.3 -	1.46 ±1.0 -	1.04 ±0.4 -	0.78 ±0.4 -	0.48 ±0.4 -	1.05 ±0.2 -	1.01 ±0.2 -	0.89 ±0.2 -	0.63 ±0.3 -	0.52 ±0.3 -
Clay (%)	9.98 ±8.0 -	9.50 ±7.9 -	10.70 ±9.4 -	12.39 ±10.2 -	12.94 ±10.2 -	5.61 ±3.3 -	6.23 ±3.5 -	6.40 ±3.3 -	6.24 ±3.8 -	6.07 ±5.1 -	5.21 ±2.4 -	5.78 ±2.9 -	5.35 ±2.9 -	5.13 ±2.7 -	5.53 ±3.0 -
PDI	0.15±0.1 -	0.13 ±0.1 -	0.09 ±0.04 -	0.05 ±0.03 -	0.04 ±0.01 -	0.23 ±0.1 -	0.22 ±0.1 -	0.16 ±0.1 -	0.09 ±0.1 -	0.04 ±0.1 -	0.21 ±0.1 -	0.18 ±0.1 -	0.16 ±0.1 -	0.11 ±0.1 -	0.06 ±0.1 -

Bray-1P (mg/kg)	39.4 ±49 -	33.92 ±45.3 -	29.53 ±34.4 -	27.03 ±28 -	22.37 ±22 -	60.55 ±47.2 -	60.30 ±46 -	5221 ±38 -	43.92± ±24.8 -	32.50 ±20.1 -	21.55 ±29 -	16.61 ±19.1 -	17.32 ±20 -	16.97 ±22.3 -	12.48 ±12 -

All numbers indicate the mean and standard deviation for each depth increment by climate zone.

**Different letters indicate statistically significant differences between climate zones ($p < 0.05$) following ANOVA using Tukey's HSD. Depth increments within a variable that have dashes indicate no significant differences between climate zones ($p > 0.05$) following ANOVA using Tukey's HSD.*

Table 1.6. *1m and 2m soil organic carbon, iron, and aluminum stocks by climate zone and vegetation type.*

Stock	Climate Zone			Vegetation Type	
	Aw	Am	Af	Savannah	Forest
SOC Stocks (1m)	7.1 ± 1.9a	10.1 ± 5.7a	6.4 ± 1.1a	7.1 ± 1.7a	8.9 ± 5.5a
SOC stocks (2m)	11.7 ± 4.1a	15.7 ± 7.9a	10.2 ± 1.7a	11.7 ± 3.4a	13.7 ± 7.6a
Fe_t stocks (1m)	13.8 ± 3.4a	13.1 ± 6.8a	33.1 ± 16.3b	15.6 ± 5.7a	26.2 ± 19.0a
Fe_t stocks (2m)	29.4 ± 7.1a	28.2 ± 14.1a	71.6 ± 34.3b	33.1 ± 11.6a	57.5 ± 40.1b
Fe_d stocks (1m)	5.4 ± 1.2a	4.7 ± 2.8a	12.3 ± 6.7b	6.1 ± 2.3a	9.5 ± 7.6a
Fe_d stocks (2m)	11.3 ± 2.5a	10.1 ± 6.0a	26.3 ± 13.7b	12.7 ± 4.7a	20.5 ± 15.9a
Fe_o stocks (1m)	1.6 ± 0.7a	3.0 ± 1.0ab	3.8 ± 1.6b	2.8 ± 1.6a	2.9 ± 1.2a
Fe_o stocks (2m)	4.1 ± 1.6a	6.6 ± 2.2ab	7.9 ± 3.6b	6.5 ± 3.3a	6.0 ± 2.6a
Al_t stocks (1m)	47.2 ± 15.4a	58.7 ± 15.9a	72.7 ± 29.0a	54.5 ± 15.4a	67.4 ± 29.3a
Al_t stocks (2m)	112.2 ± 31.8a	141.7 ± 28.1ab	167.3 ± 55.8b	126.0 ± 32.0a	161.9 ± 52.8a
Al_d stocks (1m)	1.6 ± 0.2a	2.2 ± 0.7a	2.0 ± 0.7a	2.0 ± 0.6a	1.9 ± 0.7a
Al_d stocks (2m)	3.4 ± 0.5a	5.2 ± 1.2b	4.6 ± 1.4a	4.4 ± 1.3a	4.4 ± 1.3a
Al_o stocks (1m)	1.7 ± 0.6a	3.4 ± 1.7b	1.7 ± 1.0a	2.5 ± 1.3a	1.9 ± 1.6a
Al_o stocks (2m)	5.0 ± 2.3a	10.7 ± 6.4b	4.2 ± 2.5a	7.0 ± 3.3a	6.4 ± 6.9a

All numbers indicate the mean and standard deviation for each depth increment by climate zone.

**Different letters indicate statistically significant differences between climate zones ($p < 0.05$) following ANOVA using Tukey's HSD.*

Al_t = total aluminum, Fe_t = total iron, Al_o = ammonium oxalate extractable aluminum, Fe_o = ammonium oxalate extractable iron, Al_d = citrate-dithionite extractable aluminum, Fe_d = ammonium oxalate extractable iron.

Table 1.7. *Average and standard deviation of soil properties by depth increment between vegetation types.*

Depth (cm)	0-10	10-20	20-50	50-100	100-200	0-10	10-20	20-50	50-100	100-200
SOC	2.42±3.79 -	0.99±0.66 -	0.70±0.53 -	0.47±0.41 -	0.34±0.20 -	0.73±0.10 -	0.69±0.10 -	0.56±0.13 -	0.42±0.17 -	0.32±0.13 -
pH	3.81±0.27 A	3.92±0.16 A	4.10±0.20 A	4.37±0.30 A	4.52±0.41 A	4.31±0.13 B	4.33±0.12 B	4.42±0.12 B	4.64±0.32 B	4.96±0.25 B
Al_t	3.12±1.66 -	3.77±2.25 -	4.77±2.55 -	5.92±2.45 -	7.06±1.98 A	3.21±0.82 -	3.30±0.84 -	3.77±1.08 -	4.31±1.40 -	5.16±1.20 B
Fe_t	1.41±1.00 -	1.58±1.28 -	1.91±1.56 -	2.15±1.61 A	2.28±1.58 A	1.01±0.31 -	1.02±0.30 -	1.12±0.40 -	1.18±0.45 B	1.28±0.42 B
Al_o	657.65 ±460.63 A	953.34 ±1426.08 -	1120.94±1 507.47 -	1715.83±14 98.54 -	3090.05±43 01.12 -	1449.16±5 42.98 B	1452.54±5 36.72 -	1545.46±57 3.78 -	2190.07±1448. 15 -	3017.03±1539.8 4 -
Fe_o	1643.10±8 71.79 -	1809.43±7 12.23 -	2115.01±8 52.24 -	2390.48±12 25.23 -	2315.46±11 13.91 -	1627.14±9 44.86 -	1629.15±9 40.63 -	1780±1043. 95 -	2416.95±1443. 11 -	2617.18±1243.4 9 -
Al_d	817.88±55 8.01 A	1034.28±8 34.45 -	1226.43±7 69.28 -	1687.52±60 5.24 -	1883.72±55 7.03 -	1274.58±3 03.43 B	1311.83±2 84.34 -	1364.40±28 7.87 -	1572.77±614.1 7 -	1696.39±529.11 -
Fe_d	5762.45±4 960.99 -	6167.47±5 166.17 -	7454.87±5 842.97 -	8107.29±60 46.44 -	8677.69±17 26.37 -	3995.68±1 132.86 -	3898.86±1 077.74 -	4106.96±13 62.46 -	4735.27±1958. 91 -	4912.22±1726.3 7 -
Al_{ex}	1.32±0.89 -	1.20±0.93 -	1.03±0.37 -	0.91±0.30 A	0.71±0.29 A	1.09±0.22 -	1.06±0.23 -	0.87±0.25 -	0.58±0.23 B	0.44±0.27 B
Clay	9.86±7.24 A	9.88±7.12 A	10.48±808 3 -	11.67±9.70 A	11.82±10.19 -	4.82±2.08 B	5.13±2.45 B	5.40±2.20 -	5.44±2.68 B	5.82±2.82 -
Bray-P	18.91±22. 47 A	17.95±21. 36 A	19.97±23. 73-	22.51±22.34 -	17.36±17.60 -	58.56±50.0 6 B	55.57±49.1 1 B	45.74±38.28 -	36.18±29.61-	27.51±21.39-
VC	9.3±13.6 -	8.6±5.8 -	12.0±6.0 A	18.0±7.0 -	0.4±0.3 -	5.7±6.2 -	6.1±6.0 -	7.1±3.0 B	16.1±8.5 -	0.4±0.7 -

All numbers indicate the mean and standard deviation for each depth increment by climate zone.

**Different capital letters indicate statistically significant differences between climate zones ($p < 0.05$) following ANOVA using Tukey's HSD. Depth increments within a variable that have dashes indicate no significant differences between vegetation types ($p > 0.05$) following ANOVA using Tukey's HSD.*

Table 1.8. *Family level classification of investigated pedons in DRC.*

Climate	Site	Vegetation	Land-use	Soil Classification
Tropical Rain Forest (Af)	Lomela – Mukumari (LM)	Forest	Cultivated	Typic Kandiudult, Fine-loamy, kaolinitic, acid, iso-hyperthermic (LM2)
				Typic Acrudox, Fine-loamy-kaolinitic-acid-isohyperthermic (LM3)
			Uncultivated	Typic Kandiudult, Sandy-kaolinitic-acid-iso-hyperthermic (LM1)
				Typic Kandiudult, Fine-loamy-kaolinitic-acid-iso-hyperthermic (LM4)
		Savanna	NA	NA
	Lomela-Ekomakoko (LE)	Forest	Cultivated	Udoxic Quartzipsamment, Acid-isohyperthermic-coated (LE1)
				Udoxic Quartzipsamment, Acid-isohyperthermic-coated (LE3)
			Uncultivated	Udoxic Quartzipsamment, Acid-isohyperthermic-coated (LE2)
				Psammentic Humudept, Siliceous-isohyperthermic (LE6)
				Typic Haplorthod, Sandy-kaolinitic-subactive-acid-isohyperthermic (LE7)
		Savanna	Uncultivated	Udoxic Quartzipsamment, Acid-isohyperthermic-coated (LE4)
				Psammentic Humudept, Siliceous-isohyperthermic (LE5)
Tropical Monsoon (Am)	Katako-Kiete (KK)	Forest	Cultivate	Psammentic Humudept, Siliceous-acid-isohyperthermic-coated (KK4)
			Uncultivated	Acrudoxic Kandiudult, Sandy-kaolinitic-acid-isohyperthermic (KK3)
		Savanna	Cultivated	Psammentic Humudept, Siliceous-acid-isohyperthermic-coated (KK1)
			Uncultivated	Psammentic Humudept, Siliceous -acid-isohyperthermic-coated (KK2)
	Katako-Ovungu (KO)	Forest	Cultivated	Oxic Dystrudept, Coarse-loamy- Siliceous-subactive-acid, isohyperthermic (KO4)
			Uncultivated	Cumulic Humaquept, sandy- Siliceous -subactive-acid-isohyperthermic (KO3)
		Savanna	Cultivated	Psammentic Humudept, Siliceous -acid-isohyperthermic-coated (KO1)
			Uncultivated	Psammentic Humudept, Siliceous -acid-isohyperthermic-coated (KO2)
Tropical Savanna (Aw)	Lubefu: Eshima-Ngandungandu (EN)	Forest	NA	NA
		Savanna	Cultivated	Typic Humustept, Sandy, Siliceous, Acid, Isohyperthermic (EN1)
				Typic Humustept, Sandy, Siliceous, Acid, Isohyperthermic (EN2)
				Typic Humustept, Sandy, Siliceous, Acid, Isohyperthermic (EN3)
				Typic Humustept, Sandy, Siliceous, Acid, Isohyperthermic (TU)
	Lubefu: Eshima-Maluanyi (EM)	Savanna	Uncultivated	Typic Humustept, Sandy, Siliceous, Acid, Isohyperthermic (EM1)
				Typic Humustept, Sandy, Siliceous, Acid, Isohyperthermic (EM2)
				Typic Humustept, Sandy, Siliceous, Acid, Isohyperthermic (EM3)

This page left intentionally blank

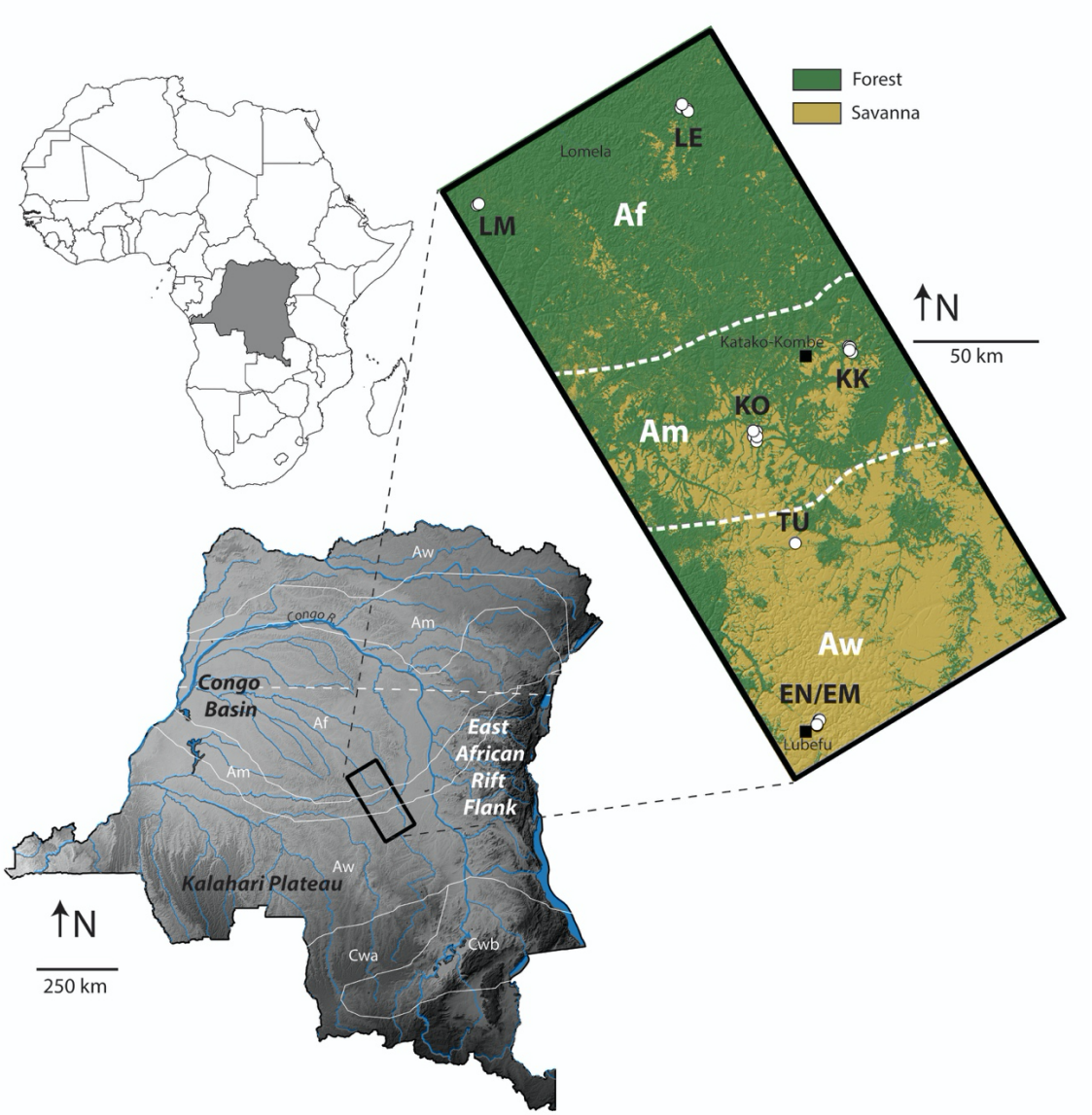

Figure 1.1. *Location of study area, location of site clusters and investigated soils in relation to the country boundaries of Democratic Republic of Congo (DRC), major geomorphic provinces, Köppen climate zones (Af – equatorial forest; Am – tropical monsoon; Aw – tropical savanna) and major vegetation types. LE = Lomela Ekomakoko, LM = Lomela Mukumari, KO = Katako Ovungu, KK = Katako Kiete, TU = Tshumbe, EN = Eshima Ngandungandu, EM = Eshima Maluanyi.*

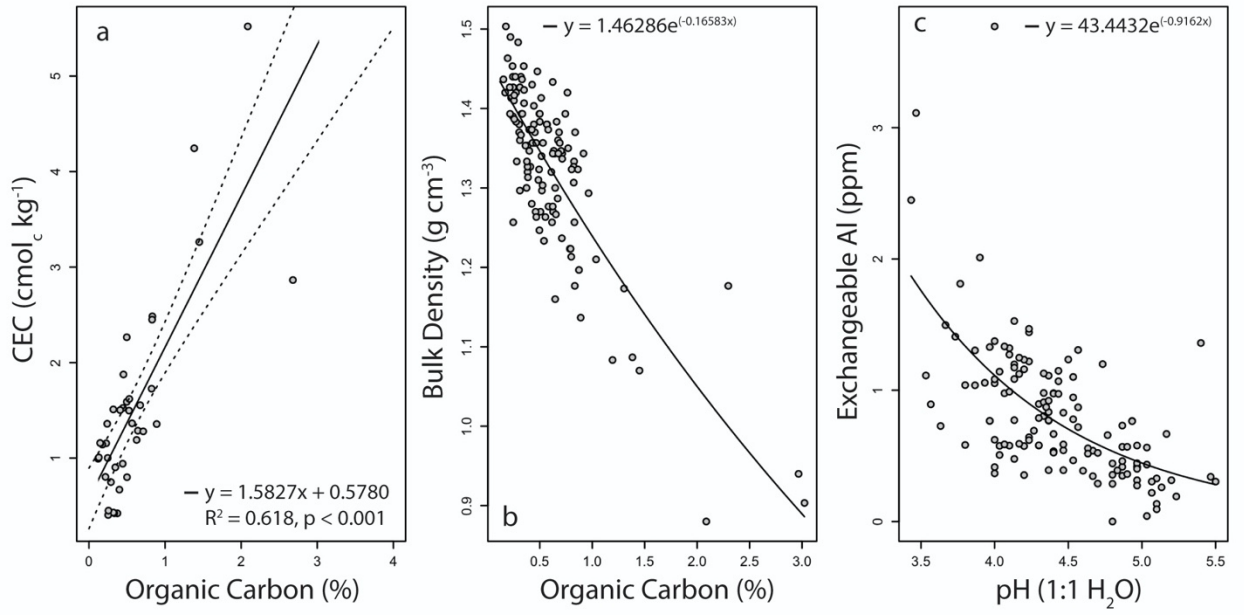

Figure 1.2. *Relationships between a) soil organic carbon and cation exchange capacity (CEC), b) soil organic carbon and bulk density, and c) pH and exchangeable Aluminum (Al_{ex}) across all samples. Note there are fewer data points displayed in panel a than in panels b and c because the number of samples analyzed for CEC was fewer (n = 40) than for bulk density (n = 124) and organic carbon (n = 149) and exchangeable aluminum (n = 147) and pH (n = 143). The dashed lines in panel (a) represent the 95% confidence interval around the slope of the regression line. R^2 is not displayed on panels b and c because the lines shown represent non-linear regressions, for which R^2 is not meaningful in comparison.*

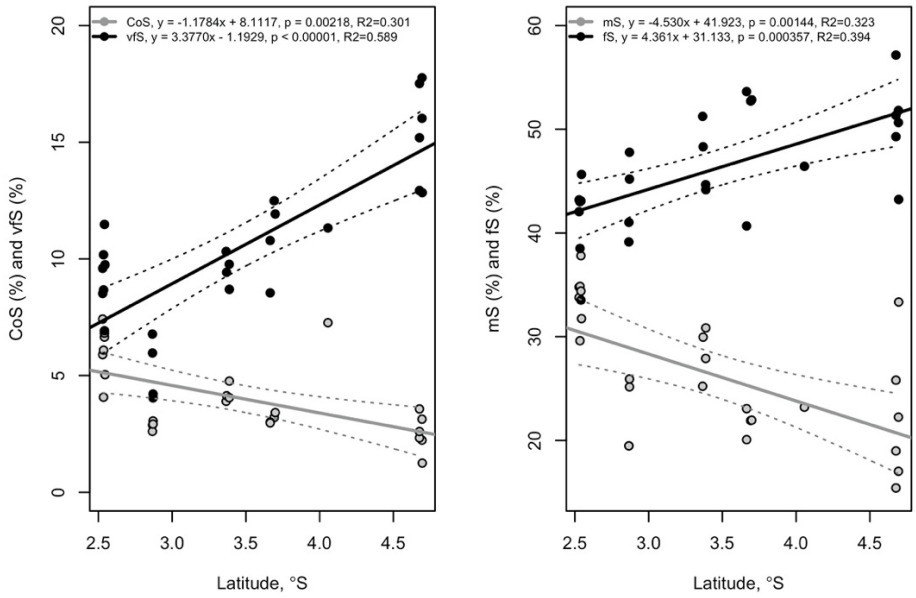

Figure 1.3. *Relationship of a) coarse sand and very fine sand and b) medium and fine sand fractions with latitude across the Sankuru transect. Dotted lines represent the 95% confidence interval around the slope of the regression lines.*

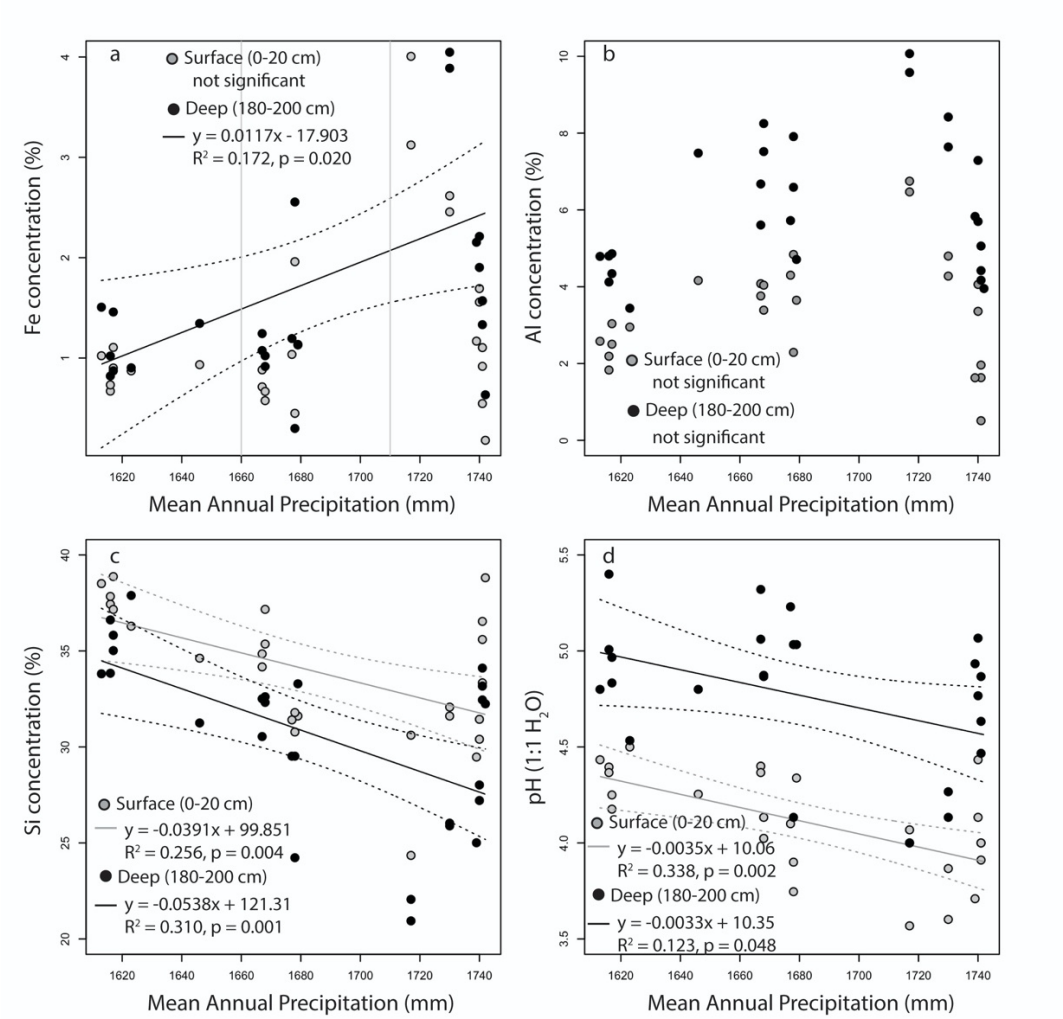

Figure 1.4. *Relationship of surface (0-20cm) and deep (180-200cm) a) total iron (Fe_t), total aluminum (Al_t), c) total Si, and pH with mean annual precipitation (mm yr^{-1}) across the Sankuru transect. Dotted lines represent the 95% confidence interval around the slope of the regression lines.*

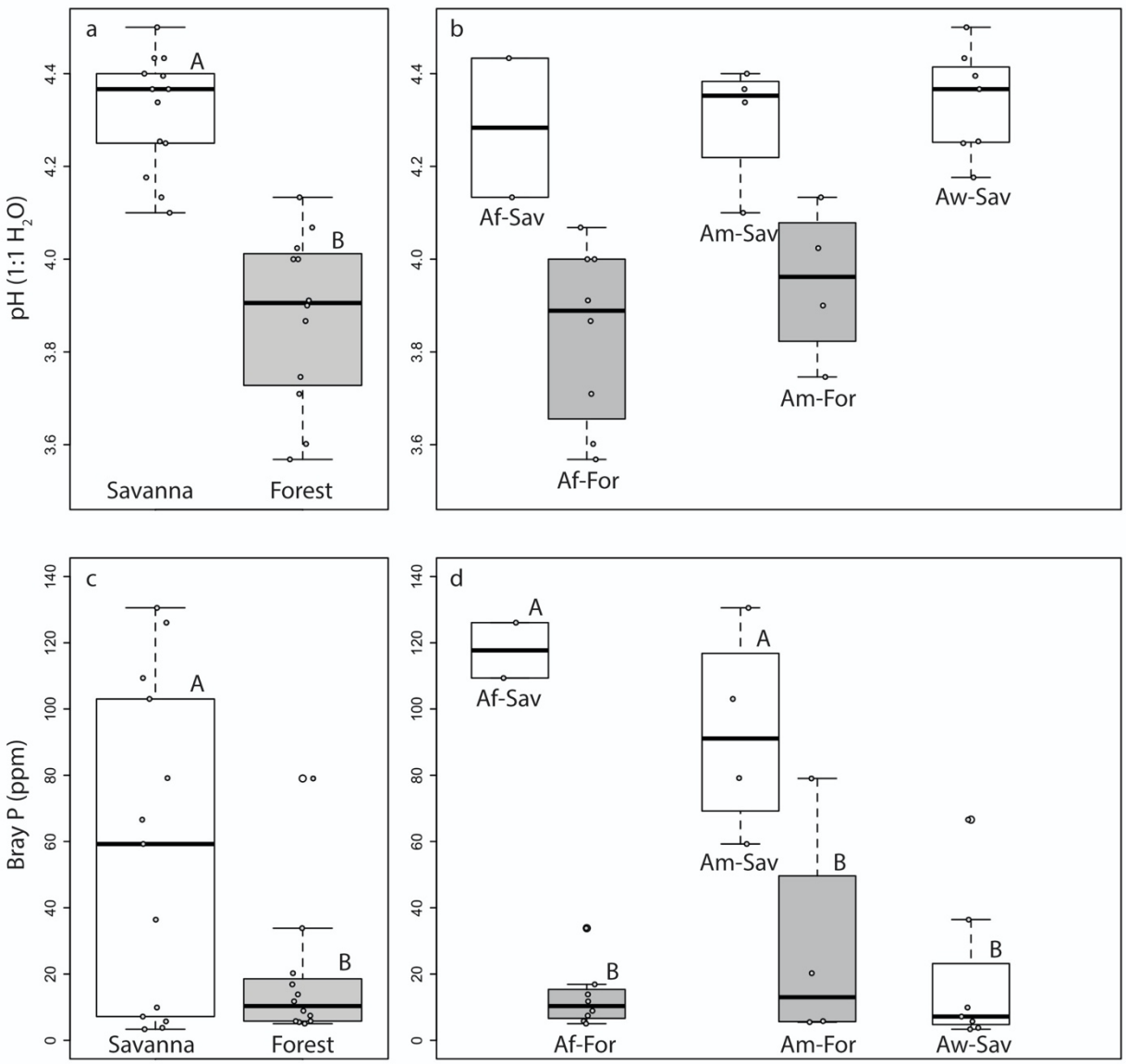

Figure 1.5. *Boxplots of surface (0-20cm) pH and Bray P by vegetation type (a, c) and vegetation type within Köppen climate zones (b, d) across the Sankuru transect. Af-Sav and Af-For represent savanna and forest vegetation in the Af climate zone, respectively, Am-Sav and Am-For represent savanna and forest vegetation in the Am climate zone, respectively, and Aw-Sav represents savanna vegetation in the Aw climate zone.*

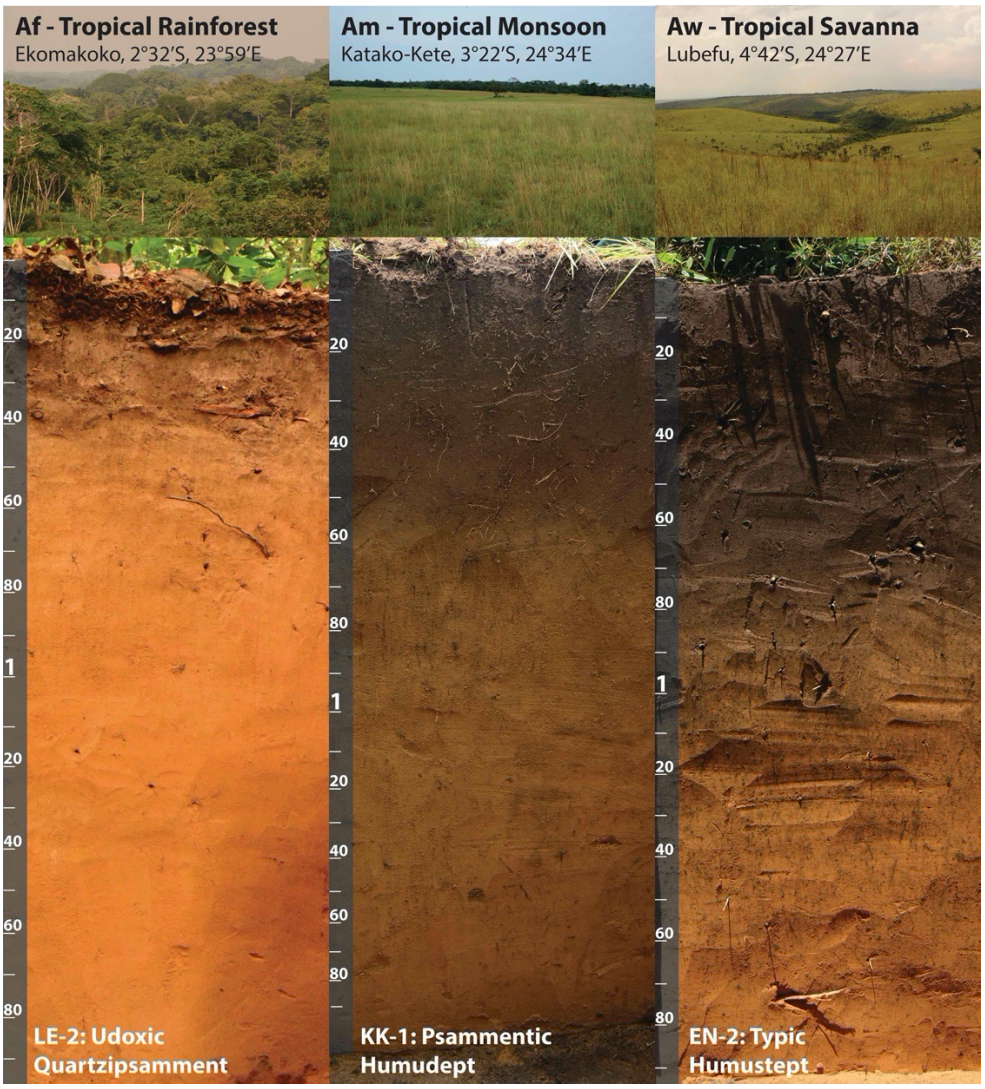

Figure 1.6. *Representative landscapes, vegetation, soils, and soil classification across the Sankuru transect.*

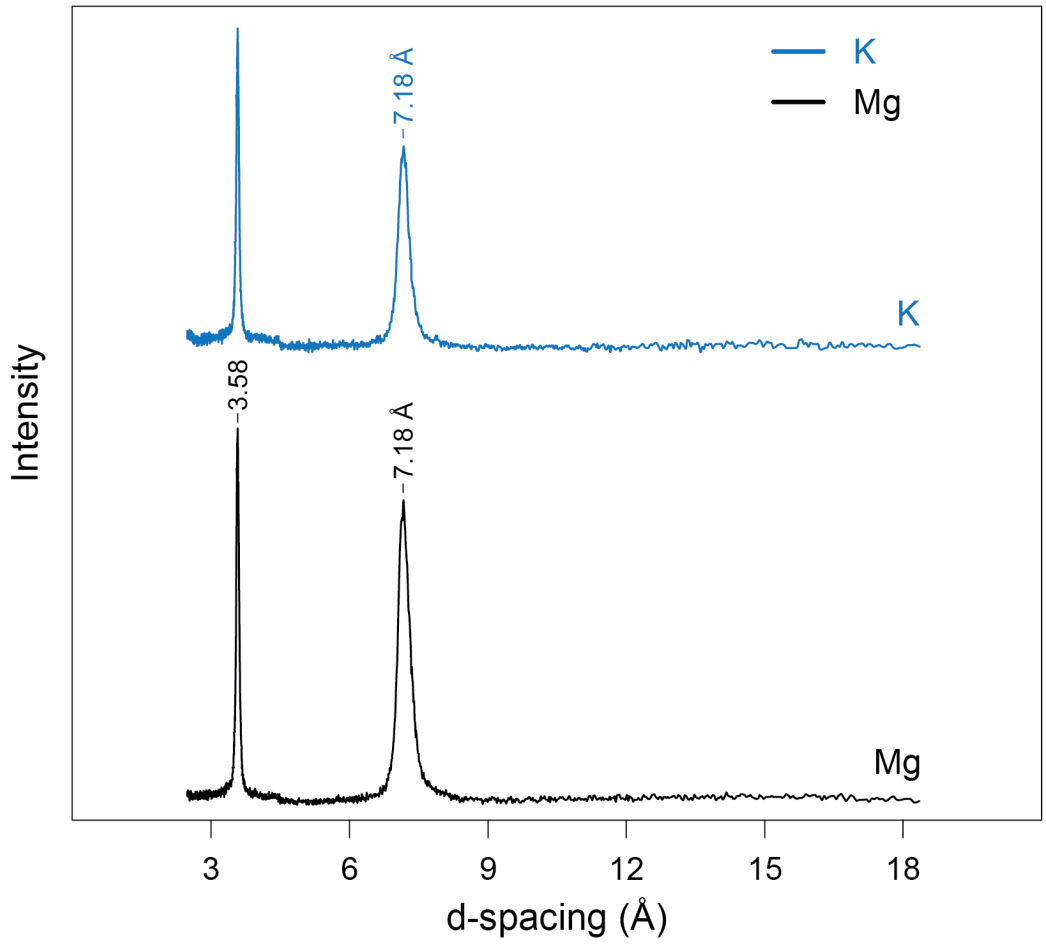

Supplementary Figure 1.S1. *X-ray powder diffraction spectra plotted from 5° to 36° 2θ (Cu–Kα radiation, λ = 1.54059 Å) for the <2–μm sized fraction of sample KO-4BTM. The x-axis is plotted as d-spacing (Angstroms, Å) rather than 2θ (Cu–Kα) for visualization purposes. Treatment types (Mg– and K–saturated) are listed on the right (legend top right). Kaolinite (~7.15 Å and ~3.58 Å) is the only clay (<2μm) phase present.*

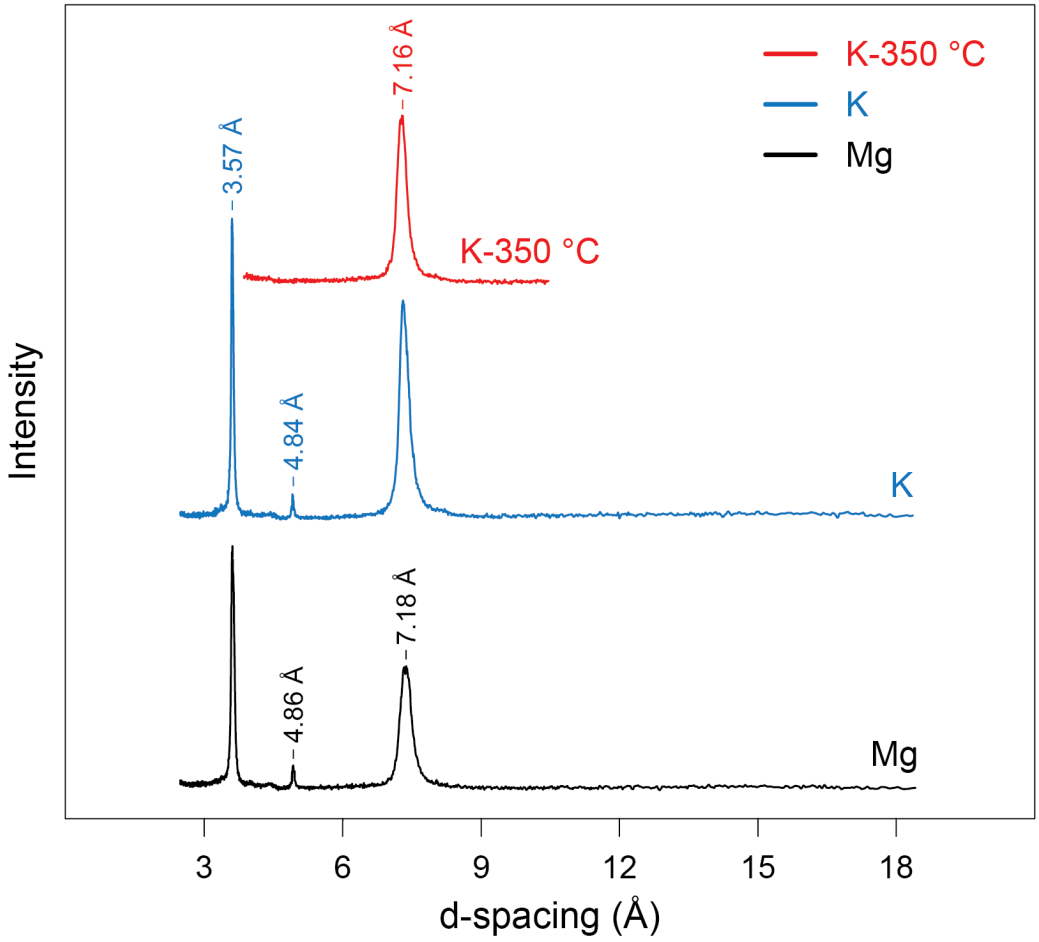

Supplementary Figure 1.S2. *X-ray powder diffraction spectra plotted from 5° to 36° 2θ (Cu–Kα radiation, λ = 1.54059 Å) for the <2μm sized fraction of sample LE 5-4: The K–350 °C spectra (top) only spans from 10° to 27° 2θ. The x-axis is plotted as d-spacing (Angstroms) rather than 2θ (Cu–Kα) for visualization purposes. Treatment types (Mg–, K–saturated, and K–350 °C) are listed on the right (legend top right). Kaolinite (~7.15 Å, ~3.58 Å) and gibbsite (~4.85 Å, ~4.37 Å peak not visible) are the two clay phases present. Note the collapse of the ~4.85 Å gibbsite (α–Al(OH)₃) peak in the K–350 °C scan (red line, top spectra).*

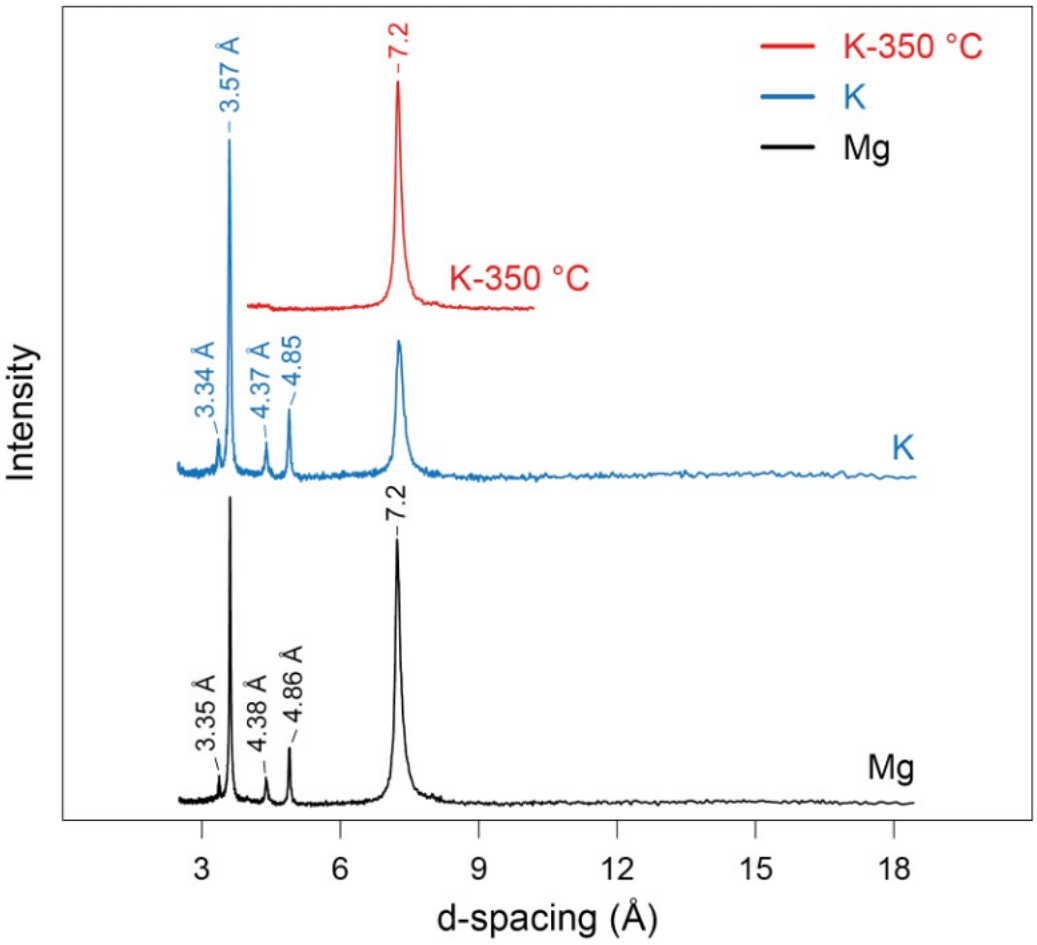

Supplementary Figure 1.S3. *X-ray powder diffraction spectra plotted from 5° to 36° 2θ (Cu–Kα radiation, λ = 1.54059 Å) for the <2μm sized fraction of sample EM-2 BTM: the K–350 °C spectra (top) only spans from 10° to 27° 2θ. The x-axis is plotted as d-spacing (Angstroms) rather than 2θ (Cu–Kα) for visualization purposes. Treatment types (Mg–, K–saturated, and K–350 °C) are listed on the right (legend top right). Kaolinite (~7.15 Å, ~3.58 Å), gibbsite (~4.85 Å, ~4.37 Å), and quartz (~3.34 Å) are the clay (<2–μm) phases present. Note the collapse of the ~4.85 Å and ~4.37 Å gibbsite peaks in the K–350 °C scan (red line, top).*

CHAPTER 2

Stable carbon isotope (^{13}C) and magnetic susceptibility provide evidence of past vegetation change and the response of iron minerals to climate variability in central Democratic Republic of Congo (DRC)

2.1 Introduction

Soil records offer a unique opportunity to untangling complex environmental histories of vegetation and climatic changes to improve understanding the effects of long-term climatic vagaries on ecosystems (Schaetzl and Anderson, 2005). Particularly in central Africa, where climatic and vegetation transitions are sharp and available evidence in the literature is sparse (Schwartz et al., 1996), understanding paleo-environmental change is important for predicting future changes (Willis et al., 2013). Soil ^{13}C isotope values ($\delta^{13}C$) and the magnetic properties of soil iron (oxy)hydroxides minerals, are pedo-signature proxy variables useful for understanding the impacts of complicated paleo-environmental histories driven by shifting vegetation and climatically influenced weathering intensities (Verosub et al., 1993, Maher and Thompson, 1995, Reynolds and King, 1995, Maher, 1998, Bokhorst et al., 2009, Balsam et al., 2011, Maxbauer et al., 2016, Maxbauer et al., 2017). Importantly, these signatures tend to record environmental change over different timescales. While vegetation histories on the order of decades to millennia may be captured by changes in the ^{13}C of soil organic carbon, the magnetic properties of iron oxyhydroxides (and their speciation) may record climatic and paleo-precipitation change on the order of millennia to tens of millennia (Long et al, 2016, Maxbauer et al., 2016) in well drained soils, and are highly sensitive (changing on the order of years) to changes in soil moisture states or accompanying redox conditions (Hall et al., 2013). Although these indicators have been explored across climatic and vegetation gradients in temperate ecosystems and in West Africa (Schwartz et al., 1996, Bekele et al., 2003, Bekele et al., 2006, Sugihara et al., 2014), little data is available to place context on our understanding of Holocene vegetative and climatic change in central Africa and the Congo Basin in particular (Bremond et al., 2017). The Congo River basin is the second largest river basin in the world (after the Amazon Basin) and has experienced dramatic climatic swings from the early Miocene (23 Ma) to Holocene (Zachos et al., 2001, Hoag and Svenning, 2017).

The ratio of stable carbon (C) isotopes ^{13}C to ^{12}C ($\delta^{13}C$) can be used as a proxy for the turnover of soil organic carbon (SOC) between C_3 and C_4 vegetation (Camino-Serrano et al., 2019) and is widely applied for paleo-ecosystem reconstruction. In Amazonia, for example, $\delta^{13}C$ values of soil organic carbon has been instrumental in identifying vegetative

changes throughout the Holocene (Pessenda et al., 1996, Pessenda et al., 2004). In a chronosequence assessment of the impact of 101-year land use change from Amazon Forest to pasture, 85% of forest-derived (largely C_3) SOC at 0-10 cm depth disappeared within the first 25 years of the conversion to a C_4 pasture grass but the remaining forest-derived SOC fraction persisted for the remainder of the century (Durrer et al., 2021). In other studies, $\delta^{13}C$ analysis revealed the predominance of C_4 and CAM (crassulacean acid metabolism, a typical carbon fixation mechanism for crassulacean (succulent) plant family) plants by comparing ^{13}C content in phytolith and soil organic matter (SOM) (Tapia and Adriano-Morán, 2012), or vegetation changes from C_4-dominated to C_3-dominated plant communities across hillslopes (Biedenbendera et al., 2004). Wittmer et al. (2010) used $\delta^{13}C$ and C_3/C_4 ratio to trace grass distribution under high altitude and arid ecosystem in Mongolia and their impact on biomass production, SOC storage, water use, and nutrient cycling.

The objectives of this study were to 1) examine the variability of soil magnetic properties across a gradient from forest to savanna in central DRC, as this information can help inform the relationship between climate, weathering intensity, and secondary or pedogenic iron minerals, which can serve as a record of climatic transitions, and 2) to determine the vegetation histories in the forest-savanna transition zone in central DRC by utilizing $\delta^{13}C$ values of SOC as a record of historic vegetation change.

2.2. Methods

2.2.1. Study Area and Background

Field work was completed in two phases from August 2015 to January 2016 and June to August 2017 in Sankuru Province, central Democratic Republic of Congo (DRC) (Figure 1.1), across a transect along a steep (~250km) climate gradient from tropical rainforest (Köppen: Af) in the north, through tropical monsoon (Köppen: Am) to tropical wet savanna (Köppen: Aw) in the south (Peel et al. 2007) (Figure 1.1). The area is occupied by the Tetela tribe. Mean annual precipitation (MAP) in the study area varies between 1613 mm in the south of the transect (near Lubefu) to 1742 mm in the north near Ekomakoko, however this data is known to be uncertain in central DRC because there is a lack of long-term data from the region (Fick and Hijmans, 2017, Figure 1.1). However, given the need

to draw on a continuous dataset to provide estimates of MAP across the transect, we relied on the best available continuous data (Africlim 3.0, Fick and Hijmans, 2017) despite the uncertainty. Importantly, although MAP varies by only ~130 mm across the transect, the seasonality of precipitation is strikingly different from south to north (Herrmann and Mohr, 2011, Munzimi et al., 2015). In the north (Af), there is no seasonality to the precipitation regime, while the Am is characterized by a single, bimodal wet season (longer wet season, bimodal), and sites in the Aw experience a shorter, unimodal wet season (Herrmann and Mohr, 2011, Munzimi et al., 2015). Additionally, this transect lies across the Udic-Ustic soil moisture regime (SMR) transition zone in central DRC, with sites in Af and Am under a Udic SMR and sites in Aw in an Ustic SMR (Soil Survey Staff, 2007, Soil Survey Staff, 2014b). Along this gradient, six site clusters were established in Lomela (under Af) at Mukumari (2.92°S; 23.48°E) and Ekomakoko (2.70°S, 24.16°E), in Katako-Kombe (under Am) at Kiete (3.62°S, 24.57°E) and Ovungu (3.82°S, 24.39°E), and in Lubefu (under Aw) at Tshumbe (4.15°S; 24.59°E), Eshima Ngandungandu/Maluanyi (4.88°S, 24.56°E (Figure 1.1). The choice of these site clusters was driven by the steep climatic and vegetation gradient, accessibility, and lack of local soil related data in the area.

Vegetation in Sankuru province is largely distributed as forest in the north and savanna in the south and southeast, reflecting the climate gradient from Af to Aw (Figure 1.1). The tropical rainforest in the north is also synonymously termed equatorial forest or broadleaf evergreen forest (Sanchez, 2019) with at least a two-strata canopy, highly diversified tree species, and few to no herbaceous species on the floor. Savanna vegetation is of the "tall grass-low tree" type, a mix of *Hyparrhenia* sp., *Imperata* sp. and other grasses, and low, scattered trees. The precipitation range across this transect (1613 to 1742 mm/yr) is in the range where alternation between stable states of forest and savanna is predicted on the African continent (Hirota et al., 2011). On a local scale in equatorial forest, isolated savanna vegetation can occur within a matrix of forest (Markham and Babbedge, 1979, Lehmann et al., 2011). These isolated savannas may be driven by interactions among soil and disturbance factors, and provide an opportunity to separately evaluate the impacts of both climate and vegetation on soil properties across this ecotone (Bowman and Perry, 2017).

Soils across the study transect are predominantly sandy (87%), with some loamy-fine sands in the south and sandy-clay loam textures in the north of the transect. Parent materials for Sankuru soils derive from the sand sheets of the Salonga and Yangambi groups (Beernaert, 1999), which are underlain by consolidated and unconsolidated materials of the Kalahari Group that covers most of the Congo Basin (Linol et al., 2015). The Salonga formation has also been synonymously termed the “Plateau sands" and is likely of early- (on the outer, upper plateau steps of the Congo basin) to late-Pleistocene (on the lower, inner plateau steps) age (Beernaert, 1999, Senut et al., 2009). The exact origins of this sand sheet appear to be complex, and it has previously been characterized as of mixed fluvial and eolian origins (Beernaert, 1999, Baert et al., 2009, Senut et al., 2009, Baert et al., 2013, Guillocheau et al., 2015). Soil organic carbon values are relatively low, decreasing on average within the top 50 cm from 1.2 % in forested sites in Af to 0.6 % under savanna in Aw (Table 1.7). Soils are strongly acidic (pH < 5) and the 50 cm average soil pH decreases from Aw (pH 4.4) to Am (pH 4.2) and Af (pH 4.0). Base saturation values are very low (< 5.5 %), with sub-active cation-exchange activity class (CEC / % clay < 0.24) (USDA, 2014). X-Ray Diffraction (XRD) studies revealed no trace of 2:1 phyllosilicate in the colloidal fraction. Instead, kaolinite (1:1 clay type), gibbsite, and free Al and Fe, which indicates advanced soil weathering states across the transect.

A total of 130 horizons from 26 soil profiles were sampled across the transect (Figure 1.1) and triplicate samples were collected from each genetic horizon using the soil core method for bulk density measurement: a sliding hammer carefully drives a metallic cylinder sampler into the soil to minimize structure disturbance of the mineral soil samples, which is imperative for accurate soil bulk density evaluation. Samples were weighed immediately in the field then bagged before air-drying. The samples were oven-dried for 24 h at 105°C, weighed, and sieved to separate the fine earth (< 2 mm) from coarse fragments (> 2 mm). The fine earth fraction (< 2 mm) was utilized for chemical and physical characterizations.

2.2.2. Iron concentrations

The total elemental concentrations of Fe were quantified by X-Ray Fluorescence (XRF), using an Olympus Delta P4000EX portable XRF (p-XRF) instrument (Olympus, Inc)

which is equipped with a silicon drift detector (SDD), that has a resolution better than 155 eV in practice. During analysis, the instrument was mounted in a Innov-X System Stand for stability and operated remotely through a computer console. We operated the instrument in the "mining" mode, which uses the fundamental parameters (FP) approach to correct the measured X-rays for a variety of physical phenomena (e.g., absorption and fluorescence, attenuation from incoherent scattering and the photoelectric effect, differences in characteristic X-ray intensities). Measuring the elements of interest used three proprietary, built-in X-ray filters (main – tube voltage of 40kV, tube current of 50 μA; low -20kV and 100 μA; and light 6kV and 200 μA). Analytical times were 20 s for both the "main" and "low" X-ray filters and 80 s for the "light" mode. Consequently, the total analytical time was 120 s for each individual measurement.

In addition to measurements of total iron (Fe_t), "free" or pedogenic Fe (Fe_d) was extracted by selective dissolution using Dithionite-Citrate solution (Jackson et al., 1986, Soil Survey Staff, 2014a). Briefly, 0.4 g of sodium dithionite (a reducing agent) and 25 ml of 0.57 M sodium citrate is added to 0.75 g of < 2 mm soil material and shaken overnight. The solution is subsequently centrifuged and an aliquot is removed for analysis of Fe by ICP-OES (Soil Survey Staff, 2014a). A subset of this pedogenic Fe, amorphous "active" Fe (Fe_o), was selectively extracted with 0.2 M ammonium oxalate buffered to pH 3.0 in a mechanical vacuum extractor under darkness over a period of 12 h (Soil Survey Staff, 2014a).

2.2.3 Magnetic Analysis

Magnetic analysis of soil samples was conducted at the Institute of Rock Magnetism (IRM) laboratory at the University of Minnesota Twin cities campus. Soil samples weighing about 2.5 g each were compressed into small diamagnetic plastic cups, and individually analyzed for 15 minutes each using a Princeton Measurements Corporation Micromag vibrating sample magnetometer (VSM), TVSM and IVSM models, at room temperature in fields up to 1Tesla (T). VSM generates hysteresis loops and backfield remanence curves which portray the sample's magnetization variation and provide indirect evidence of predominant magnetic mineral species. Saturation magnetization (M_s), saturation remanent magnetization (M_{rs}) equivalent to saturation

isothermal remanent magnetization (SIRM), coercivity (B_c), and coercivity of remanence (B_{cr}) are all derived from observed hysteresis loops and backfield measurements.

The magnetization energy conveys information about the particle magnetic domain behavior, grain size, and nature captured by the remanent magnetization (M_r) and saturation magnetization (M_s) ratio. M_r is also a reflection of anisotropy energy quantified by microscopic coercivity (B_{cr}) and bulk coercivity (B_c). The magnetization ratio (M_r/M_s) and coercivity ratio (B_{cr}/B_c) provide a snapshot view of the assemblage magnetic state. Under a shifting external magnetic field, an induced magnetization can be plotted as a hysteresis loop (a memory curve of applied field) characterized by magnetization saturation (M_s), remanence (M_r), bulk coercivity (H_c), and S-ratio (Butler, 2004; Tauxe, 2008, Maxbauer et al., 2016). The hysteresis loop illustrates the magnetic retentivity which is enabled by the magnetic anisotropy energy barrier (Darby and Isaac, 1974, Butler, 2004, Tauxe, 2008). The saturation magnetization is stronger in magnetite (Fe_3O_4) (92 Am^2/kg) and maghemite (Υ-Fe_2O_3) (74 Am^2/kg) than in hematite (α- Fe_2O_3) (0.4 Am^2/kg) and goethite (α-FeOOH) (1 Am^2/kg) (Tauxe et al., 2008, Jiang et al., 2014).

The remanence is held by magnetic minerals between 100 mT and 1 T of the backfield, and is referred to as the "hard" IRM (HIRM), where HIRM = 0.5 x (SIRM + IRM_{-300mT}). The S-Ratio parameter can be used to determine the proportion of the soft magnetic minerals (e.g., magnetite/maghemite) relative to the hard magnetic minerals (i.e., hematite/goethite) in the soil sample (Stober and Thompson, 1979). Mathematically, it is computed as follows:

S-Ratio = $\frac{SIRM-IRM}{2SIRM}$ where SIRM is the saturation isothermal remanent magnetization and IRM is the isothermal remanent magnetization at -300mT (Maxbauer et al., 2016).

Magnetism derives from the magnetic dipole moment associated with electronic orbitals and 3d unpaired spins angular momentum (Butler, 1992, Tauxe et al., 2008). In reaction to the application of an external magnetic field, the electronic magnetic moment generates three different types of induced magnetization (diamagnetism, paramagnetism, and ferromagnetism), contingent upon the chemical nature of the material being magnetized (Butler, 1992, Tauxe et al., 2008). Induced magnetization (M_i), a function of the material susceptibility (χ) and the applied magnetic field (H), will oppose or align with

the applied magnetic field (i.e., negative or positive): $M_i = \chi H$ (Tauxe et al., 2008). Diamagnetism is generated by the reaction of the electronic orbital magnetic moments to the applied external magnetic field (H), resulting in a weak induced magnetization (M_i). The common diamagnetic minerals are quartz (SiO_2) and carbonate ($CaCO_3$) due to the lack of the unpaired spins as all subshell orbitals are saturated (Tauxe et al., 2008). The inexistence of unpaired spins and the mutual offset of paired electrons moments lead to these minerals' zero net magnetic moment. Diamagnetic susceptibility, $\chi_d = M_i/H$, is negative (M_i opposing H) and very small because M_i is weak. For example, Quartz's χ_d is -0.62×10^{-9} (Tauxe, 2008). Paramagnetism (Tauxe, 2008) emerges from non-diamagnetic minerals such as the phyllosilicates biotite and smectite, where unpaired electronic spins develop a conditional magnetization; i.e., there is a net magnetization (M_i) only under external magnetic field (H) or exchange interactions. If there is no H, no M_i because, in the absence of these conditions (and consistent with Langevin theory), thermal agitation randomizes the magnetic moments orientations and results in a zero-net magnetization. The magnetic moments of these spins are temperature sensitive; their alignment requires low temperature (Curie Law) and strong magnetic field to overcome the antagonistic effect of temperature and magnetic field. The ratio of M_i/H defines paramagnetic susceptibility (χ_p) whose magnitude is positively proportional to Mi ($\chi_p = M_i/H$).

Ferromagnetism rises from ferromagnetic minerals such as magnetite (Fe_3O_4), maghemite (Υ-Fe_2O_3)/hematite (α-Fe_2O_3). Ferromagnetization is the spontaneous exchange energy between unpaired 3d spins of adjacent atoms through a direct overlap or an oxygen bridge (Tauxe, 2008, Naseem et al., 2018). This exchange interaction (coupling) establishes a permanent magnetization with a density energy as high as 1000Tesla (Tauxe, 2008). In addition to the immense magnetic energy density potential, unlike paramagnetic and diamagnetic materials, ferromagnetic minerals can conserve paleomagnetism on the order of millions to billions of years, and thus act as a critical record of the paleo-environment (Tauxe, 2008). Ferromagnetic mineral grains can naturally harbor superparamagnetic (SP), stable single domain (SSD), or multi domain (MD) components, depending on, among other factors, the density of the saturation magnetization energy (M_s) which delineates the grain size threshold between single domain and multidomain (Butler, 2004). Lower Ms energy leads to larger grain size threshold; for example, a hematite grain

with 2 Am^{-1} magnetization energy, remains SD up to 15μm threshold grain size, above which MD structure can materialize. For magnetite, this grain size threshold between SD and MD would be down to 50nm due to the mineral's higher M_s energy (Butler, 2004). The stable single domain magnetite carries more effectively the natural remanent magnetization (NRM) (Butler and Banerjee, 1975) owing to its interaction energy and the magnetic anisotropy energy (from magneto-crystalline, shape anisotropy, and stress anisotropy) which gauges the microscopic coercivity (Butler, 2004, Tauxe et al. 2008). However, in the absence of the applied magnetic field, the magnetic stability of the magnetic single domain (SSD) may become perilous under the continuous thermal agitation during the relaxation time (τ) (the time necessary for the remanence magnetization, under zero external field, to decay to 1/e of its initial magnetization) (in congruity with the Néel theory) (Tauxe et al., 2008, Gehring et al., 2009, Maxbauer et al., 2016).

Unlike diamagnetism and paramagnetism, ferromagnetism is the most consequential form of magnetism in paleo-environmental analysis due to the pedogenic origin of the magnetic minerals (Maxbauer et al., 2017). Soil magnetic susceptibility enhancement depends on the ultrafine grained (< 30nm) ferromagnetic minerals concentration (< 0.1 %) (Mullins, 1977) and grain saturation magnetization all of which result essentially, directly or indirectly, from pedogenic processes which are sometimes intensified under hot and humid climate (Verosub et al., 1993, Maher and Thompson, 1995). Laterization and latosolization processes can enable Fe mobility and precipitation (Ghosh and Guchhait, 2020) which, ultimately, raise magnetic susceptibility ensuant to magnetite (Fe_3O_4) and maghemite (γ-Fe_2O_3) accumulation (Mullins, 1977, Maher, 1998). Ferromagnetic (e.g., Fe_3O_4) and ferrimagnetic (e.g., γ-Fe_2O_3) minerals are generated by soil redox cycles consequent to waterlogging and good drainage sequences (Mullins, 1977, Maher, 1998). These cycles drive post depositional ferro-material weathering, ferrous ions translocation, and ferric ions illuviation resulting in the formation of the ultra-fine (< 30 nm) and fine (30-75 μm) magnetite and maghemite grains for soil magnetic susceptibility enhancement (Mullins, 1977, Maxbauer et al., 2016).

Ultrafine-grained magnetite is produced inorganically (Taylor et al. 1987, Maher and Taylor, 1988, Maher, 1991) and biogenically (Blakemore, 1982, Konhauser, 1997).

The authigenic inorganic process involves the adsorption of Fe^{+2} on lepidocrocite (γ-FeOOH), goethite (α-FeOOH), or hematite (α-Fe_2O_3) to enable contemporaneous authigenic magnetite (Fe_3O_4 or "$FeOFe_2O_3$"): $Fe^{+2} + 2\gamma FeOOH \rightarrow Fe_3O_4 + 2H^+$ above pH 7.3 at 25 °C (Tamaura et al., 1983). The Fe^{+2} cation derives from either the pH related metal (Fe^{+3}, Al^{+3}) hydrolysis process (Essington, 2015) or chelation process (Van Hees et al., 2000). The magnetite biomineralization process takes place inside the microaerophilic magnetotactic bacteria through the reduction process of 30 % of the ferric ions in the ferrihydrite ($5Fe_2O_3.9H_2O$) to ferrous ions (Blakemore, 1982, Maher, 1991). The resulting aggregate (Fe^{+2}, Fe^{+3}) that makes up magnetite, the main component of intracellular magnetosomes (Blakemore, 1982, Konhauser, 1997), will be exposed to the sediments after cellular lysis (Moskowitz et al., 1989). Biogenic magnetite occurs also in anaerobic conditions where bacteria, e.g., GS-15, Geobacter metalloreducens (Lovley et al., 1987), generate extracellular ultrafine-grained magnetite (a dissimilatory process as opposed to intracellular process with magnetotactic) by using amorphous ferric oxides as electron sink during respiration process (Lovley et al., 1987).

2.2.4 Carbon-13 Analysis

Samples from all described horizons were sent to the University of California (UC-Davis) Stable Isotope Facility (ISF) Laboratory for isotope carbon-13 analysis. Individual mineral sample weight ranged from 5.91 mg to 74.997 mg and organic samples from 1.903 mg to 2.995 mg depending on the concentration of carbon and nitrogen in the sample (smaller sample for higher carbon content). Samples were enclosed in micro tin capsules, weighed in micro-balance, and loaded in a 96-well tray for shipment. At the UC-Davis SIF, soil samples were analyzed for ^{13}C using an Elementar Vario EL Cube or Micro Cube elemental analyzer (Elementar Analysensysteme GmbH, Hanau, Germany) interfaced to either an Isoprime VisION IRMS (Elementar UK Ltd, Cheadle, UK) or a PDZ Europa 20-20 isotope ratio mass spectrometer (Sercon Ltd., Cheshire, UK). Samples were combusted at 1080°C in a reactor packed with chromium oxide and silvered copper oxide. Following combustion, oxides were removed in a reduction reactor (reduced copper at 650°C). The final delta ^{13}C values, reported here, are expressed relative to international standards VPDB (Vienna Pee Dee Belemnite). (https://stableisotopefacility.ucdavis.edu/13cand15n.html).

Due to its low abundance relative to ^{12}C, the stable carbon isotope ^{13}C, in organic tissue, is used by ecologists to define carbon flow paths in the trophic chain and identify biomass carbon origin (Rounick and Winterbourn, 1986, O'Leary, 1988, Müldner, 2019). It has also enabled soil scientists to determine the source of carbon in the soil organic matter and connect it to the paleo-ecosystem (Schwartz et al., 1986). The isotope ^{13}C content estimate in organic matter, $\delta\,^{13}C$ (‰), derives from $^{13}CO_2$ / $^{12}CO_2$ ratios comparison between the sample and standard CO_2 content as shown in the following formula, after organic tissue carbon has been converted into CO_2 in a mass spectrometer (Craig, 1957):

$$\delta\,^{13}C_{\,(‰)} = [(\frac{\{613CO2/\,612CO2\}\,(sample)}{\{613CO2/\,612CO2\}\,(standard)} - 1)\text{x}1000] \qquad (1),$$

where "standard" refers to the CO_2 content of the PDB, a calcium carbonate, reacting with 100 % phosphoric acid at 25.2 ^{o}C (Craig, 1957).

The values of $\delta\,^{13}C$ in plant tissues are, on average, -28 ‰ for C_3 plants and -14‰ for C_4 plants (Bender, 1968, Bender, 1971, Smith and Epstein, 1971). In the SOC, the $\delta\,^{13}C$ values help trace back to the original vegetation type (Balesdent and Mariotti, 1996). The discrimination against isotope ^{13}C due to its mass (O'Leary, 1988) occurs during isotope fractionation at the moment of photosynthesis (Vogel, 1980). In C_3 plants, the rubisco, Calvin cycle enzyme, discriminatory performance accentuates fractionation and slows carboxylation of ribulose bisphosphate as well as CO_2 uptake so that isotope ^{13}C content drops and $\delta\,^{13}C$ value becomes more negative up to -36 ‰ (O'Leary, 1988, Smith and Epstein, 1971, Guy et al., 1986). In C_4 plants, however, $\delta\,^{13}C$ values are less negative, up to -1‰) (O'Leary, 1988, Smith and Epstein, 1971) because Rubisco's isotope carboxylation fractionation impact has diminished due to the natural adaptation of the photosynthesis architectural framework (i.e., mesophyll cells and bundle sheath cells). This modification, however, enables the diffusion process to amplify isotope fractionation in C_4 more than in C_3 plants (Vogel, 1980). Rubisco, in bundle sheath cells, is prefaced with malate, a carboxylated PEP (phosphoenolpyruvate) in the mesophyll cells (Deines, 1980). The sequential decarboxylation of the malate in the bundle sheath sustains the CO_2 supply to the Calvin cycle (O'Leary. 1988), minimizes rubisco isotope fractionation, and elevates $\delta\,^{13}C$ values for C_4 plants. The magnitude of the carbon isotope fractionation during photosynthesis in C_3 and C_4 plants, depends on the relative importance of CO_2 diffusion

from air through stomata to mesophyll cells and on the enzymatic carboxylation rate (Craig, 1954). In C_3, rubisco carboxylation resistance (limited carboxylation rate) is the most snagging step while in C_4, carbon dioxide diffusion is potentially more hampering due mainly to the isotope ^{13}C mass and its low solubility (Vogel, 1980, O'Leary, 1988) and low reactivity (Farquhar et al., 1982).

The term "C_3 plant" relates to the 3-carbon sugar molecule identified as G3P (glyceraldehyde 3-phosphate) which is the Calvin cycle anabolic output after CO_2 fixation. Some crops such as soybeans (*Glycine max*), rice (*Oryza* sp), and wheat (*Triticum* sp) are known to be C_3 plants (Guede et al., 2017). The term "C_4 plant" derives from the 4-carbon sugar molecule (e.g., malate) generated in the mesophyll cells during the PEP carboxylation (Hatch and Slack, 1966) prior to Calvin cycle (O'Leary, 1988). Millet (Pennisetum), corn (Zea mays), and sugarcane (Saccharum officinarum) are some of the plants following the C_4 photosynthetic pathway (Smith and Epstein, 1971, Guede et al., 2017). Thus, it can be seen that, in C_3, carboxylation and sugar synthesis both occur in the stroma during the Calvin cycle process but in different time while, in C_4, both happen in different time also but in different structural cells (mesophyll cells and bundle sheath cells).

2.2.5. Statistical Analyses

All statistical analyses were performed in R (version 3.3.1, R Core Team, 2019). Post-hoc analyses for significant differences in response variables between groups after ANOVA analyses were conducted using Tukey's Honest Significant Difference (HSD) in group means. Unless otherwise mentioned in manuscript text or figure captions, all reported uncertainties represent a single standard deviation around the mean.

Because our dataset represents a mixture of sites sampled by genetic horizon, we chose to modify the Land Degradation Surveillance Framework (LDSF) (Vågen et al., 2013) standardized depth increments (0–20 cm, 20–50 cm, and 50–80, and 80-100 cm) by splitting the 0-20 cm depth increment into 0-10 cm and 10-20 cm and by combining the 50–80 cm and 80–100 cm LDSF standardized depth increments into one 50–100 cm increment. We then computed weighted averages to compare soil properties by depth between sites. We calculated the weighted averages of all available soil properties by depth increment for each sampling site using the "slab" function in the AQP package in R

(Beaudette et al., 2013, R Core Team, 2019). These standardized depth-increment weighted averages were utilized to examine the relationships between soil properties and site-level characteristics such as vegetation and climate using ANOVA.

2.3. Results

2.3.1. Magnetic parameters across climatic zones and vegetation types

Magnetic S-Ratio values by climate and vegetation type as well as their variations among standardized depth increments are summarized in Table 1.1. S-Ratios generally exhibited a numerical decline with depth, indicating a greater predominance of soft magnetic minerals (i.e., magnetite and maghemite) at shallower depths. This decline is evident in all investigated profiles and among average depth profiles for all climatic and vegetation groupings. Soils in Af exhibited a decreasing trend in S-ratio means from 0.79±0.12 Am^2/kg at 0-10 cm to 0.62±0.19 Am^2/kg at 100-200 cm of depth. In Am, S-Ratios decrease from 0.93±0.02 Am^2/kg at 0-10 cm to 0.85±0.03 Am^2/kg at 100-200 cm of depth. Finally, in Aw, S-Ratios decline from 0.94±0.06 Am^2/kg at 0-10 cm to 0.83±0.07 Am^2/kg at 100-200 cm deep. S-Ratios are lower across all depth increments in Af soils ($p < 0.05$, Tukey's HSD) than S-Ratios in Am and Aw soils, indicating a lower relative proportion of soft magnetic minerals (magnetite and maghemite) regardless of depth.

S-Ratio values also change with depth within distinct vegetation types, regardless of climate zone. Under forested sites, S-Ratios decrease from 0.81±0.18 Am^2/kg at 0-10 cm to 0.66±0.20 Am^2/kg at 100-200 cm of depth. The same trend is apparent in the savanna from 0.92±0.07Am^2/kg at 0-10 cm to 0.83±0.06 Am^2/kg at 100-200 cm deep. S-Ratio values drop more rapidly with depth in the forest than in the savanna, and forested sites show significantly lower S-Ratio values across all depth increments. S-ratio values across all samples were linearly and inversely related to both CBD (citrate bicarbonate dithionite) extractable iron (Fe_d) ($R^2 = 0.65$, $p < 0.001$) and total iron (Fe_t) $R^2 = 0.62$, $p < 0.001$) (Figure 2.1).

M_r/M_s ratios increase systematically with depth increments across the climate gradient but more noticeably in Af (0.19 to 0.27, Table 2.2) and under forest (0.20 to 0.25, Table 2.2). At every depth increment below 10 cm, M_r/M_s ratios in Af are higher than in Am and Aw. M_r/M_s ratios across all samples were linearly related to both Fe_d ($r = 0.75$, p

< 0.001) and Fe_t (r = 0.71, p < 0.001) (Figure 2.1). No significant relationships were observed between M_r/M_s ratios and AmmOx extractable iron (Fe_o). Ratios of the coercivity of remanence (B_{cr}) and bulk coercivity (B_c) are higher in Af than in Am and Aw between 10 cm and 100 cm of depth and also significantly elevated under forest vegetation than savanna (Table 2.3). No significant relationships were observed between B_{cr}/B_c ratios and any iron forms. Figure 2.2 reflects on the correlation between magnetization ratios (M_r/M_s) and coercivity ratios (B_{cr}/B_c) in Aw, Am, and climate (Af). The magnetizations of all three climate zones largely cluster around an M_r/M_s ratio of 0.2, but the M_r/M_s ratio of Af subsoils differ significantly from samples at all depth increments in Aw and Am (Figure 2.2). In Af in particular, therefore (unlike in Aw and Am), M_r/M_s ratios are correlated to B_{cr}/B_c ratios.

2.3.2. $\delta^{13}C$ across climatic zones and vegetation types

Across the climate gradient and depth to 300 cm, all $\delta^{13}C$ values systematically increase from Af to Am to Aw (Figure 2.3). They are significantly different between Af and Aw but not significantly different between Af and Am (Table 2.4, Figure 2.3). In Af, $\delta^{13}C$ values vary from -26.3 ± 6.8 ‰ between 0 cm and 10 cm to -25.7 ± 0.4 ‰ at 300 cm of depth. In Am, $\delta^{13}C$ values decline from -20.9 ± 7.7 ‰ at the top of the profile to -25.5±0.4 ‰ at 300 cm of depth. In Aw, $\delta^{13}C$ values progressively decrease with depth from -14.3±1.0 ‰ to -17.0±2.9 ‰ between 0 cm and 100 cm and, from 100 cm to 300 cm, $\delta^{13}C$ values decrease further from -20.7±3.0 ‰ to -22.3±1.4 ‰ (Table 2.4).

Across vegetation types (forest to savanna) (Table 2.4), $\delta^{13}C$ values are significantly lower under forest than under savanna (Figure 2.3). In forest, the $\delta^{13}C$ values increase consistently with depth (from -29.08±1.0 ‰ at 0-10 cm to -25.76±1.9 ‰ at 300 cm) but remain within the range of C_3 plants (Deines, 1980). In savanna, however, the $\delta^{13}C$ values decrease with depth from -13.96±0.83 ‰ at 0-10 cm to -23.49±0.4 ‰ at 300 cm, indicating the contribution of C_4 plants within the top 100 cm and C_3 plants below 100cm. ^{13}C values drop with depth in the savanna but increase with depth in the forest. The ^{13}C distribution in savanna sites, regardless of climate zone (Figure 2.3) suggests a historical vegetation change.

2.4. Discussion

2.4.1. Climatic boundaries recorded in soil magnetic properties

The relative decrease of the "soft" magnetic minerals (such as magnetite and maghemite called "soft" due to their high magnetic susceptibility) with depth (i.e., the weakening of the magnetic susceptibility with depth) across the climate gradient (Aw, Am, and Af) is most prominent in Af. The magnetic enhancement at the surface depth of the profiles in these tropical climates as well as in temperate climates (Maxbauer et al., 2017) indicates intensive biological and/or inorganic pedogenic activities such as authigenesis of ferromagnetic and ferrimagnetic minerals (Taylor et al.,1987, Balsam et al., 2011). The increase in the "hard" magnetic minerals (hematite, goethite, etc.) with depth as reflected in the S-ratios (Table 1.1), may be due to a reduction in magneto-pedogenic activity with depth. In addition, the marked increase of hard magnetic minerals with depth in Af may result from the effective lessivage of the hard magnetic minerals along with the soft magnetic minerals which can be converted by oxidation to hard magnetic minerals during the clay material translocation spurred by intense equatorial precipitation and further enabled by a porous soil matrix (87% sand on average). The clay fraction steadily increases with depth in Af but shows distinct peaks with depth in Am and Aw at approximately 50 cm. The mixing of the hues (10YR, 7.5YR, and sometimes 5YR) in all sampled sola indicates the prevalence of "hard" magnetic minerals (minerals with low magnetic susceptibility such as hematite, goethite, lepidocrocite, etc.) reflecting a brown and yellowish-brown dominant spectrum (Schwertmann, 1993).

Often, soil magnetism development has been found to be positively and strongly correlated to precipitation in diverse environmental settings (Balsam et al., 2011). However, the prevalence of soft magnetic minerals (i.e., magnetic susceptibility) across the climate gradient (Table 2.1) in this study appears to show a different trend. S-ratios drop in Af but rise in Aw and Am. Maxbauer et al. (2017) observed a similar soil magnetism drop in temperate forest in northeastern Minnesota. The apparent inconsistency between magnetic susceptibility (M_s) and rainfall emerges at the mineral production stage where the formation of soft magnetic minerals stagnates, and their preservation becomes precarious due to the lasting anaerobic conditions following soil saturation (even under good drainage conditions) that often occurs under intense and continuous equatorial

precipitations. Balsam et al. (2011), using a global dataset, concluded that magnetic mineral formation grows linearly with rainfall up to approximately 2000 mm yr^{-1}, at which point hard magnetic mineral formation becomes thermodynamically unfavored, magnetite solution accelerates (under the effect of organic acid also) and maghemite may be transformed back to magnetite. Ultimately, beyond this threshold, M_s decreases and a negative correlation result between M_s and rainfall. This phenomenon may explain why the soft magnetic minerals ratios dropped in Af (where soil is rarely, if ever dry) but remained high in Aw and Am where the soil is seasonally dry.

Extrapolating the work of Maxbauer et al. (2017), there are three concomitant challenges to soft magnetic mineral persistence in equatorial forest: low rate of formation, increased rates of destruction, and intensified lessivage. While soft magnetic mineral formation is lower in equatorial forest, pedogenesis, brought on by weathering of minerals (Jackson and Sherman, 1953, Schwertmann, 1991, Reynolds & King, 1995), is intensified by lessivage under equatorial heavy rains, which precludes the accumulation of soft magnetic minerals relative to Am and Aw, where lessivage is seasonally limited. In the sandy soils of Sankuru, this process translocates clay materials (including magnetite) down the profile into a well-drained sandy environment that enhances oxidation which promotes the conversion of magnetic minerals from "soft" to "hard" magnetic materials. As a consequence, hard minerals content rises from 21 % within the top 10 cm to 38 % between 100 and 200 cm deep in Af. Biomineralization (Blakemore, 1982, Kukla et al., 1988), in a wet and warm climate, may be an additional source of soft magnetic materials that are also prone to lessivage.

Regardless of soil type and climatic zone (Af, Am, Aw), the soft magnetic mineral ratio remains consistently high at the top of every profile, probably because of the relatively intense biological and inorganic pedogenic activities at those locations (Maher, 1998, Balsam et al., 2011). In Am and Aw, seasonal wet and dry alternations (and good drainage) create conditions favoring the formation of magnetite and maghemite, both genetically related (Chen et al., 2010, Maxbauer et al., 2016). Moreover, the burning of the vegetation and heating of topsoil (like during the frequent savanna fires in Aw and Am in Sankuru) may promote magnetite and maghemite formation (Mullins, 1977, Stanjek, 1987). Unlike in Af, the lessivage of these minerals in Aw and Am is seasonally limited (to the wet

season) which may explain their relatively small drop with depth in comparison with Af climatic zone.

Finally, while magnetite and maghemite can very likely be authigenic across the climate gradient, a portion of these minerals may be of geologic origin based on the history of the Congo River basin (Myers et al., 2011, Roberts et al., 2015) which includes the parent material's eolian origin. These intermittent global arid conditions affected the central African region (including the Congo River basin) in the quaternary, and enabled regional eolian activity across the Sankuru transect (Zachos et al., 2001, Plana, 2004, Hoag and Svenning, 2017).

M_r/M_s and B_{cr}/B_c ratios are the magnetic hysteresis parameters which can indicate differences in magnetic particle size and domain state despite some interpretive limitations (Tauxe, 2008). The low ratios of remanent magnetization ($0.16 < M_r/M_s < 0.3$) (Table 2.2) suggest PSD (pseudo single domain) particle predominance, indicating potential particle sizes of 75-100 nm (Maxbauer et al., 2017) in Af, Am, and Aw regardless of vegetation type. B_{cr}/B_c ratio values remain between 1.5 and 5 (Table 2.3) and are sensitive only to non-SP particles (Tauxe, 2008). The positive correlation between M_r/M_s and B_{cr}/B_c in Af (Figure 2.2) may be conveying a mineral assemblage presence likely dominated by PSD and MD. A weaker correlation prevails in Am and Aw very likely insinuating stronger SP presence.

2.4.2. Vegetative shifts recorded in $\delta^{13}C$ of soil organic carbon

Across the climate gradient, soil $\delta^{13}C$ values systematically increase from Af to Am to Aw at all depths, consistent with the current vegetation gradient dominated by C_3 plants (forest) in Af (average $\delta^{13}C$ of -25.6 ‰) to C4 dominated vegetation (grasses) in Aw (average $\delta^{13}C$ of -17.3‰) coinciding with the major current ecotone boundary across the study transect (Winowiecki et al., 2017) (Table 2.4).

The range of $\delta^{13}C$ values (-19.50 ‰ to -33.18 ‰) in the Af (rainforest) climatic zone and especially their distribution with depth from -33.18 ‰ at the top to -25.32 ‰ at the bottom definitely reflects C_3 plant signatures (Smith and Epstein, 1971, Deines, 1980), predominantly trees which are the major contributor of the SOM (soil organic matter) in Af. This range of the $\delta^{13}C$ values in Af is also consistent with the common scale of the C_3

plant $\delta^{13}C$ values -20 ‰ to -35 ‰ averaging -27 ‰ (Pessenda et al., 1996, Schaetzl and Thompson, 2015). More localized studies in West and west-central Africa have also resulted in similar ranges of $\delta^{13}C$ under stable forest. Schwartz et al. (1986) in the Congo Republic (adjacent to DR Congo) measured $\delta^{13}C$ values -27.8 ‰ in the rainforest A horizon, while Bremond et al. (2017) identified similar $\delta^{13}C$ values from -30 ‰ to -27.1 ‰ at the top to -26.7 ‰ to -24.5 ‰ at the bottom of the profile. Also, the $\delta^{13}C$ values throughout the solum in Af are comparable to those in the O horizon (which average -30.4 ‰) suggesting a direct supply of the SOM from the present litter. Thus, the $\delta^{13}C$ values enable traceability of soil carbon's parent vegetation (Balesdent and Mariotti, 1996). The largely similar depth-wise values in Af infers that SOM likely originates solely from C_3 plants, indicating forest origins.

The distribution of the $\delta^{13}C$ values with depth in Af and Am (Table 2.4 and Figure 2.3) reveals a marginal increase of $\delta^{13}C$ values in both zones with depth. Although in some cases the slight rise of $\delta^{13}C$ with depth in the soil under forest has been interpreted as evidence of historical savanna vegetation (Bekele and Hudnall, 2006), given that this trend has been observed in soils under forest around the world, it is much more likely that this increase reflects a combination of atmospheric ^{13}C abundance over time in combination with fractionation due to increased decomposition or modification of organic matter with depth (Bostrom et al., 2007). Given that all soils under forest vegetation across our study transect show a relatively small range of uncertainty, even in deeper depths, and even the least negative values at the deepest depths remain solidly within the range expected for C_3 vegetation (Figure 2.3), we interpret this as evidence of stable forest vegetation on these sites.

The average depth profile for Am $\delta^{13}C$ values (Figure 2.3), is intermediate between Af and Aw $\delta^{13}C$ values (Table 2.4). The Am climate zone, with $\delta^{13}C$ values averaging -20.9 ± 6-7 ‰ between 0 cm and 200 cm of depth, appears to be a mixed carbon source model from C_3 (-28 ‰) and C_4 (-14 ‰) (Deines, 1980) as suggested by the large standard deviation of the $\delta^{13}C$ values (± 6-7 ‰) (Figure 2.3). Desjardins et al. (2013) brought forth the rationale of mixed vegetation (C_3 and C_4 plants) to corroborate the $\delta^{13}C$ values range (-17 ‰ to -20 ‰) recorded in savanna between 130 cm and 390 cm of depth in central Cameroon.

In the Aw zone, the vegetation shift from historic C_3 vegetation (forest) to C_4 plants is apparent from the profile of $\delta^{13}C$ with depth. The $\delta^{13}C$ values within the top 100 cm in Aw (-14.3 ± 1.0 ‰ to -17.0±2.9 ‰) are clearly indicative of C_4 plants (grasses), known for their $\delta^{13}C$ values range of -9 ‰ to -17 ‰ (Deines, 1980, Schaetzl and Anderson, 2005). Below 100 cm, $\delta^{13}C$ values (-20.7±3.0 ‰ to -22.3±1.4 ‰) are strongly indicative of C_3 plants signature. A similar distribution of $\delta^{13}C$ with depth was also observed at the forest-savanna boundary in Congo-Brazzaville by Schwartz et al. (1986) with $\delta^{13}C$ values of -14.3 ‰ in A horizon and -25.2 ‰ to -27.5 ‰ in B_h horizon (105-250 cm) of a spodosol indicating a local vegetation switch from historic forest to savanna. The $\delta^{13}C$ values diminishing with depth in all profiles in Aw suggests the SOM turnover from past forest vegetation to savanna: the current vegetation, savanna, overprinting on the previous carbon pool (Balesdent & Mariotti, 1996, Krull et al., 2002) while the forest characteristics remain at the bottom of the profile (Jenkinson and Rainer, 1977) assuming increasing carbon age with depth in the profile (Bremond et al., 2017). The C_3 vegetation, which has therefore been stable in Af, appears to be in transition to C_4 plants in Am, and has fully shifted to C_4 (from forest to savanna) in Aw. The mixed SOM supply model evoked above in Am, could conceptually include CAM plants whose $\delta^{13}C$ values are intermediate between C_3 and C_4 plants $\delta^{13}C$ values (Deines, 1980). However, the tropical CAM species are not widespread or abundant enough to substantially impact soil isotope $\delta^{13}C$ values.

Pleistocene and Holocene vegetation change in DRC, like everywhere else in the tropics, has been driven by major climatic fluctuations. In the Cenozoic, climate varied from the thermal maximum (at 55 Ma) in late Paleocene/early Eocene epoch (Zachos et al., 2001) to the last glacial maximum (at 21,000 YBP) in late Pleistocene (Hoag and Svenning, 2017). The continuous glacial and interglacial cycles throughout the Pleistocene and Holocene, resulted in global arid and humid cycles (Dupont, 2011) that promoted long intervals of interpluvial and pluvial conditions in tropical Africa, leading to the regional forest contraction and expansion (Hoag and Svenning, 2017). Savanna expanded while forest contracted during glacial periods and reversed course through interglacial periods (Dupont, 2011).

The forest-savanna boundary in central Africa has been highly dynamic in the distant and recent past, vegetation change is recorded in the $\delta^{13}C$ of soil organic matter on

maximum timescales of millennia in the humid tropics (Schwartz et al., 1992, Schwartz et al., 1996). In deep time, the central African rainforest originated in Oligocene (Plana, 2004) and became widespread during the warming period between late Oligocene (~26 Ma) and early Miocene (~15 Ma) in the Tertiary period (Zachos et al., 2001). The initially widespread rainforest in early Miocene shrunk to small patches (refugia) in the Late Miocene (15-5 Ma) under arid conditions and expanded in the Early Pliocene (5-3.5 Ma) with the return of moist climates. African rainforest contracted again in the Late Pliocene (3.5-1.5 Ma) and savanna also retracted during the Late Pliocene major drought (3.2-3.0 Ma) (Plana, 2004).

In the Quaternary era (1.8 Ma to present), climate swing patterns persisted with high amplitude in the Pleistocene and mild variation in the Holocene (Cohen et al., 2007, Hoag and Svenning, 2017). The glacial periodicity reached two maxima in the Pleistocene at 160,000 to 30,000 YBP and 24,000 to 12,000 YBP which resulted in two respective phases of maximum forest fragmentation (Maley, 1996, Cohen et al., 2007). The recovery process of the equatorial forest which restarted 11,000 YBP under humid climate, reached the maximum expansion 5,000 YBP (from Guinea to the Lake Victoria through Congo River basin - Plana, 2004) before disintegrating again twice 4,000 YBP and between 2,500-2,000 YBP (Weijers et al., 2007, Nash et al., 2016, Maley et al., 2018). Currently, the Central African rainforest expansion process may be in peril as forest greenness declines due to the anthropogenic global warming (Zhou et al., 2014, Nash et al., 2016) which can raise the African rainforest temperature per 0.8-1^{o}C for 1^{o}C of global warming (Malhi et al., 2013); even though higher atmospheric CO_2 concentration would favor forest extension by boosting C_3 plants over C_4 plants (Bond, 2008). Although the $\delta^{13}C$ values of soil organic carbon can be sensitive to vegetation change in the tropics on the order of decades (Sugihara et al., 2019, Desjardins et al., 1994), these changes are usually no more than 4-10 units and typically restricted to the top 10 cm of soil. Given that the observed changes in $\delta^{13}C$ values with depth in the savanna sites across our transect, it is likely that these are recording changes in the forest-savanna boundary during the forest fragmentation periods 2,000-4,000 yBP and that these sites have remained relatively stable under savanna vegetation for at least two millennia. This is consistent with other studies in tropical soils combined with radioisotope dating of organic materials which have shown that $\delta^{13}C$ in soil

organic matter records approximately 3,000-6,000 years in the top 2 m of soil (Schwartz et al., 1992, Schwartz et al., 1996, Bremond et al., 2017).

2.5 Conclusion

Our analysis of magnetic parameters and $\delta^{13}C$ values of soil organic carbon across the Sankuru transect provides unique insights into climatic influences on magnetic mineral formation and vegetation change across the modern equatorial forest-savanna ecotone in central DRC. We conclude all sites across the transect currently under savanna vegetation were once under forest, likely on the order of 2,000 to 4,000 yBP, although we are unable to directly constrain this timeline with the data at hand. Forested sites in the Af and Am climatic zones seems to bear no sign of vegetation shift and have likely been under forest vegetation for millennia. Additionally, we find that the greater rainfall in Af is an abrupt threshold that result in less prevalent soft magnetic minerals. This may be due to lingering soil saturation under equatorial forest in Af, which may enable a reductive dissolution of the ferromagnets and ferrimagnets, weakening magnetic susceptibility. These results demonstrate the transient nature of vegetative and climatic boundaries across the sharp forest-savanna ecotone in central Africa, and provides additional perspective on pedological trends related to modern climate and vegetation.

Table 2.1. *Average S-Ratios (@300mT, Am^2/kg) by depth increments across climate zones*

	Depth (cm)	0-10	10-20	20-50	50-100	100-200
Climate	Equator. Forest (Af)	0.79±0.12a	0.67±0.18a	0.66±0.20a	0.63±0.20a	0.62±0.19a
	Trop. Monsoon (Am)	0.93±0.02b	0.90±0.05b	0.90±0.04b	0.89±0.03b	0.85±0.03b
	Trop. Savanna (Aw)	0.94±0.06b	0.93±0.07b	0.92±0.07b	0.88±0.03b	0.83±0.07b
Vegetation	Savanna	0.92±0.07a	0.92±0.07a	0.92±0.06a	0.87±0.05a	0.83±0.06a
	Forest	0.81±0.18b	0.71±0.18b	0.70±0.20b	0.68±0.21b	0.66±0.20b

All numbers indicate the mean and standard deviation for each depth increment by climate zone or by vegetation type.
**Different letters indicate statistically significant differences within climate zone categories or vegetation types ($p < 0.05$) by depth increment following ANOVA using Tukey's HSD.*

Table 2.2. *Average Mr/Ms Ratios by depth increments across climate zones*

	Depth (cm)	0-10	10-20	20-50	50-100	100-200
Climate	Equatorial Zone (Af)	0.19±0.03a	0.24±0.07a	0.25±0.07a	0.27±0.07a	0.27±0.08a
	Trop. Monsoon (Am)	0.16±0.01a	0.16±0.01b	0.15±0.02b	0.16±0.02b	0.17±0.02b
	Trop. Savanna (Aw)	0.19±0.02a	0.19±0.02b	0.19±0.02b	0.20±0.02b	0.20±0.04b
Vegetation	Savanna	0.18±0.02a	0.18±0.02a	0.18±0.02a	0.19±0.02a	0.19±0.03a
	Forest	0.20±0.05a	0.22±0.07b	0.23±0.08b	0.24±0.09b	0.25±0.09b

All numbers indicate the mean and standard deviation for each depth increment by climate zone or by vegetation type.
**Different letters indicate statistically significant differences within climate zone categories or vegetation types ($p < 0.05$) by depth increment following ANOVA using Tukey's HSD.*

Table 2.3. *Average Bcr/Bc Ratios by depth increments across climate zones*

	Depth (cm)	0-10	10-20	20-50	50-100	100-200
Climate	Equatorial Zone (Af)	2.22±1.18a	3.16±0.98a	3.20±0.87a	3.27±0.61a	3.15±0.77a
	Trop. Monsoon (Am)	2.67±0.27a	2.75±0.25b	2.64±0.22ab	2.63±0.14b	2.78±0.23a
	Trop. Savanna (Aw)	2.33±0.24a	2.33±0.24b	2.27±0.32b	2.32±0.31b	2.43±0.57a
Vegetation	Savanna	2.35±0.52a	2.35±0.51a	2.41±0.37a	2.48±0.28a	2.53±0.44a
	Forest	2.87±0.52a	3.28±0.58b	3.15±0.76b	3.16±0.62b	3.14±0.68b

All numbers indicate the mean and standard deviation for each depth increment by climate zone or by vegetation type.
**Different letters indicate statistically significant differences within climate zone categories or vegetation types ($p < 0.05$) by depth increment following ANOVA using Tukey's HSD.*

Table 2.4. *Average $\delta^{13}C$ (‰) values by depth increment across climate zones and vegetation types.*

	Climate Zone			Vegetation	
Depth (cm)	Af	Am	Aw	Forest	Savanna
0-10	-26.34±6.84	-20.86±7.73	-14.31±1.03	-29.08±0.98	-13.96±0.83
10-20	-25.88±6.20	-20.16±7.15	-14.34±1.09	-28.05±1.62	-13.98±0.88
20-50	-25.12±5.30	-20.07±7.03	-15.20±2.18	-27.17±1.42	-14.62±1.74
50-100	-25.27±2.32	-21.38±6.01	-17.03±2.93	-26.23±1.52	-17.48±3.24
100-200	-25.38±1.58	-21.97±6.16	-20.70±3.03	-26.27±1.17	-20.20±3.75
300	-25.71±0.39	-25.48±0.43	-22.29±1.35	-25.76±1.86	-23.49±0.38

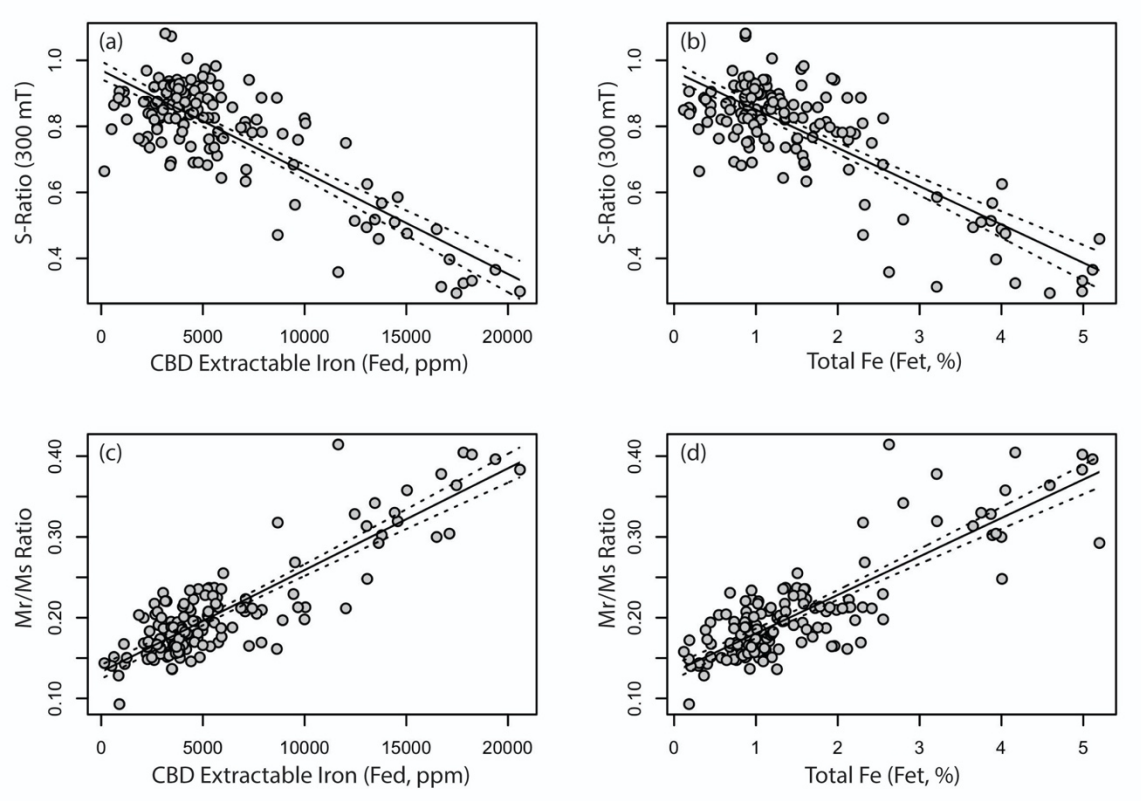

Figure 2.1. *Relationships between a) S-Ratio$_{300mT}$ and CBD (citrate-bicarbonate-dithionite) extractable iron (Fed), b) S-Ratio$_{-300mT}$ and Total iron (Fe$_t$), c) Mr/Ms Ratio and CBD extractable iron (Fe$_d$) and d) Mr/Ms Ratio and Total iron (Fe$_t$) across all samples. Dotted lines represent the 95% confidence interval around the slope of the regression line.*

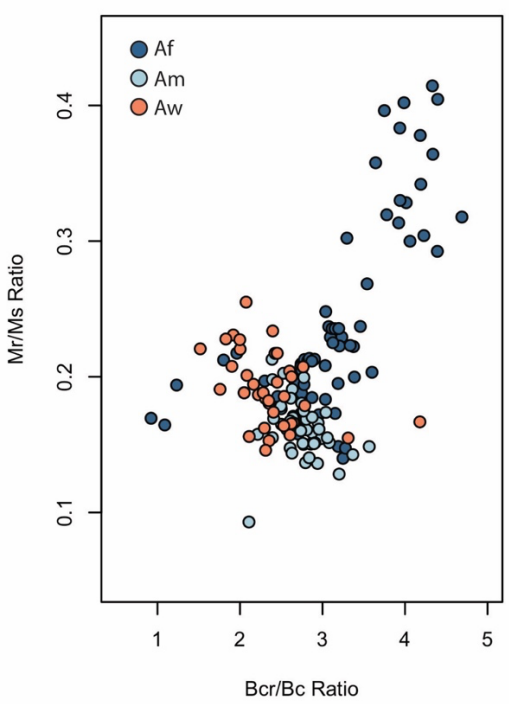

Figure 2.2. *"Day" plot of magnetic parameters (B_{cr}/B_c ratio vs M_r/M_s ratio) for all samples, colored by climate zone.*

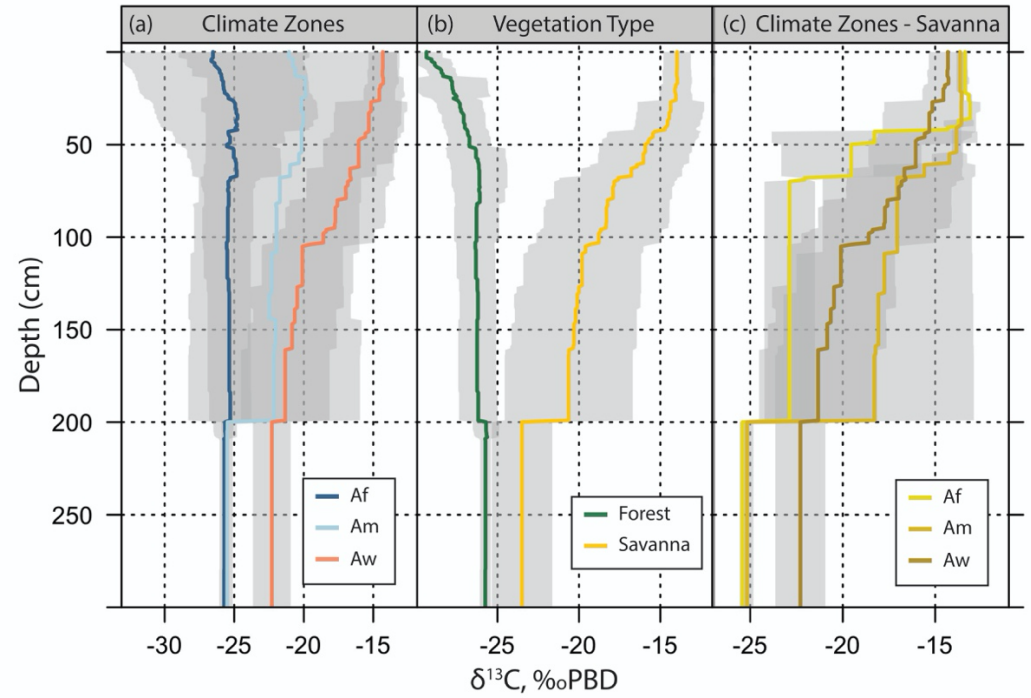

Figure 2.3. *Average $\delta^{13}C$ values with depth from the soil surface for investigated soils by a) climate zone, b) vegetation type, and c) by climate zone for sites under savanna vegetation only. $\delta^{13}C$ values are reported as the difference from PBD standard per mil (‰).*

CHAPTER 3

Phosphorus fractions and stocks across a combined climo- and bio-sequence in Sankuru Province, central Democratic Republic of Congo (DRC)

3.1. Introduction

Soil phosphorus (P) cycling in tropical environments is unique: despite the fact that the weathering of primary minerals, secondary minerals, and decomposition of organic matter is accelerated in high temperature and rainfall environments, resulting in P release in available form to the soil solution (Tiessen and Moir, 2006), P occlusion (P which has been physically or chemically sequestered and is not extractable by standard wet chemical procedures) in highly weathered soils can also restrict P availability over long time periods (Smeck, 1973, Walker and Syers 1976, Negassa and Leinweber 2009). In highly weathered soils prevalent in humid tropical environments, the iron and aluminum oxides to clay ratio can be very high (Sanchez, 2019), reacting with P to produce P occlusion (Smeck, 1973) and nutrient limitation (Walker and Syers, 1976, Yang and Post, 2011, Wardle et al., 2004, Turner et al., 2007). In some regions in tropical Latin America and Africa, up to 80 % of the soils may be P limited (Sanchez, 2019, Hou et al., 2020) resulting in restrictions to crop productivity (Lynch, 2011) and decreases in microbial activity when the soil nitrogen to phosphorus (N:P) ratio is greater than 16 and the soil carbon to phosphorus ratio (C:P) is greater than 200 (Wardle et al., 2004, Turner et al., 2007). These deficiencies can be exacerbated by initially P-poor soil parent material (Walker and Adams, 1957). Therefore, understanding the evolution of soil phosphorus under unique combinations of climate, vegetation, and parent material is critical for managing soils appropriately to meet global food production demands.

The Walker and Syers (1976) model is one of the most widely used conceptual models to understand the fate of the P during pedogenesis, involving various P bio-geotransformations (Hedley et al., 1982) used as pedogenic markers (Smeck, 1973, Walker and Syers, 1976, Tiessen et al., 1984, Cross & Schlesinger, 1994, Yang and Post, 2011, Turner and Condron, 2013). Although the Walker and Syers conceptual model is often interpreted as a strict chronosequence, in reality it was implemented on a combined climo-geo-chronosequence with differing parent materials (outwash, alluvium, and eolian sands) in humid temperate New Zealand, with a MAT (mean annual temperature) averaging 11ºC, mostly forest vegetation, and a mean annual precipitation (MAP) varying from 650 mm to 5090 mm (Walker and Syers, 1976). Despite these confounding factors, this seminal study helped frame the “classical” concept of the pedogenic P transformational trajectory, over

time and space, from its initially high content in soil parent materials (predominantly as apatite) to its ultimate organic accretion and mineral occlusion in the soil "terminal" state leading to the prospect of ecosystem regression following soil P limitation (Walker and Syers, 1976, Wardle et al., 2004, Turner and Condron, 2013). This had led to wide generalizations regarding the nature of soil P pools, assessed operationally using sequentially extractable P fractions, in highly weathered tropical soils.

However, Crews et. al. (1995) expanded on this initial framework using a soil chronosequence in Hawaii. Their findings supported the Walker and Syers predictions: the drop of Ca-associated P and the rise of the occluded P fraction in older soils. Nevertheless, the non-occluded P pool made up a significant proportion of total P (P_t) well into what would have been interpreted as a highly weathered, terminal state in the Walker and Syers model (at 1.41M & 4.1M yrs). Crews et al. (1995) also found that the maximum total soil P (kg/m^2 up to 50 cm) recorded after 150,000 years (Crews et al., 1995) was much higher than expected under the Walker and Syers model due to potential allochthonous P supply from dust additions as well as mycorrhizal P mining from the parent material and Fe/Al occluded P. The existence of a large non-occluded pool of phosphorus in many highly weathered soils has been corroborated by subsequent meta-analyses (Yang et al., 2011, Yang et al., 2014).

Biogeochemical P transformations over short timescales (months to centuries) can regulate P availability (Yang et al., 2011) and thus need to be incorporated into earth system models, particularly in tropical environments for which there is limited data (Mcdowell et al. 2007, Brenner et al., 2019). Primary P mineral dissolution, mineralization (McGill and Cole, 1981), P sorption and desorption from clay materials (Walker and Syers, 1976, Parfitt and Smart, 1978), and mycorrhizal mutualisms (Zhu et al., 2001, Smith et al., 2003) are the geochemical and biological processes (Cross and Schlesinger, 1995) that collectively determine soil phosphorus supply to organisms (Condron and Newman, 2011). In Indonesia, Schlesinger et al. (1998) reported P limitation in the surface horizons due to high organic P accumulation (likely as phosphomonoesters, which can be resilient to mineralization (Mclaren et al., 2015)), which thwarted upland rice growth in a young soil (110 yrs) derived from pyroclastic ashfall with up to 384 mg/kg Ca-associated P (apatite). Tiessen et al. (1984) showed that, in Ultisols, mineralization of P from organic forms

contributed to 80 % of P availability, as Al/Fe complexes with P were less likely to dissolve naturally in highly weathered soils. Additional work has expanded on the Walker-Syers model with more strictly controlled chronosequence studies (Crews et al., 1995), as well as with climatic gradients (Feng et al., 2016), and vegetative boundaries (Lloyd et al., 2015), gradients in soil parent material P concentrations (Porder and Ramachandran, 2013, Mou et al. 2020), and land use conversions (Yang et al., 2021). This research has shown that, for pedogenetic factors in addition to time, and in different biophysical contexts (such as the humid tropics) the Walker and Syers model may not accurately reflect soil phosphorus dynamics.

Despite the importance of understanding soil P dynamics in humid tropical environments where P can often be a limiting nutrient (Hou et al., 2020), only limited work has been done on P transformations in equatorial regions, particularly central Africa (Hou et al., 2018c). Therefore, the objectives of this study were to investigate soil phosphorous distributions, fractions, and transformations on a combined bio-climosequence across the tropical savanna-equatorial forest ecotone (the Sankuru transect) on P-poor parent materials (eolian sands) in central Democratic Republic of Congo. By integrating the results of this study into existing conceptual models, advances in our understanding of soil P dynamics in these environments could have large real-world implications, particularly in P-limited agronomic systems where management practices and amendments could affect major changes in P availability.

3.2 Materials and Methods

3.2.1 Study Area, Climate, Vegetation, and Soils

Field work was completed in two phases from August 2015 to January 2016 and June to August 2017 in Sankuru Province, central Democratic Republic of Congo (DRC) (Figure 1.1), across a transect of ≈250 km entailing a steep climate gradient from tropical rainforest (Köppen: Af) in the north, through tropical monsoon (Köppen: Am) to tropical wet savanna (Köppen: Aw) in the south (Figure 1.1). The area is occupied by the Tetela tribe. MAP in the study area varies between 1613 mm in the south of the transect (near Lubefu) to 1742 mm in the north near Ekomakoko (Fick and Hijmans, 2017, Figure 1.1). Importantly, although MAP varies by only ~130mm across the transect, the seasonality of

precipitation is strikingly different from south to north (Herrmann and Mohr, 2011, Munzimi et al., 2015). In the Af in the north, there is no seasonality to the precipitation regime, while Am is characterized by a single, bimodal wet season (longer wet season, bimodal), and sites in Aw experience a shorter, unimodal wet season (Herrmann and Mohr, 2011, Munzimi et al., 2015). Additionally, this transect lies across the Udic-Ustic soil moisture regime transition zone in central DRC, with sites in Af and Am under a Udic soil moisture regime (SMR) and sites in the Aw in an Ustic SMR (Soil Survey Staff, 2007, Soil Survey Staff, 2014b). Along this gradient, six site clusters were established in Lomela (under Af) at Mukumari (2.92°S; 23.48°E)and Ekomakoko (2.70°S, 24.16°E), in Katako-Kombe (under Am) at Kiete (3.62°S, 24.57°E) and Ovungu (3.82°S, 24.39°E), and in Lubefu (under Aw) at Tshumbe (4.15°S; 24.59°E), Eshima Ngandungandu/Maluanyi (4.88°S, 24.56°E (Figure 1.1). These site clusters were chosen to capture a steep climatic and vegetation gradient, as well as accessibility and the lack of local soil data in the area.

Vegetation in Sankuru province is split between forest in the north and savanna in the south and southeast, consistent with the climate gradient from Af to Aw (Figure 1.1). The tropical rainforest in the north is also synonymously termed equatorial forest or broadleaf evergreen forest (Sanchez, 2019) with at least a two-strata canopy, highly diversified tree species, and few to no herbaceous species on the floor. Savanna vegetation is of the "tall grass-low tree" type, a mix of *Hyparrhenia* sp., *Imperata* sp. and other grasses, and low, scattered trees. The precipitation range across this transect (1620 to 1740 mm/yr) is in the range where alternation between stable states of forest and savanna is predicted on the African continent (Hirota et al., 2011). On a local scale in equatorial forest, isolated savanna vegetation can occur within a matrix of forest (Markham and Babbedge, 1979, Lehmann et al., 2011). The occurrence of these isolated savannahs may be driven by interactions among soil and disturbance factors (such as natural or anthropogenic fires), and provide an opportunity to separately and interactively evaluate the impacts of both climate and vegetation on soil properties across this ecotone (Bowman and Perry, 2017).

Soils across the study transect are predominantly sandy (87 %), with some loamy-fine sands in the south and sandy-clay loam textures in the north of the transect. Parent materials for Sankuru soils derive from the sand sheets of the Salonga and Yangambi groups (Beernaert, 1999), which are underlain by consolidated and unconsolidated

materials of the Kalahari Group that covers most of the Congo Basin (Linol et al., 2015). The Salonga formation has also been synonymously termed the “Plateau sands" and is likely of early- (on the outer, upper plateau steps of the Congo basin) to late-Pleistocene (on the lower, inner plateau steps) age (Beernaert, 1999, Senut et al., 2009). The exact origins of this sand sheet appear to be complex, and it has previously been characterized as of mixed fluvial and eolian origins (Beernaert, 1999, Baert et al., 2009, Senut et al., 2009, Baert et al., 2013, Guillocheau et al., 2015). Soil organic carbon concentrations are low, decreasing on average within the top 50cm from 1.2% in forested sites in the Af climate zone to 0.6 % under savanna in the Aw climate zone. Soils are very acidic (pH < 5) and the 0-50 cm depth average soil pH decreases from Aw (pH 4.4) to Am (pH 4.2) and Af (pH 4.0). Base saturation values are also very low (< 5.5 %), with sub-active cation-exchange activity class (CEC / % clay < 0.24) (USDA 2014). X-Ray Diffraction (XRD) studies revealed no trace of 2:1 phyllosilicate in the colloidal fraction (< 2 μm of diameter). Instead, kaolinite (1:1 clay type), gibbsite, and free Al and Fe predominated, indicating a state of advanced soil weathering across the transect.

A total of 130 horizons from 26 soil profiles were sampled across the transect and triplicate samples were collected from each genetic horizon using the soil core method for bulk density measurement: a sliding hammer carefully drives a metallic cylinder sampler into the soil to minimize structure disturbance of the mineral soil samples, which is imperative for accurate soil bulk density evaluation. Samples were weighed immediately in the field then bagged before air-drying. The samples were oven-dried for 24 h at 105°C, weighed, and sieved to separate the fine earth (< 2 mm) from coarse fragments (> 2 mm). The fine earth fraction (< 2 mm) was utilized for chemical and physical characterizations. As it is inappropriate to use the clod or ring methods on organic materials, surface organic horizon bulk densities were collected using a serrated knife to cut blocks of 5 cm x 5 cm x 10cm from the pit surface before excavation. Soil morphology was described in the field, and morphological properties including soil color, structure, texture, and visual differences in volume estimates of coarse fragments were utilized to define genetic horizons (Schoeneberger et al., 2012).

Using US Soil Taxonomy, a total of 5 soil orders (Entisols (15 %), Inceptisols (62 %), Spodosols (4 %), Ultisols (15 %) and Oxisols (4 %)), 9 suborders, and 10 soil Great

Groups were identified across the Sankuru study transect. Most of the taxonomic diversity occurred at the suborder level, and Inceptisols (Humustepts and Humudepts, 62 % of all profiles) predominated in the tropical wet savanna (Aw) and tropical monsoon (Am) climate zones. In contrast, Ultisols (Kandiudults), and a single Oxisol (Acrudox) and Spodosol (Haplorthod) (23 % of all investigated profiles) were located primarily in the tropical rainforest (Af); and Entisols (Quartzipsamments, 15 % of all investigated profiles) were also identified in Af zone (Figure 1.6).

3.2.2. Soil Carbon, pH, Iron and Aluminum characterization

Total soil carbon (TC, g $100g^{-1}$) and nitrogen (TN, g $100g^{-1}$) were determined by dry combustion at 800 ºC using a LECO 2000 CN analyzer (LECO Corporation, 2003). Soil pH for mineral samples was determined in 1:1 slurry of 5 g of air-dried soil and 5 ml of water (pHH2O) followed by additional 5 ml of 0.01M $CaCl_2$ (pHCaCl2) (Soil Survey Staff, 2014a). Total elemental concentrations of Al and Fe were quantified by X-Ray Fluorescence (XRF), using an Olympus Delta P4000EX portable XRF (p-XRF) instrument (Olympus, Inc) which is equipped with a silicon drift detector (SDD), that has a resolution better than 155 eV in practice. During analysis, the instrument was mounted in a Innov-X System Stand for stability and operated remotely through a computer console. We operated the instrument in the "mining" mode, which uses the fundamental parameters (FP) approach to correct the measured X-rays for a variety of physical phenomena (e.g., absorption and fluorescence, attenuation from incoherent scattering and the photoelectric effect, differences in characteristic X-ray intensities). Measuring the elements of interest used three proprietary, built-in X-ray filters (main – tube voltage of 40kV, tube current of 50 μA; low -20kV and 100 μA; and light 6kV and 200 μA). Our analytical times were 20 s for both the "main" and "low" X-ray filters and 80 s for the "light" mode. Consequently, the total analytical time was 120s for each individual measurement.

In addition to measurements of total iron and total aluminum (Fe_t and Al_t), "free" or pedogenic Fe and Al (Fe_d and Al_d) were extracted by selective dissolution using Dithionite-Citrate solution (Jackson et al., 1986, Soil Survey Staff, 2014a). Briefly, 0.4g of sodium dithionite (a reducing agent) and 25 ml of 0.57M sodium citrate is added to 0.75 g of < 2 mm soil material and shaken overnight. The solution is subsequently centrifuged

and an aliquot is removed for analysis of Fe and Al by ICP-OES (Soil Survey Staff, 2014a). The dithionite-citrate selective extraction is thought to predominantly extract non-crystalline, amorphous, and organically-complexed Fe and Al, but is a poor extractor of crystalline Fe and Al (Wada, 1989). It is thus a reasonable measure of the total pedogenic Fe and Al oxy-hydroxides in the soil. A subset of these pedogenic Fe and Al oxy-hydroxides, amorphous "active" Fe and Al (Fe_o and Al_o), were selectively extracted with 0.2M ammonium oxalate buffered to pH 3.0 in a mechanical vacuum extractor under darkness over a period of 12 h (Soil Survey Staff, 2014a).

Assuming that Fe_t represented both crystalline and non-crystalline iron and Fe_o represented amorphous or non-crystalline iron, we estimated crystalline iron (Fe_{crys}) concentrations as the difference between Fe_t and Fe_o

$$Fe_{crys} = Fe_t - Fe_o \qquad (1),$$

where Fe_t is total iron measured by XRF and Fe_o is the concentration of iron extracted by ammonium oxalate.

3.2.3. Soil Phosphorus Extraction

3.2.3.1 Hedley Method

The Hedley extraction process is a widely used sequential extraction method to fractionate soil phosphorus into operational pools that characterize biogeochemical P dynamics and plant availability (Cross and Schlesinger, 1995, Condron and Newman, 2011, Do Nascimento et al. 2015). The Hedley method has been modified multiple times by Condron and Goh (1989), Chen et al. (2000), and Moir and Tiessen (2007). A modified Hedley sequential phosphorus extraction methodology (Margenot et al., 2017) was employed to separate P into operational pools. Anion exchange membrane (AEM) and H_2O were used in initial steps for extraction of inorganic and organic P loosely bound in the diffuse ion swarm (AEM-P_i and H_2O-P_o); $NaHCO_3$ to capture inorganic and organic P ($NaHCO_3$-P_i and $NaHCO_3$-P_o) in the outer-sphere surface complex zone; NaOH to extract inorganic and organic P (NaOH-P_i and NaOH-P_o) inside the inner-sphere surface complex; and HCl to dissolve recalcitrant and/or primary inorganic P from Ca-associated P mineral (HCl-P_i). The final outputs of this process therefore led to four operational inorganic P

pools (AEM-P_i, $NaHCO_3$-P_i, NaOH-P_i, and HCl-P_i) and three operational organic P pools (H_2O-P_o, $NaHCO_3$-P_o, and NaOH-P_o).

The solid-solution interface, a site of intense surface complex development due to chemical interactions between soil solution solutes and surface functional groups of the soil exchange complex (charged sites on soil colloids), is the focal location for orthophosphate extraction. Aqueous ortho-phosphate anions in soil solution form complexes with surface functional groups of phyllosilicate and metal oxides/hydroxides/oxyhydroxides of Al^{+3}, Fe^{+3}, Ca^{+2}, etc. (Essington, 2015, Xu et al., 2016). The interface structure encompasses the following surface charge density components from the soil solid surface into the soil solution: net proton (pH dependent) charge (σ_H), inner-sphere charge (σ_{is}), out-sphere charge (σ_{os}), and diffuse ion swarm charge (σ_d) (Essington, 2015). These charges define adsorption planes (or layers): s-plane with σ_H charges at mineral solid surface, inner-sphere plane with σ_{is} charges for complex ions, out-sphere plane with σ_{os} for ion pair, and d-plane with σ_d for counterions. Ions at every adsorption layer, contribute to neutralize intrinsic mineral charges (σ_{is}+ σ_o), where σ_o is permanent structural charge density from isomorphic substitution (Essington, 2015).

This structure is the chemical and electrochemical framework from where phosphate fractions are presumed to be extracted sequentially from d-plane through os-plane to is-plane with increasing extractant power (resin, $NaHCO_3$, NaOH, and HCl) as the orthophosphate ligand exchange process (phosphate ion replacing hydration molecule) grows stronger from the diffuse zone to the inner-sphere by forming potentially various surface complexes of the nature of monodentate-mononuclear, bidentate-mononuclear, and bidentate-binuclear (Essington, 2015, Parfitt and Smart, 1978). Nevertheless, the actual P extraction may not be occurring as strictly sequential and contained within the boundaries of discrete P fractions (Guo and Yost, 1998, Condron and Newman, 2011). Guo and Yost (1998) recognized difficulties of identifying discrete phosphorus pools due to the complexity of soil phosphorus chemistry and mineralogy, as phosphorus availability may best be viewed as a continuum.

Utilizing the Hedley method therefore requires understanding important caveats with regard to assigning operational Hedley P pools to discrete P fractions as is often done in the literature. For example, resin-P_i and $NaHCO_3$-P_i and P_o are often assigned to labile

or easily mineralized P pools, while NaOH-P_i is ascribed to secondary mineral P_i adsorbed to Fe and Al oxy-hydroxides, NaOH-P_o is ascribed to stable P_o, and HCl-P_i is ascribed to Ca-P or apatite P (Yang et al., 2011, Yang et al., 2014, Barrow et al., 2021). However, these sequentially extracted pools are not necessarily strictly selective (Gu et al., 2020, Barrow et al., 2021), and assigning Hedley pools to discrete soil P fractions may be depending in part on the bio-geochemical context (edaphic properties, mineralogy) of a given soil (Gu and Margenot, 2021). Additionally, P in soils may be more likely to exist in adsorbed forms which can penetrate variable charged particles rather than as discrete precipitates (Barrow, 2020). Nevertheless, provided that Hedley operational P pools are not automatically taken as representative of discrete soil P pools in all contexts, the Hedley procedure can provide important insights into transformations and lability of the soil P (Gu and Margenot, 2021).

Sequential extraction methods have also led to the assignment of sequential Hedley P pools as requiring more and more efforts from plants to extract and longer timeframes of P turnover (Hou et al., 2019), despite the fact that plants can draw down on multiple P pools simultaneously (Guppy, 2021). Extractable phosphorus simply estimates soil buffering capacity in short term (labile-P), moderate, or long-term depending on the type of extracted phosphorus fraction. For example, in natural (unfertilized) ecosystem, labile-P fraction (resin-P_i and $NaHCO_3$-P_i) is considered a rapid turnover P form (Cross and Schlesinger, 1995) within a few days (Hou et al., 2018a); NaOH-P_i fraction can become available in months (Hou et al., 2018b) and is seen as a slow turnover form of P (Cross and Schlesinger, 1995); availability of organic P form ($NaHCO_3$-P_o, NaOH-P_o) can occur in weeks (Hou et al. 2018a); and HCl-P_o/P_i turnover is very slow and can happen in decades (Hou et al., 2018b). Guo and Yost (1998) suggested three soil P pools: readily available (AEM-P_i and $NaHCO_3$-P_i), reversibly available (NaOH-P_i, NaOH-P_o, $NaHCO_3$-P_o, and HCl-P), and sparingly available (residual-P absent in younger soil). However, in reality, plants are able to draw down soil P from multiple operational fractions at the same time (Guppy, 2021).

3.2.3.2 Total P Analysis

Total soil P was measured via digestion with nitric acid and hydrogen peroxide (Kimbrough and Wakakuwa, 1989). In brief, 0.250 g of soil ground to <0.1 mm diameter was incubated in 2.000 mL of 15.9 M (glacial) nitric acid (trace metal grade) for 16 h at room temperature. The mixture was subsequently incubated at 100 ℃ in a block heater for 1 h. After cooling to room temperature, 0.125 mL of 30 % hydrogen peroxide (trace metal grade) was slowly added, and the mixture was incubated at 100 ℃ for an additional 0.5 h. This was repeated twice. Finally, 0.250 mL of hydrogen peroxide was added and the mixture was incubated at 100 ℃ for a final 3 h until the total volume was reduced to 2 ml. The resulting digest was diluted to a final volume of 10 mL using 18.2 MΩ-cm water. Orthophosphate-P in the resulting solution was quantified by molybdate colorimetry at 882 nm (Murphy and Riley 1962). The difference between P_t and the sum of Hedley extractable P fractions was assumed to represent occluded P (P_{occ}) (sometimes termed "residual P") within the context of the Hedley fractionation:

$$P_{occ} = P_t - \sum P_{Hedley} \quad (2),$$

where ΣP_{Hedley} = AEM-P_i + H_2O-P_o + $NaHCO_3$-P_i + $NaHCO_3$-P_o + NaOH-P_i + NaOH-P_o + HCl-P_i.

3.2.3.3 Bray P1 Available P

The Bray-Kurtz P1 test (Bray P1 test, or "standard" Bray) is a chemical extraction to estimate soil phosphorus lability and the amount of soil phosphorus that can become quickly available to satisfy plant phosphorus needs (Bray and Kurtz 1945). During the extraction process, diluted reactants hydrochloric acid (0.025M HCl) and ammonium fluoride (0.03M NH_4F) respectively promote P mineral dissolution and P desorption which increase the soil solution orthophosphate concentration. Simultaneously, Al^{+3} and Fe^{+3} precipitate in the form of AlF_3 and FeF_3, a process that prompts further dissolution and desorption, consistent with mass action law. In acidic soils (such as those on the Sankuru transect, which have an average pH of 4.2), strengite ($FePO_4 \bullet 2H_2O$) and variscite ($AlPO_4 \bullet 2H_2O$) control soil solution P concentration. The concentration of P measured by Bray 1P depends on the existence of acid-soluble and adsorbed forms of soil phosphorus that are tested more appropriately in acid soil (pH ≤ 7), where adsorbed P content is the highest (Bray and Kurtz, 1945). Adsorbed P is the most effective soil P form relative to

plant nutrient demand with instant implication to plant development (Bray and Kurtz, 1945) as supported by high correlation coefficients of 0.74 to 0.94 between P plant uptake and P concentration recorded in the Midwest, USA (Watson and Mullen 2007).

3.2.3.4 P_{ox} and P_{CBD} extraction

From the soil mineral weathering process (Schwertmann, 1991, Sokolova, 2013), iron and aluminum are released as $(Fe^{3+})_{aq}$ and $(Al^{3+})_{aq}$ into soil solution where they react with soil phosphate through inner- and outer-sphere complexes (Scarseth, 1935). These new ion complexes will precipitate and either crystallize or remain noncrystalline (Jones and Uehara, 1973, Shen et al., 2000). P associated with ammonium oxalate extractable Fe and Al (P_{ox}), and citrate-dithionite extractable Fe and Al (P_d) was measured in solution following extractions with each process as described in section 2.2.

3.2.4. Statistical Analysis

All statistical analyses were performed in R (version 3.3.1, R Core Team, 2019). We utilized Pearson's correlation coefficient (with the Bonferroni correction for multiple comparisons) to examine the relationship between measured soil properties across all samples. Post-hoc analyses for significant differences in response variables between vegetation, climate, and depth groupings following ANOVA analyses were conducted using Tukey's Honest Significant Difference (HSD) in group means. Unless otherwise mentioned in manuscript text or figure captions, all reported uncertainties represent a single standard deviation around the mean.

Because our dataset represents a mixture of sites sampled by genetic horizon, we chose to utilize Land Degradation Surveillance Framework (LDSF) (Vågen et al., 2013) standardized depth increment (0–20 cm, 20–50 cm, and 50–100 cm (combining the 50–80 cm and 80–100 cm LDSF standardized depth increments into one 50–100cm increment) weighted averages to compare soil properties by depth between sites. We calculated the weighted averages of all available soil properties by depth increment for each sampling site using the "slab" function in the AQP package in R (Beaudette et al., 2013, R Core Team, 2019). These standardized depth-increment weighted averages were utilized to examine the relationships between soil properties and site-level characteristics such as land use,

landscape position, vegetation, and climate using ANOVA. The effects of climate and vegetation on soil physical and chemical properties were evaluated using both ANOVA (for categorical variables vegetation and Köppen climate zone) and regression models (for the continuous covariates mean annual precipitation (MAP) and latitude). Because the soils investigated in this study were coarse fragment-free, we calculated stocks of soil constituents for a defined depth increment by multiplying the concentration of individual soil constituents by the bulk density of the fine-earth and the increment thickness. All unit conversions were made to the original data prior to calculating stocks. Constituent stocks were expressed in g/m^2 for P_t and individual P fractions.

To assess the nature of the relationship between the many P pools measured in this study, in addition to correlation analysis, we conducted cluster analysis and structural equation modelling. For cluster analysis, ascendant hierarchical clustering of the full dataset of P pools measured for all samples was conducted using the *hclustvar* function in the *ClustofVar* package in R (Chavent, 2017). In this function, the aggregation criterion is the decrease in homogeneity for the clusters being merged. The homogeneity of a cluster is the sum of the correlation ratio (for qualitative variables) and the squared correlation (for quantitative variables) between the variables and the center of the cluster which is the first principal component from principle components analysis (PCA) of the data.

Structural equation modeling or path analysis followed the procedure in Wade et al. (2020) and Hou et al. (2018a), with some modifications. An initial conceptual model was constructed with two exogenous variables (Mean Annual Precipitation (MAP), and vegetation type), a number of soil chemical properties known to influence P cycling and transformations in soil (SOC, pH, Fe_t, Fe_d, Fe_o, Al_t, Al_d, Al_o), and all measured soil P pools, with Bray P as the ultimate response variable (Figure 3.1). We calculated the standardized total effects of the exogeneous and endogeneous variables for each path in the initial conceptual model. Secondary variables and paths were excluded from the final model if they did not have a significant effect ($\alpha = 0.05$) on any additional variables. Since we were only evaluating a single model, goodness of fit indices (which are relative measures) were not conducted on the final model.

3.3. Results

3.3.1. Fe, Al, pH, and Organic Carbon

Across all samples, Fe_t concentrations ranged from 0.1 to 5.2 % (mean 1.51 ± 1.10 %) and Al_t concentrations varied from 0.5 to 10.8 % (averaging 4.94 ± 2.07 %) (Table 3.1), and Fe_t and Al_t were moderately correlated (Pearson's r = 0.66) and linearly related (R^2 = 0.43, $p < 0.001$) (Table 3.1). However, iron and aluminum extractable by CBD (Fe_d and Al_d, respectively) and iron and aluminum extractable by ammonium oxalate (Fe_o and Al_o, respectively) were not significantly correlated or linearly related. Pedogenic or "free" iron (Fe_d) was strongly correlated to Fe_t across all samples ($r = 0.96$, $p < 0.01$), while Fe_o was not significantly correlated to Fe_t. Fe_d accounted for 37 ± 8% of Fe_t (157 to 20,588 mg/kg), while Fe_o accounted for 18 ± 10% of Fe_t (92 to 5,330 mg/kg). Non-crystalline iron proportion of pedogenic iron (Fe_o/Fe_d) ranged from 2.7 to 171%, with an average of 52.1 +/- 30.2%. Fe_{crys} concentrations were highly variable across samples, but ranged from 946 mg/kg to 50,622 mg/kg, with an average of 13,152 ± 10,994 mg/kg.

Al_d accounted for 3 ±2 % of Al_t (229 to 3,848 mg/kg), while Al_o accounted for 5 ±5% of Al_t (127 to 16,876 mg/kg) (Table 3.1). Across all samples, soil pH ranged from 3.4 to 5.5 with a mean of 4.4 ± 0.4. Al_d and Al_o increased with increasing pH ($r = 0.31$ and 0.58, respectively, $p < 0.01$), while Fe_d showed a weak decrease with increasing pH ($r = -0.25$) and Fe_o was not significantly related to pH. Soil carbon concentrations ranged from 0.1 to 26.3% SOC (17.2-26.3% SOC were measured in the organic litter layers of forested sites, but otherwise the maximum SOC concentration observed was 5.5%), but were generally very low (mean 0.9 ± 0.3%, median = 0.5%).

3.3.2. Absolute magnitude and relative proportions of soil P fractions

Total soil P concentrations across all sites and depths ranged from 41.8 to 675.3 mg/kg (averaging 210.8 ± 135.4 mg/kg), while Hedley extractable P ranged from 22.4 to 504.7 mg/kg (mean 157.2 ± 11.8 mg/kg) (Table 3.1). Among Hedley P fractions, NaOH-Pi (72.0 ± 64.6 mg/kg) and NaOH-P_o (38.1 ± 30.4 mg/kg) made up the largest proportion of Hedley extractable P, accounting for, on average 44.0 ± 18.0 % and 30.2 ± 17.1 % of

total Hedley extractable P, respectively, or nearly 75% of Hedley extractable P combined. The remainder of Hedley extractable P was relatively evenly distributed between $NaHCO_3$-P_i (average of 5.6 ± 3.8% of Hedley Extractable P), $NaHCO_3$-P_o (average of 6.8 ± 5.4% of Hedley extractable P), HCl-P_i (5.8 ± 4.7% of Hedley P), and H_2O-P_o (average of 4.9 ± 4.7% of Hedley P), along with AEM-P_i made up the smallest proportion of Hedley P (2.6 ± 3.5 of Hedley P).

Among organic P fractions, NaOH-P_o made up, on average, over 70% of total Po (70.9 ± 14.4 %), with $NaHCO_3$-P_o and H_2O-P_o making up approximately even proportions of the remaining organic P (16.0 ± 10.0 and 13.0 ± 10.8, respectively). Total-Po ranged from 2.6 to 189.5 mg/kg (average of 52.1 ± 39.6 mg/kg), and made up, on average 24.6 ± 21.5 % of Hedley P and 30.0 ± 18.2 % of P_t. P_{occ}, the difference between the sum of Hedley extractable P fractions and P_t, Equation 1) was highly variable, averaging 58.8 ± 66.9 mg/kg across all samples and making up, on average, 28.4 ± 22.4 % of P_t.

Bray P ranged from 1.5 to 133.6 mg/kg across all samples (mean 32.5 ± 31.6 mg/kg, with a median value of 20.9 mg/kg), and accounted for, on average 14.6 ± 0.9% of P_t. P_d and P_{ox} concentrations, on average, exceeded all individual Hedley fractions by a minimum factor of 2 to 3. P_d (205.2 ± 138.2 mg/kg) was nearly equivalent to P_t (210.8 ± 135.4 mg/kg) in absolute magnitude, and in fact 57% of all samples had a higher concentration of P_d than P_t . P_{ox} ranged from 13.0 to 659.2 mg/kg across all samples (average of 164.1 ± 139.9 mg/kg) and comprised an average of 76% of P_t and 92% of P_d.

3.3.3. Linear Relationship Tests between measured P fractions

Multiple correlation tests were performed (Pearson's correlations, with Bonferroni correction for multiple tests) among different P fractions to better understand their inter-relationships (Table 3.2). The three Hedley organic P fractions (H_2O-P_o, $NaHCO_3$-P_o, and NaOH-P_o) were correlated most strongly to each other (Table 3.2), with only weak or non-significant correlations with the inorganic P fractions and Bray P, P_d and P_{ox}. The only exception to this was that H_2O-P_o was moderately correlated to AEM-P_i and $NaHCO_3$-P_i (r = 0.63 and 0.56, respectively). AEM-P_i was most strongly correlated to $NaHCO_3$-P_i (r = 0.85), but was also strongly and significantly correlated to Bray P (r = 0.75), P_d (r = 0.71), H_2O-P_o (r = 0.63) and P_d (r = 0.71). $NaHCO_3$-P_i, NaOH-P_i, HCl-P_i, and Bray P were all

strongly and significantly positively correlated to P_{ox} and P_d. $NaHCO_3$-P_i was also strongly and significantly correlated to NaOH-P_i ($r = 0.66$) and Bray P ($r = 0.74$), and HCl-P_i was strongly correlated to Bray P ($r = 0.62$). Occluded P was unique in that was not significantly correlated (or only very weakly correlated) to any of the other extracted P fractions. Bray P was most strongly correlated with AEM-P_i ($r = 0.75$) and $NaHCO_3$-P_i ($r = 0.74$), followed by HCl-P_i ($r = 0.62$).

Hierarchical cluster analysis revealed four major clusters of P fractions and six minor clusters (Figure 3.2). Partition stability for the clusters reached a minimum at six clusters, so the tree containing six minor clusters was retained. This analysis shows that AEM-P_i and H_2O-P_o, fractions most associated with highly labile P_i and P_o, were uniquely and closely associated. P_{occ} was largely excluded from clustering with other variables, and the two other Po fractions ($NaHCO_3$-P_o and NaOH-P_o) formed a cluster. A major cluster was formed with the remaining measured P fractions. Three pairs of P fractions, including NaOH-P_i and HCl-P_i, $NaHCO_3$-P_i and Bray P, and P_{ox} and P_d, respectively were closely clustered and on a single branch of the tree distinct from the highly labile fractions (AEM-Pi and H_2O-P_o), the major organic fractions ($NaHCO_3$-P_o and NaOH-P_o), and P_{occ}.

3.3.4. Relationships between P fractions and Fe, Al, pH, and organic carbon

The major variables investigated as influencing P fractions were assumed to be organic carbon, pH, Fe and Al and the two derived Fe variables: non-crystalline iron proportion (Fe_o/Fe_d) and crystalline iron concentration (Fe_{crys}). Total P_o (the sum of all three Hedley P_o fractions) was weakly but significantly linearly related to organic carbon concentration ($r = 0.12$, $p < 0.001$) (Figure 3.3). Organic carbon to organic phosphorus ratios (C:P_o) ranged from 28 to 513 across all samples (mean of 151 ± 94), and were significantly linearly related to both organic carbon concentration ($p = 0.03$) and pH ($p < 0.001$) ($r = 0.22$, $p < 0.001$, multiple linear regression).

AEM-P_i was only very weakly related to any measured non-P variables. Although AEM-P_i was significantly related to pH, Fe_o, and organic carbon, these relationships were weak. At pH values greater than 4.5, AEM-P_i concentrations were significantly reduced (Figure 3.3b). $NaHCO_3$-P_i was significantly linearly related to only two non-P variables, pH and Fe_o ($r = 0.29$, $p < 0.001$). NaOH-P_i was significantly linearly related to only one

non-P variable, Fe_o; with the exception of the relationships between P_{occ} and iron fractions (discussed below), the relationship between NaOH-P_i and Fe_o was the second strongest between any of the P fractions and a non-P variable in our dataset ($r = 0.44$, $p < 0.001$, Figure 3.3c). NaOH-P_i and Al_o were not significantly linearly related ($p > 0.10$, Figure 3.3c). HCl-P_i is typically assumed to represent the P fraction associated with Ca. However, our study sites' soils are extremely acidic and calcium concentrations are very low and sometimes below detection limits. Therefore, it is unlikely that for these soils HCl-P_i represents Ca associated P, but rather an additional Fe and Al associated P fraction not extracted by NaOH. This is supported by the fact that HCl-P_i is significantly linearly related to Fe_o and in fact this is the strongest relationship between any P fraction and non-P variable in our dataset ($r = 0.56$, $p < 0.001$, Figure 3.3d).

P_{occ} was significantly linearly related to Fe_{crys} concentration ($r = 0.38$, $p < 0.001$), total Fe_t ($r = 0.56$, $p < 0.001$, Figure 3.3e), and Fe_d ($r = 0.49$, $p < 0.001$). Additionally, as Fe_t increased, the proportion of P_t that was occluded increased significantly. As Fe_t concentrations increased above 3 %, proportion of P_t that was occluded abruptly increased to > 60%. P_{ox} was most closely related to Fe_o, and they were linearly and significantly related ($r = 0.41$, $p < 0.001$, Figure 3.3f). Interestingly, P_d was not significantly related to Fe_d or any other exogenous measured or derived variables, but was significantly linearly related to Fe_o ($r = 0.32$, $p < 0.001$) as well. Bray P was significantly linearly related to both $NaHCO_3$-Pi ($r = 0.83$, $p < 0.001$, Figure 3.3g) and NaOH-P_i ($r = 0.71$, $p < 0.001$, Figure 3.3h).

3.3.5. Variability of Fe, Al and P concentrations with depth across climate and vegetation gradients

Major differences in Hedley P fractions by vegetation type were limited primarily to NaOH-P_i and NaOH-P_o, and sum of Hedley P. In the case of each of these fractions, soils under savanna vegetation, on average, had values nearly double those of soils under forest vegetation in the top 20 cm with the exception of NaOH-P_i, which remained significantly higher under savanna vegetation as deep as 100 cm (Table 3.3). Inorganic P (P_i) fractions were insensitive to the climate zone. However, there was a significant interaction of vegetation and climate zone ($p < 0.001$, ANOVA). In the top depth

increments (0-10 and 10-20 cm), AEM-P_i, $NaHCO_3$-P_i, NaOH-P_i, and HCl-P_i were higher in soils under savanna vegetation in Af and Am, than soils under forest vegetation in Af and Am, and also significantly higher than soils under savanna vegetation in Aw (Table 3.3). These differences were less pronounced through the 20-50 cm depth increment, and became largely non-significant in the deepest depth increments (50-100 and 100-200), with the exception of HCl-P_i, where soils under savanna remained significantly higher than other vegetation/climate zone categories even in the deepest depth increments (Table 3.3). P_{occ} was higher in Af than Am or Aw soils across all depth increments, but did not differ by vegetation categories. However, for vegetation/climate zone combinations, occluded P was highest in Af savanna and Af forest across the 20-50 and 100-200 cm depth increments, and highest in Af savanna in the 0-10 and 50-100 depth increments (Table 3.5, 3.6, 3.7).

Total P_o was greatest in soils of the Am for all depth increments below 10 cm (Table 3.4), and was higher in savanna vegetation relative to forest vegetation in the 0-10, 10-20 and 20-50 cm depth increments (Table 3.3). For vegetation/climate zone combinations (Table 3.5), Am savanna soils had significantly higher Total P_o concentrations than all other vegetation/climate zone combinations in the 0-50 (Table 3.5), 50-100 (Table 3.6) and 100-200cm (Table 3.7) depth increments. Am forest soils and Am savanna soils were significantly higher in Total P_o than other vegetation/climate zone combinations in the 20-50cm depth increment. C:P_o ratios were higher than all other climate zone/vegetation combinations in Af forest soils for the 0-10, 10-20, and 20-50cm depth increments. For these same depth increments, Am forest soils had higher C:P_o ratios than Am savanna soils, although both of these were still lower than Af forest soils.

Fe_t was highest in soils of the Af climate zone ($p < 0.000$) across nearly all depth increments, but there were no significant differences in Fe_t for vegetation type or Al_t for either climate zone or vegetation type. No significant differences between Fe_t and Al_t were detected between climate zone/vegetation combinations at any depth. No significant differences were detected in Fe_d and Al_d for the top depth increments 0-10, 10-20 cm, but Aw savanna soils had lower values than other groups in lower depth increments (100-200 cm for Al_d, 20-50, 50-100, 100-200 for Fe_d). Fe_o concentrations were higher in Af savanna than Am and Aw savanna in the top depth increment (0-10 cm), and higher than Aw

savanna in the 10-20 and 20-50 cm depth increments. In the deepest depth increments, Af savanna had greater Fe_o than soils under forest vegetation and Aw savanna.

P_t was highest in Af and Am relative to Aw in the deepest depth increments 50-100 and 100-200, but not significantly different in the top depth increments 0-10, 10-20, 20-50. No significant differences were detected between forest and savanna vegetation at any depth. However, between climate zone/vegetation categories, P_t was highest in Af forest and Af savanna in the top depth increments (0-10, 10-20), while for all other depth increments Af savanna soils exceeded all other climate zone/vegetation categories in P_t concentrations 20-50, 50-100, 100-200. Bray P did not differ by climate zone or vegetation, but was significantly different between climate/vegetation combinations. Bray P was highest ($p < 0.001$) under savanna vegetation in the Af and Am climate zones in the top depth increments (0-10 and 10-20cm), while significant differences were not detected below 20cm.

3.3.6. P stocks across climate and vegetation gradients

Phosphorus stocks in the top 50 cm across the climate gradient in the Sankuru transect are shaped by three major pools with the following average proportions of P_t: organic phosphorus (P_o) (~33 %), P_{occ} (~21 %), and non-occluded phosphorus (non-occ P_i) (~44 %) (Figure 3.4d). P_o stock proportion remained almost constant in Am and Aw (about 42 % & 43 % respectively) but was over 3-fold lower in Af (~14 %). P_{occ} is the predominant pool in the Af zone (~ 41%) especially in Af-forest (~51%). The non-occluded P pool (which is the largest pool) increases to about 54 % of total-P in the Am zone and up to around 57 % in Am-savanna (Figure 3.4d).

Stocks of H_2O-P_o, $NaHCO_3$-P_o, and NaOH-P_o, sum of Hedley extractable P and total P_o were greatest in Am soils (165 ± 94.6 g m^{-2} and 72 ± 29 g m^{-2}, respectively, (Figure 3.4a). Stocks of P_t, $NaHCO_3$-P_i and NaOH-P_i were highest in savanna soils in the Af and Am climate zones (Figure 3.4a). This mirrored patterns of P_d and Fe_o, which were also highest in savanna soils in the Af and Am. Stocks of P_{occ} (Equation 2) were significantly higher in soils of the Af climate zone (average of 68.9 ± 7.3 g m^{-2}) than in soils of the Am and Aw climate zones (7.3 ± 9.0 and 15.0 ± 10.4 gm^{-2}, respectively), regardless of vegetation type. Stocks of P_{ox}, Fe_t, and Fe_d were also highest in soils of the Af climate zone

relative to the Am and Aw climate zones, regardless of vegetation type. Patterns of soil P stocks in the top 50 cm (the most critical zone for plant roots and nutrient access, Table 3.5) did not significantly differ from the relative rankings or patterns of P stocks in deeper increments (50-100 cm and 100-200 cm). Therefore, although we present data on P stocks in those depth increments in Tables 3.6 and 3.7, only P stocks in the top 50 cm are discussed here.

Furthermore, some individual P fractions have exhibited relative prevalence in their respective combined pools (Table 3.5) within the top 50 cm. Among the organic P fractions ($NaHCO_3$-P_o, NaOH-P_o, and H_2O-P_o), the NaOH-P_o fraction constituted about 71% of the total-P_o across the climate gradient and reached about 78 % of Total-P_o in Aw (Figure 3.4b). P_{occ} reaches ~ 41% of P_t in Af with a peak of 51% in Af-forest, but averages only 21% of total-P across the climosequence (Figure 3.4b). The non-occluded P_i pool, which peaks at ~58% in Am-savanna (Figure 3.4c), encompasses four different P_i fractions (AEM-P_i, $NaHCO_3$-P_i, NaOH-P_i, and HCl-P_i). The NaOH-P_i fraction is the dominant fraction in the non-occluded P_i pool with an average proportion of about 73 % of the total non-occluded P_i throughout the transect (Figure 3.4). Nevertheless, AEM-P_i and HCl-P_i share similar proportions to Total-P of about 4 % or less. $NaHCO_3$-P_i proportion to Total-P is also low and peaks at around 9 % in Am-savanna.

3.3.7. Effects of Fe, Al and P fractions on available P – Path Analysis.

Path analysis showed that our two exogenous variables (MAP and vegetation type) exerted controls on differing input variables (Figure 3.5). MAP primarily influenced Fe_t ($p < 0.05$) and Fe_o ($p < 0.0001$) (and therefore, by proxy, Fe_{crys}), while vegetation primarily influenced pH (savanna = higher pH, forest = lower pH, $p < 0.0001$) and Fe_o (savanna = higher Fe_o, forest = lower Fe_o, $p < 0.0001$). Therefore, both exogenous variables exerted a primary influence on Fe_o, which resolutely emerged as a master variable explaining P distribution and availability in our dataset (Figure 3.5). Fe_o increases with increasing MAP and is higher under savanna vegetation than forest vegetation in the Af and Am climate zones. SOC and Al_o (two additional variables in our dataset hypothesized to control P distribution and availability) were not significantly influenced by MAP and vegetation when using the path analysis protocol implemented in this analysis.

Fe_o, in turn, exerted a major control on all of the measured P_i fractions (Figure 3.5). The two highly labile Hedley fractions (AEM-P_i and H_2O-P_o) were inversely influenced by pH, and $NaHCO_3$-P_o and NaOH-P_o were influenced by SOC. Importantly, HCl-P_i was influenced primarily by Fe_o but also by Al_o. P_{occ} was primarily influenced by Fe_t and Fe_o (and therefore, by proxy, Fe_{crys}, $p < 0.0001$), and available P, as measured by Bray I, was most significantly influenced by the NaOH-P_i and $NaHCO_3$-P_i pools in our dataset.

3.4. Discussion

3.4.1. Association of Hedley fractions to other extractable P pools and soil properties

The results of our correlation analysis, cluster analysis, and path analysis show that several Hedley P pools share a close association with other extractable P pools and soil properties in the sandy, kaolinitic, acidic soils investigated in this study. The two major Hedley P_i pools in our soils were NaOH-P_i and $NaHCO_3$-P_i (which, together make up nearly 75 % of non-occluded P), and it is clear from our analysis that amorphous iron (as approximated by Fe_o) is the major control on these non-occluded inorganic P pools (and thus on non-occluded inorganic P in general) in Sankuru soils (Figure 3.5). This is consistent with previous studies which have shown the high importance of amorphous iron in generating reactive surface area, particularly in sandy soils (Borgaard et al., 1982, Pronk et al., 2011, Wagai et al., 2013, Gypser et al., 2018). In Sankuru soils, amorphous iron is orders of magnitude more abundant than pedogenic aluminum and thus may provide more reactive surface area for P adsorption because the parent material is predominantly siliceous, pre-weathered, and quartz dominated. Pedogenic Al is much more likely to play a major role in P adsorption in highly weathered soils which are finer in texture (Fontes and Weed, 1996) or derived from volcanic parent materials (Hashimoto et al., 2012, Takamoto et al., 2021).

Bray P was most strongly correlated with $NaHCO_3$-P_i ($r = 0.74$) and AEM-P_i ($r = 0.75$), but these two pools combined were, on average 10 to 40 mg/kg smaller than the Bray P pool. If we consider the Hedley fractions most strongly correlated to Bray P to be contributing to the available P pool, then the most likely fractions contributing to Bray P in addition to $NaHCO_3$-P_i and AEM-P_i are either HCl-P_i or NaOH-P_i.

The Hedley HCl-P_i fraction has been historically assigned to a discrete Ca-P or apatite pool, but increasing evidence indicates that – for some soils – the P_i extracted by HCl is not necessarily apatite P (Walker and Syers, 1976, Helfenstein et al., 2020). Given that Ca is often below the limit of detection in our soils, pH is generally < 5.0, and XRD analysis revealed only kaolinite, gibbsite, and quartz in the bulk soil and clay fraction, it is highly unlikely that there is any apatite or Ca-associated P in Sankuru soils (Brucker and Spohn, 2019). Across all samples in our study, the Hedley HCl-P_i fraction (which made up, on average approximately 5% of non-occluded Hedley extractable P_i) was most closely associated with Fe_o and Al_o, suggesting that in the case of these low pH, sandy soils, that the operationally defined HCl P_i fraction, usually interpreted as calcium phosphates such as apatite, may be the result of extracting more Fe and Al- associated P_i that was not extracted by the NaOH and $NaHCO_3$ steps. This phenomenon has been observed in previous studies for some soils or pure minerals (Barrow et al., 2020, Helfenstein, 2020, Gu et al., 2020), and highlights the need for context-dependent interpretation of Hedley P_i pools that depends on specific soil properties (Gu and Margenot, 2021). Taken as a whole, these results suggest that approximately 80 % of the non-occluded P in these soils is controlled by non-crystalline, amorphous iron. The remaining non-occluded P is predominantly in organic forms. Occluded P (which made up, on average, 22 % of P_t stocks in the 0-50 cm depth increment) was not driven by Fe_o but rather by Fe_t, indicating an association with crystalline iron forms not predominantly extracted by Fe_o (Schwertmann, 1973).

3.4.2. Magnitude of Sankuru P stocks and fractions in global context

The total 0-50 cm phosphorus stocks reported here were reasonably close to, but somewhat higher than expected for the Sankuru region and our study sites from previous global gridded predictions of soil P_t and operational P fractions (Yang et al., 2013, Yang et al., 2014), which predicted P_t stocks for the 0-50 cm depth of 45 to 135 g/m2 in Sankuru. Our measured P_t stocks for 0-50 cm depth ranged from 44 to 405 g/m^2, with an average of 143 ± 99 g/m^2 (Table 3.5). Our measured organic P stocks ranged from 9 to 111 g/m^2, with an average of 44 ± 28 g/m^2, while Yang et al (2013) predicted total organic P stocks to this depth for our study area of 9 to 35 g/m^2. Occluded P in our study was in line with

predictions from global datasets. Our measured P_{occ} stocks ranged from 0 g/m^2 to 135 g/m^2, with an average of 31 ± 36 g/m^2, while Yang et al (2013) predicted values for the study area ranged from 27 g/m^2 to 68 g/m^2. Our measured labile P stocks (defined by Yang as AEM-P_i + $NaHCO_3$-P_i) were significantly higher than predicted by Yang et al. (2013), ranging from 1 g/m^2 to 50 g/m^2, with an average of 13 ± 15 g/m^2, while Yang et al (2013) predicted values for the study area ranged from 3 g/m^2 to 9 g/m^2.

In our study, concentrations of P pools at the 0-30 cm depth increment were higher than expected when compared to other tropical soils, and sandy soils in particular. For example, average concentrations of most P fractions on the Sankuru transect (P_t 219 ± 162 mg/kg, total P_o 67 ± 45 mg/kg, P_{occ} 45 ± 53 mg/kg) were significantly higher than those reported in previous studies on Arenosols in the Amazon Basin (P_t 34-37 mg/kg, Total P_o of 12-15 mg/kg, and P_{occ} of 0-13 mg/kg in the upper 30cm (Quesada et al., 2010), and higher than some P fractions reported in Ultisols and Spodosols in peninsular Thailand (P_t 39-162 mg/kg, Total P_o of 20-80 mg/kg, and P_{occ} 1-64 mg/kg) (Orthong et al., 1999).

The average P_t concentration in our dataset (across all sampling depths) was 210 ± 184 mg/kg. This is in line with P_t concentrations expected for more highly weathered soils such as Ultisols and Oxisols (Yang et al., 2011). Several studies using global datasets have utilized soil order classification as a categorical variable to differentiate between soil P stocks and fractions, drawing conclusions about the impact of high weathering intensities on soil P pools (Yang et al., 2011, Uygur et al., 2017, Dzombak et al., 2020). It is important to note that while this approach may be successful in temperate ecosystems, it may be confounded in tropical environments, particularly on extremely coarse-textured soils such as our study transect in central DRC, because equating degree of weathering with central concepts of soil orders can lead to some fallacious conclusions. Soils of the Sankuru transect are highly weathered, acidic, kaolinitic soils, but the lack of major subsoil development due to sandy parent materials lead to many being classified as Entisols and Inceptisols instead of Ultisols and Oxisols. Therefore, it is more appropriate to view these soils as sandy Ultisols or Oxisols than Entisols or Inceptisols when considering their absolute age or weathering degree or when constructing conceptual models with the data.

3.4.3. Phosphorus in relation to climate, vegetation, and pedogenesis

The Sankuru transect is unique in that it consists of relatively homogeneous, sandy parent materials distributed across a climatic and vegetation gradient in the humid tropics (Figures 1.1 and 1.6). Although there have been P chronosequence studies on sandy soils (Koojiman et al., 2009) and several studies focusing on vegetative differences across ecotones with more variable parent materials (Frossard et al., 1989) in temperate and semiarid (Zhao et al., 2009) regions, to our knowledge, this is one of only a handful of studies across vegetative and climate gradients in the humid tropics (Lloyd et al., 2015, Sugihara et al., 2014) and one of the only studies to examine a well constrained bio-climosequence in the humid tropics. Other studies in the humid tropics have focused primarily on the impacts of land use change (Maranguit et al., 2017) or topography (Araujo et al., 2004) on P distribution. Additionally, the data from this study fills a major gap in soil P studies in central Africa and the Congo Basin (Hou et al., 2018).

Although the initial conceptual model developed by Walker and Syers (1974) conceptualized P in highly weathered soils as predominantly in organic or occluded form, this conceptual was built from a chronosequence confounded by climate and parent material differences in a temperate climate. Subsequent research (Crews et al., 1995, Yang et al., 2011) has developed a more nuanced view of soil P dynamics in highly weathered soils, which includes large proportions of P in non-occluded form. Similar to Yang et al., 2011, we find that even on these sandy, highly weathered soils in central DRC, secondary mineral P_i (non-occluded P_i in Walker and Syers) is a significant pool of non-occluded P in our soils (~80 % of non-occluded P stocks and ~64 % of P_t stocks). This suggests the persistence of a natural mechanism that feeds the non-occluded P_i pool which is made of AEM-P_i, $NaHCO_3$-P_i, NaOH-P_i, and HCl-P_i fractions. This mechanism proceeds, over time, through apatite dissolution, OM mineralization, occluded-P mycorrhizal dissolution (Tiessen et al., 1994), and possibly allochthonous P inputs (Crews et al., 1995) to sustain the dynamic equilibrium between organic P and occluded P at the soil terminal steady state (Walker and Syers, 1976).

The major novel revelation from our bio-climosequence is that climate and vegetation can interact significantly to determine soil P stocks and fractions in the humid tropics. Across the climosequence from Aw through Am to Af, total precipitation increases and the seasonality of precipitation significantly decreases. Our work shows that soil

phosphorus under forest and savanna responds differently to changes across the climatic gradient (Figure 3.4, Table 3.5). P_t stocks do not significantly change from Am to Af under forested sites, but P_{occ} becomes a larger proportion of P_t in the Af, potentially at the expense of organic P. Conversely, there is a major increase in P_t stocks under savanna from Aw to Am and Af (Figure 3.4, Table 3.5). This increase appears to be driven primarily by significant increases in P_{occ} stocks from Am to Af, and increases in non-occluded P associated with amorphous iron (NaOH-P_i and HCl-P_i) from Aw to Am to Af (Figure 3.4, Table 3.5). Other studies have shown a decreasing or flat concentrations of Hedley extractable P in both forest and savanna with increasing MAP (i.e., Lloyd et al., 2015), but importantly those studies did not measure P_{occ}, which we did in our study.

This study extends the results of Feng et al. (2016) which examined soil P transformations across a climosequence of arid and semiarid grasslands in China (MAP ranged from 34 mm/yr to 436 mm/yr). The driest tropical savanna sites in our study began with MAP of approximately 1600 mm/yr, with a highly distinct dry season. If we synthesize the results of these climosequences for grassland or savanna vegetation only, we find that Ca-associated P is largely absent in Sankuru soils, and organic P increases from Aw to Af, while non-occluded Fe-associated P increases significantly from Aw to Am, and occluded P increases significantly from Am to Af (Table 3.5). Similar to Feng et al. (2016), we found that C:P_o ratios increased significantly with increasing MAP, but were influenced strongly by vegetation type. C:P_o ratios remained significantly lower under savanna vegetation than forest vegetation in comparable climate zones (Am and Af).

Total soil phosphorus stocks within the top 50 cm, accumulate more substantially in savanna (168 ± 117 g m^{-2}) than in forest (109 ± 61 g m^{-2}) with organic P (P_o) stocks representing 32% and 27.8% of the total phosphorus in savanna and forest respectively. Labile P stocks are approximately twice as high under savanna (17 g m^{-2}) than forest (9 g m^{-2}) in Am and Af climate zones, and mirror patterns in Bray P stocks. At advanced stages of mineral weathering, crystalline and non-crystalline Fe/Al-oxides-hydroxides have been shown to be specifically involved in phosphorus adsorption process more than phyllosilicate minerals such as kaolinite (Wang et al., 2009) through inner-sphere surface complex formations, as long as PZNC (point of zero net charge) remains higher than soil pH (Arai and Sparks, 2007). PZNC is expected to be high in the weathered soils

investigated here (Xu et al., 2016) which have average pH values around ~4.2. The dominance of non-occluded P_i stocks, which are higher under savanna vegetation in Am and Af climate zone and comprise, on average, 68 % of total-P stocks in savanna and 72 % of total-P stocks in forest, is related to the higher magnitude and proportion of Fe_o under savanna vegetation in Am and Af. Interestingly, Fe_t does not vary significantly between forest and savanna vegetation in Am and Af climate zones, but amorphous iron is significantly higher under savanna vegetation (Table 3.5).

There are at least three potential explanations for these observations, which we will discuss in turn: 1) savanna vegetation fragments in Af and Am climate zones are on fundamentally different soil parent materials or drainage classes, leading to differences in iron forms and P pools that are indirectly driven by vegetation; 2) savanna vegetation directly changes the dynamics of iron and therefore phosphorus cycling in the humid tropics; 3) savanna and forest vegetation indirectly drive soil properties that influence iron and phosphorus dynamics, and 4) anthropogenic land use and land management differ on savanna soils than forested soils in Am and Af.

Different soil parent materials or drainage classes. This explanation is not supported by our fundamental soil physical, chemical and morphological analysis. Both savanna and forest soils occurred on well drained uplands, with no evidence of a shallow water table or redoximorphic features to a depth of at least 2 m. Additionally, trace element concentrations and soil particle size distributions do not differ significantly between forest and savanna soils at any depth.

Savanna vegetation directly changes the dynamics of iron and phosphorus cycling in the humid tropics. There is a distinct possibility that the differences between forest and savanna P stocks and fractions are driven primarily by biogeochemical processes that differ by vegetation type. Grasses naturally die and decompose faster than forest litter, which is reflected in the significantly lower $C:P_o$ ratios of soils under savanna vegetation than forest vegetation in Af and Am. In Sankuru, both $C:P_o$ ratio and climate are likely interacting to affect the rate of organic matter mineralization. In both climates (Af and Am), forests have higher soil $C:P_o$ ratio than their respective savannas. Increased P cycling time under savanna could raise P supply so that inner-sphere adsorption sites are overwhelmed,

favoring the formation of outer-sphere complexes and phosphate counterions swarm (Wang et al., 2009, Essington, 2015) which are easily desorbed.

Additionally, the natural predominance of arbuscular mycorrhizae in savanna could be associated with the increased effectiveness of grass P uptake (Negassa and Leinweber, 2009), leading to lower P leaching through the highly permeable sandy parent materials and the opportunity for that P to adsorb to amorphous Fe throughout the profile. A much higher proportion of the iron under savanna is in amorphous rather than crystalline form, leading to increased opportunity for non-occluded P_i to accumulate in these soils. An additional contributing factor to the increased amorphous iron under savanna could be the increased release of siderophores by graminoids, which can disrupt iron crystallinity and maintain iron in more amorphous forms (Cesco et al., 2006, Columbo et al., 2014, Reichard et al., 2005). However, this phenomenon can be highly context dependent, as differences in Fe_o concentrations between forest and savanna vegetation can be highly variable (Herold et al., 2014, Chiu et al., 2005, Chao et al., 2017, Warman et al., 2013, Sugihara et al., 2014).

Savanna and forest vegetation indirectly drive differing soil properties that influence iron and phosphorus dynamics. The relative abundance of plant available-P_i in savanna as opposed to forest could be connected to soil mineral surface charges and orthophosphate supply that differ by pH, which is significantly impacted by vegetation type. In forest, low pH (4.2 average with 3.8 minimum) may result in predominantly positive charges on the exchange complex surface area which bind phosphate anions. An extensive amount of P anions will intensely bind to Al/Fe surfaces in the inner-sphere and progressively diminish their availability (Yang et al., 2013) in the presence of increased crystalline Fe stocks in forest. In savanna, the adsorption mechanism remains the same between phosphate anions and Al/Fe oxides but, the magnitude of adsorption and bonding intensity may be lower for several reasons related to higher soil pH, increased phosphate ion supply, and fulvic acid competition for adsorption sites, resulting in elevated plant available-P content. Relatively higher savanna pH (average of 4.6 versus 4.2 in forest) may lead to increased negative charges on the exchange complex, which could potentially reduce phosphate adsorption.

Differing land use and anthropogenic management of savanna soils. A final possibility is that differences in management and land use may account for the significant

differences in P and Fe under savanna vegetation relative to forested sites in Am and Af. One main difference may be an increased frequency of fire set on savanna sites, which are likely to be burned nearly every year, as tree encroachment on savanna within decades is a certainty in the Af and Am climate zones in the absence of disturbance. Annual fires on savanna may increase mineralization of organic matter and the rate of P cycling/P release (Gonzalez-Perez et al., 2004). Local land management strategies, however, do not include the addition of P-rich amendments to soils, and there are few, if any, P-rich amendments available in central DRC as animal agriculture is largely non-existent, and it is economically unfeasible to import large quantities of inorganic fertilizer materials to the area.

3.4.4. Agronomic implications of soil P stocks and P availability

In the Sankuru transect study, soils under savanna vegetation store more labile P than forest vegetation which may make savanna more suitable for cropping activities than forest relative to P availability. However, there is an interaction between vegetation type and climate zone, and Am and Af savanna may present the best opportunities for maximizing agricultural production with respect to soil P in the absence of external inputs. It is likely that savanna soils in Af and Am have a large enough available P pool to satisfy most crop P requirements. Local soil P supply may emerge largely from the mineralization of organic matter, which is a critical step in the phosphorus cycle and a key process for meeting crop P demand in low-input regions with low P availability due to P-fixation and/or low soil P stocks. This P then becomes progressively associated with non-crystalline iron (Fe_o), and generally, high Fe_o stocks will lead to increased accumulation of non-occluded P. Therefore, "mining" these Fe_o-associated P pools represents a considerable opportunity for increasing P availability further in the soils, particularly under forest vegetation or in Aw savanna, where P stocks remain low. Locally produced amendments such as biochar may have the potential to increase soil pH and release additional P from the Fe_o-associated pools. Although it is currently economically inefficient to transport P containing fertilizers into central DRC and Sankuru, if that possibility does arise in the future, it would be important to know whether or not these soils have additional phosphorus adsorption capacity or whether they are near to P saturation.

We estimated the degree of P saturation (DPS) of these soils using concentrations of oxalate extractable P (P_{ox}), Fe (Fe_o), and Al (Al_o) described by Nair et al. (2004) for sandy soils in Florida. In this work, the authors found that water soluble phosphorus (both organic and inorganic), presumably vulnerable to leaching losses in sandy soils, increased significantly above a DPS threshold of 20 %. Although our soils were very sandy, they had Al_o and Fe_o concentrations 5 to 6 times higher than those soils investigated in other studies in temperate regions or the subtropics. For example, the surface soils evaluated by Nair et al. (2004) ranged from 15-40 mmol/kg (Al_o + Fe_o) (average of 23 mmol/kg), while for the sandy soils of sandy marine sediments on the mid-Atlantic coast of the US (Sims et al., 2002), mean Fe_o + Al_o of 52.5 mmol/kg. In our study, the mean value of Fe_o + Al_o for the surface horizons ranged from 18-125 with a mean of 68.8 mmol/kg. Thus, our estimates of DPS using this method are much lower than those reported in Nair et al (2004) because 1) Sankuru soils have higher Fe_o and Al_o and thus higher predicted P adsorption capacity, and 2) the lack of P inputs as fertilizer in Sankuru. We did find that DPS was non-linearly related to the Hedley AEM-P_i fraction investigated in our study, and that AEM-P_i (as an approximation of water-soluble P_i) began to rise at lower DPS values (~5-10%) that those reported in Nair (15-20%). These results suggest that Sankuru soils may respond to increased external P addition with increases to the water soluble and labile plant available P pools.

3.5. Conclusion

The study of soil phosphorus biogeochemical fractions in the Sankuru transect has provided an opportunity for comparative analysis to validate, in tropical environments, the Walker and Syers chronosequence model predictions of phosphorus pedogenic transformations. This study showed that both climate and vegetation can interact to drive fundamental soil properties which in turn affect soil P pools and fractions. Unlike the Walker and Syers model which identified two major pools, occluded P and organic P in highly weathered soils at a terminal steady state, the Sankuru bio-climosequence model revealed large proportions of non-occluded P_i. This non-occluded pool is most closely associated with non-crystalline iron and may be sustained by the effect of increased

mineralization of P from organic matter followed by its adsorption to non-crystalline or para-crystalline iron.

Table 3.1. *Descriptive statistics of the distribution of soil properties related to soil P for all samples across the climatic transect in Sankuru Province, DRC*

Property	Range (min-max)	Mean	Median	25th Percentile	75th Percentile	CV (%)	Skewness	Kurtosis
AEM P_i	0 – 30.75	4.14	1.61	0.34	4.74	1.49	2.16	7.34
H_2O P_o	0 – 22.23	5.38	4.26	1.97	7.40	0.92	1.66	5.93
$NaHCO_3$ P_i	0.16 – 68.40	10.80	5.18	1.68	14.40	1.23	1.83	6.40
$NaHCO_3$ P_o	0 – 61.45	8.60	5.70	2.77	9.97	1.15	2.72	12.07
NaOH P_i	0.89 – 256.86	72.00	46.24	19.60	120.50	0.90	0.90	2.79
NaOH P_o	1.65 – 126.71	38.10	27.85	14.54	50.41	0.80	1.15	3.51
HCl P_i	0.09 – 50.49	10.75	4.86	1.18	17.31	1.13	1.17	3.57
Total P_o	2.58 – 189.53	52.08	38.52	23.42	71.41	0.76	1.25	3.97
Sum Hedley P	22.43 – 504.74	157.20	113.36	56.87	237.27	0.75	0.85	2.64
Bray I P	1.52 – 133.62	32.49	20.92	6.11	51.76	0.97	1.15	3.60
Total P	41.8 – 675.3	210.76	184.3	90.93	289.30	0.64	0.91	3.41
Bray P (mg/kg)	1.5 – 133.6	32.5	20.9	6.1	51.8	0.97	1.15	3.60
Total P (mg/kg)	41.8 – 675.3	210.8	184.3	90.9	298.3	0.64	0.91	3.41
P_{ox} (mg/kg)	13.00 – 659.19	164.13	121.80	46.88	239.01	0.85	1.09	3.59
Al_{ox} (mg/kg)	127 – 16,876	2,270	1,470	812	2,721	1.13	3.42	18.01
Fe_{ox} (mg/kg)	92 – 5,330	2,200	2,012	1,278	2,959	0.52	0.47	2.60
P_d (mg/kg)	26.03 – 676.65	205.22	180.77	89.56	265.14	0.67	1.10	3.85
Al_d (mg/kg)	229 – 3,848	1,541	1,467	1,068	1,989	0.45	0.49	3.37
Fe_d (mg/kg)	157 – 20,588	5,851	4,272	3,266	7,027	0.73	1.58	4.85
Al_t (%)	0.51 – 10.77	4.94	4.67	3.48	6.09	0.42	0.40	2.73
Fe_t (%)	0.12 – 5.20	1.51	1.10	0.87	1.77	0.73	1.66	5.26

***Table 3.2**. Correlations between soil P fractions and related variables across all samples. Correlation coefficients shown are from Pearson's method, with Bonferroni correction for multiple comparisons. Significant correlations ($\alpha < 0.05$) with $r > 0.50$ are highlighted in bold. ns = not significant.*

	AEM-P_i	H_2O-P_o	$NaHCO_3$-P_o	$NaHCO_3$-P_i	NaOH-P_o	NaOH-P_i	HCl-P_i	P_{occ}	Bray-P	P_{ox}	P_d
AEM-P_i	1										
H_2O-P_o	**0.63**	1									
$NaHCO_3$-P_o	0.41	0.43	1								
$NaHCO_3$-P_i	**0.85**	**0.56**	ns	1							
NaOH P_o	ns	ns	**0.66**	0.43	1						
NaOH P_i	0.50	ns	ns	**0.66**	0.33	1					
HCl P_i	0.49	ns	ns	0.38	0.26	0.18	1				
P_{occ}	ns	ns	ns	ns	-0.28	-0.21	ns	1			
Bray P	**0.75**	ns	0.39	**0.74**	0.41	0.27	**0.62**	0.05	1		
P_{ox}	**0.60**	0.34	0.38	**0.73**	0.42	**0.77**	**0.72**	ns	**0.75**	1	
P_d	**0.71**	0.50	ns	**0.68**	ns	**0.63**	**0.56**	0.27	**0.55**	**0.55**	1

Table 3.3. *Average and standard deviations of concentrations of P fractions across depth increments for vegetation types. Different capital letters indicate significant differences (following ANOVA, Tukey's HSD) between vegetation types for the same depth increment. Depth increments within a variable that have dashes indicate no significant differences between climate zones ($p > 0.05$) following ANOVA using Tukey's HSD.*

	Forest					Savanna				
	0-10	10-20	20-50	50-100	100-200	0-10	10-20	20-50	50-100	100-200
AEM-P_i	8.24± 6.37 -	5.01± 5.82 -	3.61± 6.63 -	2.26± 5.00 -	2.88± 4.88 -	10.77± 10.11 -	9.72± 9.92 -	5.95± 7.03 -	2.48± 3.33 -	1.02± 1.20 -
H_2O-P_o	6.12± 4.52 -	5.26± 4.4 -	6.39± 5.52 -	6.01± 5.06 -	4.49± 6.04 -	8.28± 3.66 -	7.97± 3.79 -	7.79± 4.20 -	5.56± 5.44 -	2.10± 2.04 -
$NaHCO_3$-P_i	9.97± 12.06 -	7.78± 11.10 B	7.95± 11.64 -	7.14± 10.20 -	6.24± 8.82 -	25.08± 23.08 -	23.28± 22.34 A	14.96± 14.17 -	11.22± 10.69 -	7.21± 7.18 -
$NaHCO_3$-P_o	15.02± 17.39 -	11.38± 15.68 -	9.99± 11.53 -	6.44± 7.52 -	4.27± 5.49 -	14.20± 15.35 -	13.49± 15.24 -	10.51± 11.13 -	6.061± 6.29 -	4.68± 5.69 -
NaOH-P_i	32.44± 47.03 B	32.43± 41.57 B	45.02± 42.04 -	56.28± 42.85 -	67.85± 47.66 -	100.54± 81.62 A	97.05± 80.64 A	86.65± 72.06 -	87.84± 74.76 -	80.91± 68.09 -
NaOH-P_0	33.96± 16.63 B	26.13± 19.21 B	25.23± 27.73 B	20.31± 25.32 B	19.05± 20 -	65.27± 34.87 A	64. ± 34.93 A	55.77± 28.15 A	45.86± 30.70 A	30.52± 22.10 -
HCl-P_i	4.74± 6.27 -	4.75± 5.78 -	7.48± 9.01 -	8.59± 11.10 -	10.48± 12.40 -	12.71± 13.32 -	12.49± 13.29 -	12.39± 13.90 -	13.23± 14.02 -	10.84± 13.07 -
Total-P_0	55.10± 31.81 -	42.77± 31.78 B	41.61± 39.85 B	32.76± 34.45 -	27.81± 26.39 -	87.75± 50.67 -	85.47± 50.73 A	74.07± 40.17 A	58.03± 37.58 -	37.30± 27.09 -
Labile-P	18 .20± 18 -	13.75± 17.08 -	12.46± 18.33 -	10.13± 15.30 -	8.11± 13.51 -	35.85± 32.89 -	33± 31.97 -	20.91± 20.60 -	13.70± 13.62 -	8.23± 7.86 -
Σ Hedley-P	110.49± 95.72 B	98.94± 90.42 B	112± 94 -	114± 85.81 -	114.26± 89.06 -	236.85± 162.98 A	228± 161.40 A	194± 131 -	173± 121 -	137.29± 102.79 -

***Table 3.4**. Average and standard deviations of concentrations of P fractions across depth increments for climate zones. Different capital letters indicate significant differences (following ANOVA, Tukey's HSD) between climate zones for the same depth increment. Depth increments within a variable that have dashes indicate no significant differences between climate zones ($p > 0.05$) following ANOVA using Tukey's HSD.*

	Af					Am					Aw				
	0-10	10-20	20-50	50-100	100-200	0-10	10-20	20-50	50-100	100-200	0-10	10-20	20-50	50-100	100-200
AEM-P_i	9.95 ± 7.24 AB	6.94 ± 7.35 AB	3.90 ± 4.53 -	1.56 ± 1.74 -	0.83± 0.57 -	14.47 ±9.67 A	12.54 ± 10.41 A	8.99 ± 9.97 -	4.55 ± 6.85 -	2.91± 6.38 -	3.85 ± 5.56 B	2.14 ± 2.13 B	1.36 ± 1.86 -	1.15 ±1.76 -	0.87± 1.53 -
H_2O-P_o	6.24 ± 4.49 -	5.03 ± 4.18 B	4.95 ± 2.83 B	3.83 ± 2.21 B	0.77± 2.80 -	9.91 ± 4.10 -	10.13 ± 4.05 A	12.11 ± 5.27 A	9.62 ±7.55 A	4.87± 7.72 -	5.56 ± 2.22 -	5.09 ± 1.83 B	4.73 ± 2.03 B	4.49 ±2.72 BA	2.48± 2.22 -
$NaHCO_3$-P_i	19.32 ± 22.39 -	14.43 ±20.52 -	11.42 ±14.50 -	9.11± 10.28 -	7.57± 7.32 -	26.68 ± 22.44 -	25.53 ± 21.08 -	17.42 ± 14.31 -	13.20± 12.59 -	9.82± 10.73 -	8.24 ±10.65 -	5.83 ±6.27 -	4.68 ±5.92 -	4.69± ±6.96 -	2.42± 2.89 -
NaOH-P_i	69.96 ±87.92 -	57.94 ±77.27 -	66.70 ±66.61 -	80.05 ±71 -	85.30 ± 67.35 -	101.31 ±82.31 -	102.41 ±77.28 -	94.78 ±63.42 -	97.09 ±53.22 -	100± 47.24 -	37.31 ±39.20 -	32.38 ±29.46 -	31.38 ±34.73 -	30.91 ±36 -	33.16 ± 29.16 -
NaOH-P_o	35.67 ±18.71 A	25.03 ±18.36 B	18.56 ±15.07 B	13.05 ± 10.59 B	11.46 ± 9.74 B	77.46 ±40.19 B	78.13 ±39.54 A	72.89 ±33.50 A	64.00± 34.95 A	50.17 ± 19.83 A	40.43 ±10.08 A	38.77 ±10.33 B	37.95 ±12.52 B	29.24 ± 15.35 B	18.45 ± 11.44 B
HCl-P_i	11.91 ±15.13 -	9.86 ±13.34 -	13.10 ±14.49 -	14.42 ± 15.66 -	13.84 ± 15.10 -	11.06 ±10.08 -	11.22 ±9.93 -	11.46 ±10.39 -	12.74± 10.51 -	13.72 ± 11.49 -	4.12 ±6.62 -	3.69 ±5.75 -	3.22 ±5.01 -	3.32± 5.58 -	3.07± 5.15 -
Total-P_o	51.10 ±24.28 A	36.91 ±22.90 B	28.23 ±18.03 B	19.31 ± 10.61 B	16.02 ± 934 B	114.14 ±54.36 B	113.99 ±52.49 A	107.20 ±39.40 A	88.18± 37.29 A	65.56 ± 23.70 A	52.85 ±12.36 A	49.87 ±11.98 B	47.96 ±14.87 B	37.47 ± 17.84 B	23.17 ± 13.78 B

***Table 3.5**. Average and standard deviations of concentrations soil P stocks (g/m^2) in the **0-50 cm** depth increments across depth increments for climate zones, vegetation type, and combinations of climate zone and vegetation. Different letters indicate significant differences (following ANOVA, Tukey's HSD) between categories for the same depth increment.*

0-50cm	Climate Zone			Vegetation		Climate + Vegetation				
Fraction	Af	Am	Aw	Forest	Savanna	Af-Forest	Af-Savanna	Am-Forest	Am-Savanna	Aw-Savanna
AEM-P_i	4.18 ± 3.97	7.08 ± 6.50	1.32 ± 1.56	3.27 ± 4.36	5.13 ± 5.43	2.23 ± 1.82ab	10.02 ± 1.60ab	4.83 ± 6.78ab	9.34 ± 6.24a	1.32 ± 1.56b
H2O-P_o	3.90 ± 2.11a	7.55 ± 3.03b	3.40 ± 1.30a	4.56 ± 3.35	5.38 ± 2.59	2.86 ± 0.73ac	7.05 ± 1.45abc	7.11 ± 4.28bc	7.99 ± 1.62b	3.40 ± 1.30c
$NaHCO_3$-P_i	10.64 ± 11.96	13.83 ± 11.36	3.74 ± 4.42	5.95 ± 8.03	12.49± 11.52	5.21 ± 6.77a	26.93 ± 8.05b	7.07 ± 10.69ac	20.59 ± 8.06bc	3.74 ± 4.42a
$NaHCO_3$-P_o	3.75 ± 1.70a	15.60 ± 10.71b	3.90 ± 0.83a	7.76 ± 8.61	8.04 ± 8.58	3.65 ± 1.96a	4.05 ± 0.98ab	13.93 ± 11.48ab	17.28 ± 11.33b	3.90 ± 0.83a
NaOH-P_i	51.77 ± 51.22	64.98 ± 46.78	21.93 ± 22.23	28.49 ± 28.37	61.73± 50.27	25.53 ± 15.46a	130.49 ± 25.35b	32.95 ± 44.40a	97.01 ± 19.97b	21.93 ± 22.23a
NaOH-P_o	15.73 ± 11.89a	49.25 ± 23.51b	26.34 ± 7.38a	18.02 ± 14.45	40.31 ± 20.77	9.39 ± 1.94a	34.75 ± 2.63b	30.95 ± 15.75b	67.56 ± 12.18c	26.34 ± 7.38b
HCl-P_i	9.48 ± 10.14	7.57 ± 6.78	2.31 ± 3.52	4.33 ± 5.12	8.41 ± 9.08	4.45 ± 4.21a	24.59 ± 4.71b	4.16 ± 6.99a	10.98 ± 5.24a	2.31 ± 3.52a
Total P_o	23.39 ± 14.35a	72.41 ± 29.28b	33.64 ± 8.68a	30.33 ± 22.71a	53.73 ± 29.94b	15.90 ± 3.76a	45.85 ± 5.05ab	51.98 ± 21.97b	92.83 ± 20.12c	33.64 ± 8.68ab
Occluded P	68.93 ± 38.06a	7.29 ± 8.96b	14.96 ± 10.37b	36.87 ± 33.09	26.60 ± 39.48	55.72 ± 29.83a	108.57 ± 38.73b	8.60 ± 5.17c	5.97 ± 12.49c	14.96 ± 10.37c
Total P	168.39 ± 120.13	173.16 ± 94.56	77.89 ± 44.40	109.26 ± 61.04	168.08 ± 117.07	109.03 ± 43.58a	346.45 ± 83.50b	109.59 ± 89.51a	236.73 ± 45.59b	77.89 ± 44.40a

**Different letters indicate statistically significant differences between climate zones ($p < 0.05$) following ANOVA using Tukey's HSD. Depth increments within a variable that have no letters indicate no significant differences between climate zones ($p > 0.05$) following ANOVA using Tukey's HSD.*

***Table 3.6**. Average and standard deviations of concentrations soil P stocks (g/m^2) in the **50-100 cm** depth increments across depth increments for climate zones, vegetation type, and combinations of climate zone and vegetation. Different letters indicate significant differences (following ANOVA, Tukey's HSD) between categories for the same depth increment.*

50-100cm	Climate Zone			Vegetation		Climate + Vegetation				
Fraction	Af	Am	Aw	Forest	Savanna	Af-Forest	Af-Savanna	Am-Forest	Am-Savanna	Aw-Savanna
AEM-P_i	1.18 ± 1.19a	3.02 ± 4.49a	0.81 ± 1.25a	1.61 ± 3.33a	1.71 ± 2.28a	0.86 ± 0.84a	2.43 ± 1.96a	3.11 ± 5.89a	2.93 ± 3.50a	0.81 ± 1.25a
H2O-P_o	2.97 ± 1.44a	6.44 ± 5.11a	3.21 ± 1.90a	4.43 ± 3.17a	3.89 ± 3.79a	3.44 ± 1.05a	1.08 ± 1.47a	6.41 ± 5.15a	6.48 ± 5.86a	3.21 ± 1.90a
$NaHCO_3$-P_i	7.01 ± 7.16a	8.84 ± 8.37a	3.27 ± 4.84a	5.19 ± 6.78a	7.80 ± 7.43a	4.46 ± 4.90a	17.24 ± 5.58a	6.67 ± 10.40a	11.01 ± 6.52a	3.27 ± 4.84a
$NaHCO_3$-P_o	1.69 ± 0.83a	9.64 ± 4.65b	2.64 ± 1.18a	4.43 ± 4.89a	4.56 ± 4.26a	1.68 ± 0.90a	1.70 ± 0.67a	9.94 ± 5.01b	9.34 ± 5.01b	2.64 ± 1.18a
NaOH-P_i	61.89 ± 49.20a	65.32 ± 36.21a	21.78 ± 25.22a	41.42 ± 27.63a	61.30 ± 52.21a	42.20 ± 28.11a	140.66 ± 27.29b	39.88 ± 30.82a	90.78 ± 19.57b	21.78 ± 25.22a
NaOH-P_o	9.10 ± 7.76a	42.62 ± 23.02b	20.65 ± 10.60a	13.68 ± 6.39a	31.72 ± 20.39b	5.85 ± 3.42a	22.09 ± 6.14ab	29.33 ± 21.63bc	55.91 ± 17.28d	20.65 ± 10.60ab
HCl-P_i	11.17 ± 11.12a	8.57 ± 7.03a	2.33 ± 3.94a	6.35 ± 7.66a	9.26 ± 9.92a	7.06 ± 7.83a	27.61 ± 2.79b	4.93 ± 8.23a	12.21 ± 3.51ab	2.33 ± 3.94a
Total P_o	13.76 ± 7.64a	58.70 ± 24.40b	26.50 ± 12.26a	22.54 ± 22.15a	40.17 ± 25.00a	10.98 ± 4.59a	24.88 ± 8.27ab	45.68 ± 26.05bc	71.71 ± 16.10c	26.50 ± 12.26ab
Occluded P	86.85 ± 61.53a	13.94 ± 12.08b	16.63 ± 9.26b	57.50 ± 62.27a	31.27 ± 40.32a	78.83 ± 66.85ab	118.95 ± 14.83b	14.83 ± 12.24a	13.04 ± 13.72a	16.63 ± 9.26a
Total P	181.86 ± 99.64a	158.40 ± 72.43ab	71.34 ± 49.08b	134.63 ± 69.25a	151.51 ± 107.60a	144.38 ± 67.82ac	331.77 ± 31.07b	115.11 ± 78.04ac	201.69 ± 33.97a	71.34 ± 49.08c

**Different letters indicate statistically significant differences between climate zones ($p < 0.05$) following ANOVA using Tukey's HSD. Depth increments within a variable that have no letters indicate no significant differences between climate zones ($p > 0.05$) following ANOVA using Tukey's HSD.*

Table 3.7*. Average and standard deviations of concentrations soil P stocks (g/m2) in the* ***100-200 cm*** *depth increments across depth increments for climate zones, vegetation type, and combinations of climate zone and vegetation. Different letters indicate significant differences (following ANOVA, Tukey's HSD) between categories for the same depth increment.*

100-200cm	Climate Zone			Vegetation		Climate + Vegetation				
AEM-P_i	Af	Am	Aw	Forest	Savanna	Af-Forest	Af-Savanna	Am-Forest	Am-Savanna	Aw-Savanna
H2O-P_o	1.16 ± 0.78	3.29 ± 7.41	1.24 ± 2.17	2.40 ± 6.06	1.37 ± 1.64	0.87 ± 0.47	2.34 ± 0.69	5.46 ± 10.74	1.12 ± 0.64	1.24 ± 2.17
$NaHCO_3$-P_i	3.91 ± 3.96	5.70 ± 8.97	3.50 ± 3.16	5.98 ± 7.59	2.88 ± 2.76	4.89 ± 3.83	0.00 ± 0.00	8.16 ± 12.94	3.23 ± 1.99	3.50 ± 3.15
$NaHCO_3$-P_o	10.62 ± 10.26	13.06 ± 12.49	3.42 ± 4.13	8.16 ± 11.00	10.51 ± 9.79	6.35 ± 5.42a	27.71 ± 3.51b	11.79 ± 18.68ab	14.33 ± 3.28ab	3.41 ± 4.13a
NaOH-P_i	2.53 ± 1.11a	15.10 ± 9.45b	3.13 ± 2.56a	5.54 ± 6.77	7.80 ± 8.98	2.53 ± 1.19a	2.50 ± 1.02a	11.57 ± 9.61ab	18.63 ± 9.10b	3.13 ± 2.56a
NaOH-P_o	119.55 ± 93.66a	144.62 ± 73.07a	46.40 ± 41.65b	89.30 ± 58.61	123.51 ± 100.10	82.42 ± 56.52a	268.05 ± 38.00b	103.07 ± 69.00ac	186.17 ± 55.61bc	46.40 ± 41.65a
HCl-P_i	16.03 ± 13.48a	73.06 ± 34.14b	25.75 ± 16.33a	24.22 ± 23.34	48.80 ± 37.99	10.80 ± 6.79a	36.97 ± 14.73ab	51.07 ± 21.20b	95.05 ± 31.31c	25.75 ± 16.34ab
Total P_o	19.36 ± 21.05	18.67 ± 13.43	4.32 ± 7.34	13.57 ± 15.66	16.18 ± 18.10	11.60 ± 14.90a	50.39 ± 5.25b	17.51 ± 18.72a	19.84 ± 8.19ab	4.32 ± 7.34a
Occluded P	22.47 ± 12.89a	93.86 ± 39.54b	32.38 ± 19.74a	35.74 ± 31.32	59.48 ± 46.11	18.22 ± 8.66a	39.47 ± 15.75ab	70.80 ± 31.08b	116.91 ± 35.56c	32.38 ± 19.74ab
Total P	185.69 ± 108.41a	33.76 ± 21.59b	35.73 ± 19.60b	127.33 ± 114.17	65.32 ± 82.05	171.14 ± 117.05a	243.90 ± 37.21a	39.72 ± 21.73b	27.79 ± 22.82b	35.73 ± 19.60b
AEM-P_i	358.85 ± 182.07a	307.25 ± 132.22a	123.48 ± 79.06b	276.51 ± 132.16	276.37 ± 205.22	290.59 ± 126.11a	631.87 ± 25.99b	248.35 ± 159.23ac	366.16 ± 78.66a	123.48 ± 79.06c

**Different letters indicate statistically significant differences between climate zones ($p < 0.05$) following ANOVA using Tukey's HSD. Depth increments within a variable that have no letters indicate no significant differences between climate zones ($p > 0.05$) following ANOVA using Tukey's HSD.*

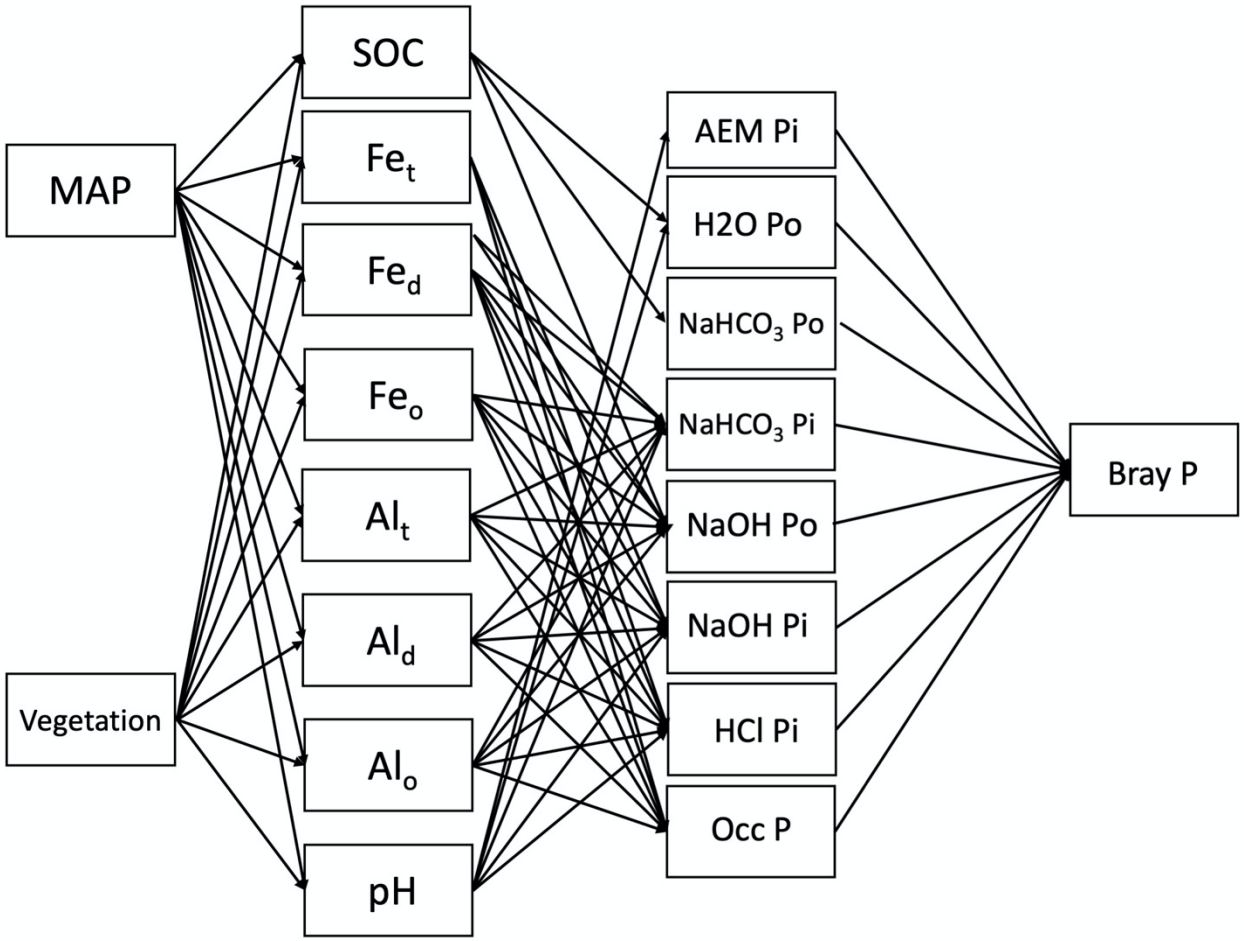

Figure 1.1. *Initial conceptual model used in structural equation modelling/path analysis.*

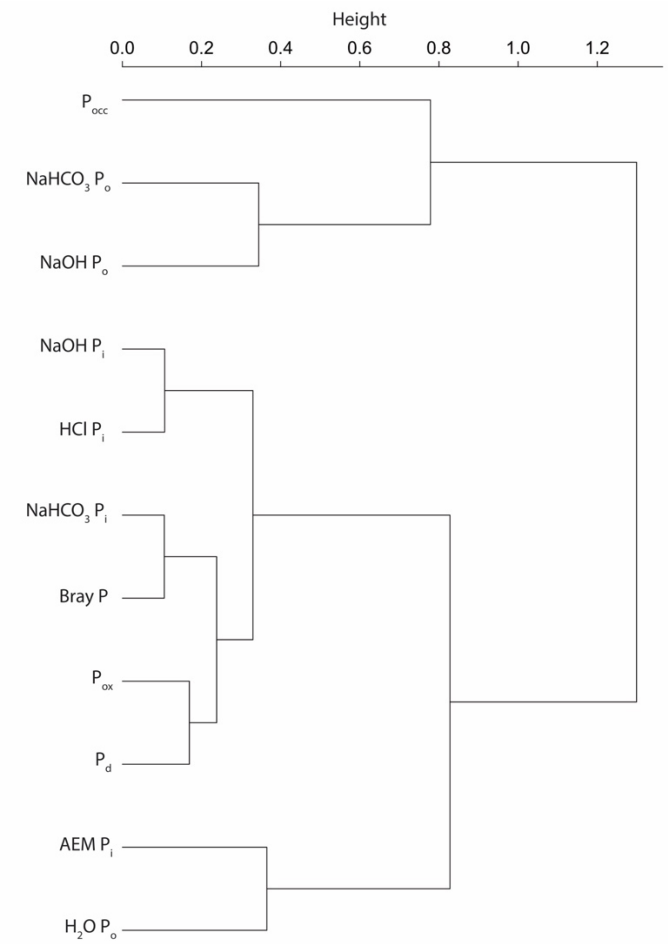

Figure 3.2. *Principle Coordinates based hierarchical cluster analysis of measured P fractions*.

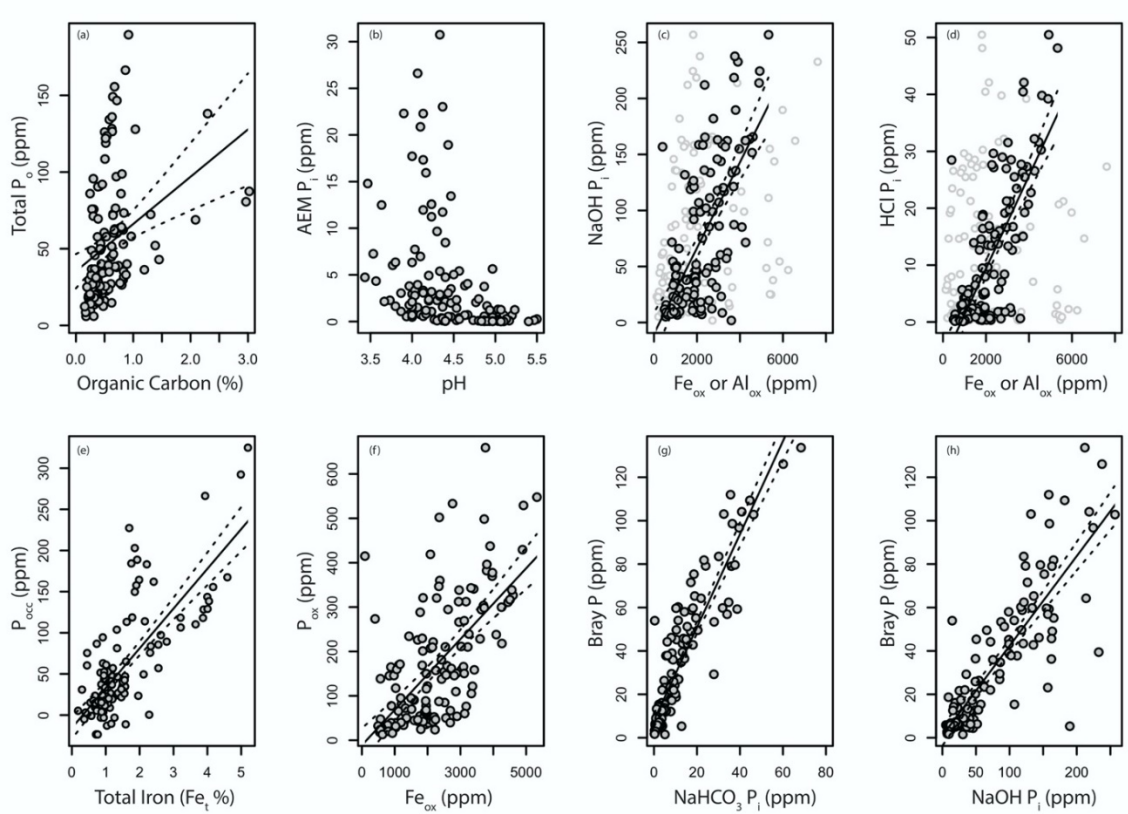

Figure 3.3. *Relationships between selected variables across all samples. For subplots (c) and (d), grey-filled points with black rings represent Fe_{ox}, while white filled points with grey rings represent Al_{ox}.*

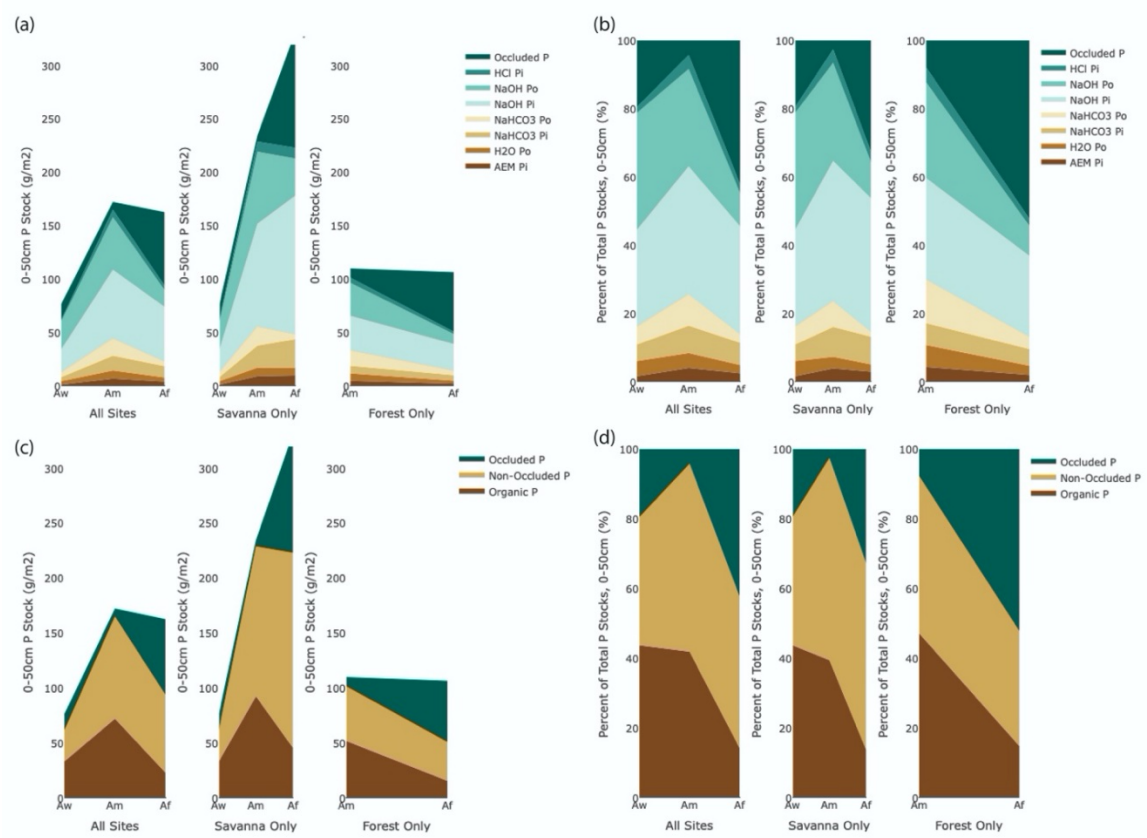

Figure 3.4. *Plots of 0-50cm soil P stocks; (a) in g/m2 for all soils across climate zones (left panel) and vegetation types (center and right panels) for individual Hedley fractions and (b) proportion of P_t for individual Hedley fractions. Plots of 0-50cm soil P stocks; (c) in g/m2 for all soils across climate zones (left panel) and vegetation types (center and right panels) for grouped Hedley fractions (occluded, non-occluded, and organic P) and (d) proportion of P_t for grouped Hedley fractions (occluded, non-occluded, and organic P).*

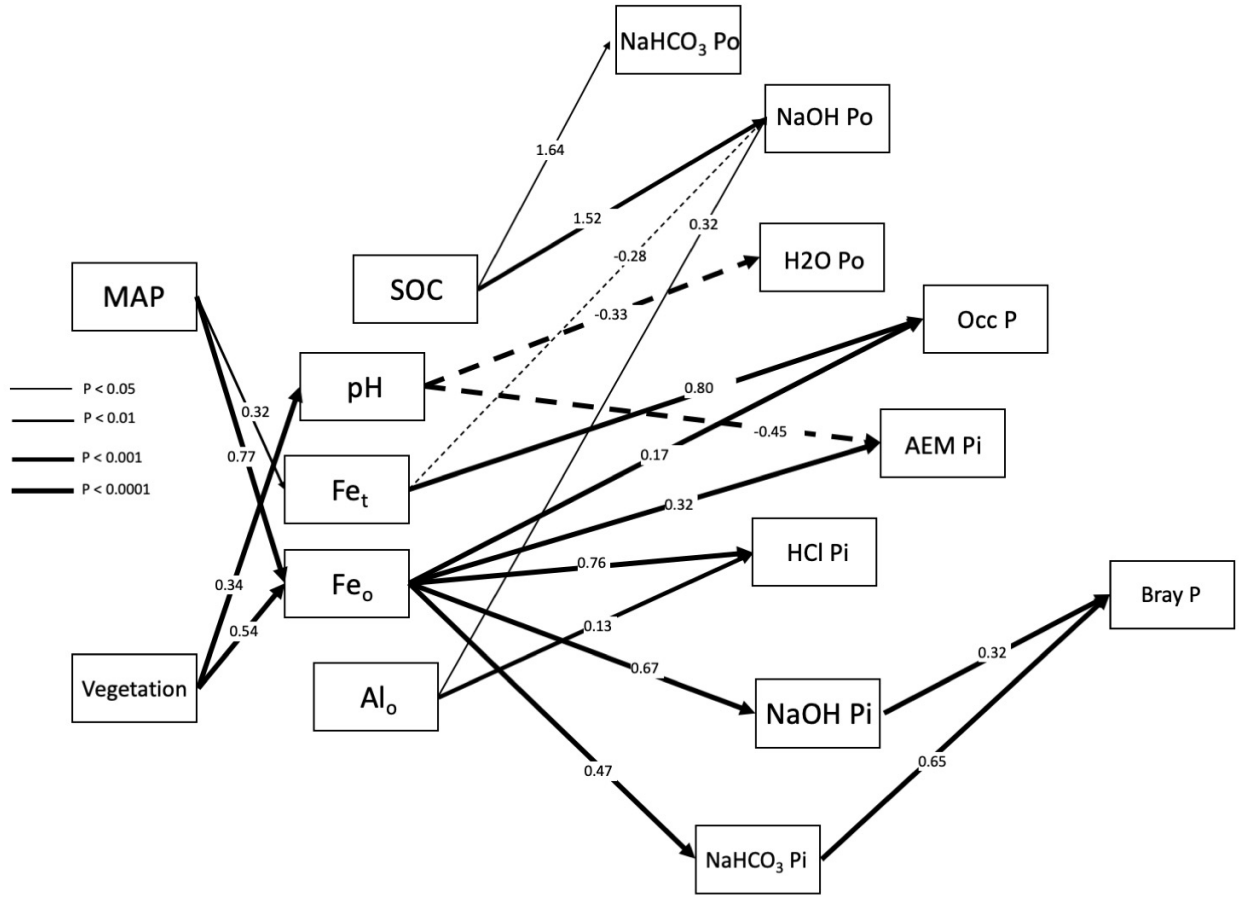

Figure 3.5*. Final path analysis diagram showing only significant relationships from the initial conceptual model (Figure 3.1). Arrow thickness indicates significance level. Dotted arrows indicate inverse relationships. Numbers associated with each path represent standardized coefficients.*

Bibliography

Aleman, J. C., Jarzyna, M. A., & Staver, A. C. (2018). Forest extent and deforestation in tropical Africa since 1900. *Nature Ecology and Evolution*, 2, 26–33. https://doi.org/10.1038/s41559-017-0406-1

Anderson, D. W. (1987). Pedogenesis in the Grassland and Adjacent Forests of the Great Plains, in: Stewart, B.A. (Ed.), Advances in Soil Science, Advances in Soil Science. Springer New York, New York, NY, pp. 53–93. https://doi.org/10.1007/978-1-4612-4790-6_2

Armolaitis, K., Aleinikovienė, J., Lubytė, J., Žėkaitė, V., & Garbaravičius, P. (2013). Stability of soil organic carbon in agro and forest ecosystems on Arenosol. *Zemdirbyste*, 100, 227-234. https://doi.org/10.13080/z-a.2013.100.029.

Arai, Y., & Sparks, D. L. (2007). Phosphate Reaction Dynamics in Soils and Soil Components: A Multiscale Approach. In D. Sparks (Ed.), *Advances in Agronomy* (pp. 135-179). (Advances in Agronomy; Vol. 94). https://doi.org/10.1016/S0065-2113(06)94003-6

Araújo, M. S. B., Schaefer, C. E. R., & Sampaio, E. V. S. B. (2004) Soil phosphorus fractions from toposequences of semi-arid Latosols and Luvisols in northeastern Brazil. *Geoderma*, 119 (3). 309-321 doi:10.1016/j.geoderma.2003.07.002

Baert, G., Van Ranst, E., Ngongo, M. L., Kasongo, E. L., Verdoodt, A., Mujinya, B. B. & Mukalay, J. M. (2009). Guide des sols en République Démocratique du Congo, tome II: description et données physico-chimiques de profils types. Univeristy of Ghent, Ghent, Belgium, 262 pp.

Baert, G., Verdoodt, A., Ngongo, M., & Van Ranst, E. (2013). Legacy soil survey data of D.R. Congo. International Conference on Nutirtion and Food Production in the Congo Basin. Brussels, Belgium, 30 September – 01 October, 2013. Royal Academy for Overseas Sciences.

Balesdent, J., & Mariotti, A. (1996). Measurement of soil organic matter turnover using 13C natural abundance. Mass Spectrom. Soils; Boutton, T.W., Yamasaki, S., Eds.; Marcel Dekker New York, 83–111.

Balsam, W. L., Ellwood, B. B., Ji, J., Williams, E. R., Long, X., & El Hassani, A. (2011). Magnetic susceptibility as a proxy for rainfall: Worldwide data from tropical and temperate climate. *Quaternary Science Reviews*, 30, 2732–2744. https://doi.org/10.1016/j.quascirev.2011.06.002

Barrow N. J., Sen, A., Roy N., & Debnath, A. (2020) The soil phosphate fractionation fallacy. *Plant and Soil*, 459,1-11. https://doi.org/10.1007/s11104-020-04476-6

Barrow, N. J. (2021). Comparing two theories about the nature of soil phosphate. *Eurasian Journal of Soil Science*, 72, 679– 685. https://doi.org/10.1111/ejss.13027

Batjes, N. H. (2009). Harmonized soil profile data for applications at global and continental scales: updates to the WISE database. *Soil Use and Management*, 25, 124–127. doi:10.1111/j.1475-2743.2009.00202.x, 2009.

Batjes, N. H., Ribeiro, E., van Oostrum, A., Leenaars, J., Hengl, T., & Mendes de Jesus, J.. (2017). WoSIS: providing standardised soil profile data for the world, *Earth Systems Science Data*, 9, 1–14, https://doi.org/10.5194/essd-9-1-2017.

Beaudette, D. E., Roudier, P., & O'Geen, A. T. (2013). Algorithms for quantitative pedology: A toolkit for soil scientists. *Computers and Geosciences*, 52, 258–268. doi:10.1016/j.cageo.2012.10.020

Beernaert, F.R. (1999). Development of a soil and terrain map/database for the Democratic Republic of Congo (DRC). UN-FAO Technical Report. 91 pp.

Bekele, A. & Hudnall, W. (2003). Stable Carbon Isotope Study of the Prairie-Forest Transition Soil in Louisiana. *Soil Science*, 168, 783-792. 10.1097/01.ss.0000100472.96182.d8.

Bekele, A., & Hudnall, W.H. (2006). Spatial Variability of Soil Chemical Properties of a Prairie–Forest Transition in Louisiana. *Plant and Soil*, 280, 7–21. https://doi.org/10.1007/s11104-005-4983-4

Bell, R.W. & Seng, V. (2007). The management of agro-ecosystems associated with sandy soils. In: Management of Tropical Sandy Soils for Sustainable Agriculture: Symposium on the Management of Tropical Sandy Soils, 27th November – 2nd December 2005, Khon Kaen, Thailand, pp 298-304.

Belsky, A.J., Mwonga, S.M., Amundson, R.G., Duxbury, J.M., & Ali, A.R. (1993). Comparative effects of isolated trees on their undercanopy environments in high- and low-rainfall savannas. *Journal of Applied Ecology*, 30, 143-155. https://doi.org/10.2307/2404278

Bender, M. M. (1968). Mass spectrometric studies of carbon-13 variations in corn and other grasses. *Radiocarbon*, 10, 468–472.

Bender, M. M. (1971). Variations in the 13C/12C ratios of plants in relation to the pathway of photosynthetic carbon dioxide fixation. *Phytochemistry* 10, 1239–1244. https://doi.org/10.1016/S0031-9422(00)84324-1

Bera, R., Seal, A., Banerjee, M., Dolui, A. (2005). Nature and profile distribution of iron and aluminum in relation to pedogenic processes in some soils developed under tropical environment in India. *Environmental Geology*, 47, 241-245. 10.1007/s00254-004-1149-2.

Biedenbender, S., McClaran, M., Quade, J., & Weltz, M. (2004). Landscape patterns of vegetation change indicated by soil carbon isotope composition. *Geoderma, 119*, 69-83.

Birkeland, P. W., Machette, M. N., & Haller, K. M. (1991). Soils as a tool for applied quaternary geology. Miscellaneous Publication 91-3, Utah Geological and Mineral Survey, Utah Department of Natural Resources.

Blakemore, R.P. (1982). Magnetotactic bacteria. *Annual Review of Microbiology*. 36, 217–238. https://doi.org/ doi: 10.1146/annurev.mi.36.100182.001245.

Blanchart, E., Albrecht, A., Bernoux, M., Brauman, A., Chotte, J.-L., Feller, C., Ganry, F., Hien, E., et al. (2005). Organic matter and biofunctioning in tropical sandy soils and implications for its management. Management of Tropical Sandy Soils for Sustainable Agriculture. A holistic approach for sustainable development of problem soils in the tropics, Nov 2005, Khon Kaen, Thailand. pp.224-241. hal-01420428

Blume, H. P. & Schwertmann, U. (1969). Genetic Evaluation of Profile Distribution of Aluminum, Iron, and Manganese Oxides. *Soil Science Society of America Journal*, 33, 438-444. https://doi.org/10.2136/sssaj1969.03615995003300030030x

Bockheim, J. G., & Schliemann, S. A., 2014. Soil richness and endemism across an environmental transition zone in Wisconsin, USA. *Catena*, 113, 86–94. https://doi.org/10.1016/j.catena.2013.09.011

Bokhorst, M. P., Beets, C. J., Marković, S. B., Gerasimenko, N. P., Matviishina, Z. N., & Frechen, M. (2009). Pedo-chemical climate proxies in Late Pleistocene Serbian-Ukranian loess sequences. *Quaternary International*, 198, 113–123.

Bond, W. J. (2010). Do nutrient-poor soils inhibit development of forests? A nutrient stock analysis. *Plant and Soil*, 334, 47–60. https://doi.org/10.1007/s11104-010-0440-0

Bond, W. J., Woodward, F. I., Midgley, G. F. (2004). The global distribution of ecosystems in a world without fire. *New Phytologist*, 165, 525–538. https://doi.org/10.1111/j.1469-8137.2004.01252.x

Bond, W. J. (2008). What limits trees in C4 grasslands and savannas? Annual Review of *Ecology and Evolutionary Systematics*, 39, 641–659. https://doi.org/10.1146/annurev.ecolsys.39.110707.173411

Borgaard, O. K. (1982), The influence of iron oxides on the surface area of soil. *Journal of Soil Science*, 33, 443-449. https://doi.org/10.1111/j.1365-2389.1982.tb01779.x

Bortoluzzi, E., Samudio P. C., Ardisson, J., Tiecher, T., & Caner, L. (2015). Occurrence of iron and aluminum sesquioxides and their implications for the P sorption in subtropical soils. *Applied Clay Science*. 104, 196-204. 10.1016/j.clay.2014.11.032.

Boström B., Comstedt D., Ekblad A. (2007). Isotope fractionation and 13C enrichment in soil profiles during the decomposition of soil organic matter. *Oecologia*, 153(1), 89-98. doi: 10.1007/s00442-007-0700-8.

Bowman, D. M. J. S. (1992) Monsoon Forests in North-Western Australia. II. Forest-Savanna Transitions. *Australian Journal of Botany*, 40, 89-102.

Bowman, D. & Perry, G. (2017). Soil or fire: what causes treeless sedgelands in Tasmanian wet forests? *Plant and Soil*. 420, 1-18. 10.1007/s11104-017-3386-7.

Bray, R. H., & Kurtz, L. T. 1945. Determination of Total, Organic, and Available Forms of Phosphorus in Soils. *Soil Science*, 59, 1, 39-46.

Bremond, L., Bodin, S. C., Bentaleb, I., Favier, C., & Canal, S. (2017). Past tree cover of the Congo Basin recovered by phytoliths and δ 13 C along soil profiles. *Quaternary International,* 434, 91-101.

Brenner, J., Porter, W., Phillips, J. R., Childs, J., Yang, X. and Mayes, M. A. (2019) Phosphorus Sorption on Tropical Soils with Relevance to Earth System Model Needs. *Soil Research*, 57, 17-27. https://doi.org/10.1071/SR18197

Bronger, A. (1991). Argillic Horizons in Modern Loess Soils in an Ustic Soil Moisture Regime: Comparative Studies in Forest-Steppe and Steppe Areas from Eastern Europe and the United States, in: Lal, R., Stewart, B.A. (Eds.), Soil Restoration, Advances in Soil Science. Springer New York, New York, NY, pp. 41–90. https://doi.org/10.1007/978-1-4612-3030-4_2

Bruand, A., Hartmann, C., & Lesturgez, G. (2005). Physical properties of tropical sandy soils: A large range of behaviours. Management of Tropical Sandy Soils for Sustainable Agriculture. Management of Tropical Sandy Soils for Sustainable Agriculture. A holistic approach for sustainable development of problem soils in the tropics, Nov 2005, Khon Kaen, Thailand. pp. 148-158. hal-01420428

Brucker, E., & Spohn, M. (2019). Formation of soil phosphorus fractions along a climate and vegetation gradient in the Coastal Cordillera of Chile. *Catena, 180*, 203-211.

Butler, R.F. (1992). Paleomagnetism: magnetic domains to geologic terranes. Blackwell Scientific Publications, Oxford, UK. https://doi.org/10.5860/choice.29-5708

Butler, R.F., & Banerjee, S.K. (1975). Theoretical single-domain grain size range in magnetite and titanomagnetite. *Journal of Geophysical Research*, 80, 4049–4058. https://doi.org/10.1029/jb080i029p04049

Cesco, S., Rombolà, A. D., Tagliavini, M., Varanini, Z., & Pinton, R. (2006). Phytosiderophores released by graminaceous species promote ^{59}Fe-uptake in citrus. *Plant and Soil*, 287, 223–233. https://doi.org/10.1007/s11104-006-9069-4

Chadwick, O. A., & Chorover, J. (2001). The Chemistry of Pedogenic Thresholds. *Geoderma*, 100 (3-4), 321-53.

Chao, J., Chen, S., Hu, R., & Li, Y. (2017). Aggregate stability and size distribution of red soils under different land uses integrally regulated by soil organic matter, and iron and aluminum oxides. *Soil and Tillage Research*, 167, 73-79.

Chavent, M.C., Kuentz, V., Liquet, B., & Saracco, J. (2017). *ClustOfVar*. R Package. https://cran.r-project.org/web/packages/ClustOfVar/ClustOfVar.pdf

Chen, C. R., Condron, L. M., Davis, M. R., & Sherlock, R. R. (2000). Effects of Afforestation on Phosphorus Dynamics and Biological Properties in a New Zealand Grassland Soil. *Plant and Soil*, 220(1–2), 151–63. https://doi.org/10.1023/A:1004712401721.

Chen, T., Xie, Q., Xu, H., Chen, J., Ji, J., Lu, H., & Balsam, W. (2010). Characteristics and formation mechanism of pedogenic hematite in Quaternary Chinese loess and paleosols. *Catena*, 81, 217–225. https://doi.org/10.1016/j.catena.2010.04.001

Chiu, C.-Y., Pai, C.-W., & Yang, K.-L. (2005). Characterization of phosphorus in sub-alpine for- est and adjacent grassland soils by chemical extraction and phosphorus-31 nuclear magnetic resonance spectroscopy. *Pedobiologia*, 49, 655–663.

Cohen, A.S., Stone, J.R., Beuning, K.R.M., Park, L.E., Reinthal, P.N., Dettman, D., Scholz, C.A., Johnson, T.C., King, J.W., Talbot, M.R., Brown, E.T., & Ivory, S.J. (2007). Ecological consequences of early Late Pleistocene megadroughts in tropical Africa. *Proceedings of the National Academy of Sciences*, 104, 16422e16427.

Colombo, C., Palumbo, G., He, J.-Z., Pinton, R., & Cesco, S. (2014). Review on iron availability in soil: interaction of Fe minerals, plants, and microbes. *Journal of Soils and Sediments*, 14, 538–548. https://doi.org/10.1007/s11368-013-0814-z

Condron, L. M., & Goh, K. M. (1989). Effects of Long-term Phosphatic Fertilizer Applications on Amounts and Forms of Phosphorus in Soils under Irrigated Pasture in New Zealand. *Journal of Soil Science*, 40(2), 383–95. https://doi.org/10.1111/j.1365-2389.1989.tb01282.x.

Condron, L. M., & Newman, S. (2011). Revisiting the Fundamentals of Phosphorus Fractionation of Sediments and Soils. *Journal of Soils and Sediments*, 11(5), 830–40. https://doi.org/10.1007/s11368-011-0363-2.]

Coward, E., Thompson, A. & Plante, A. (2017). Iron-mediated mineralogical control of organic matter accumulation in tropical soils. *Geoderma*, 306, 206-216. 10.1016/j.geoderma.2017.07.026.

Craig, H. (1954). Carbon 13 in Plants and the Relationships between Carbon 13 and Carbon 14 Variations in Nature. *Journal of Geology*, 62, 115–149. https://doi.org/10.1086/626141

Craig, H. (1957). Isotopic standards for carbon and oxygen and correction factors for mass-spectrometric analysis of carbon dioxide. *Geochimica et Cosmochimica Acta*, 12, 133–149.

Crews, T. E., Kitayama, K., Fownes, J. H., Riley, R. H., Herbert, D. A., Mueller-Dombois, D., & Vitousek, P. M. 1995. Changes in Soil Phosphorus Fractions and Ecosystem Dynamics across a Long Chronosequence in Hawaii. *Ecology*, 76(5), 1407–1424. https://doi.org/10.2307/1938144.

Cross, A.F ., & Schlesinger, W. H. (1995). A Literature Review and Evaluation of the Hedley Fractionation: Applications to the Biogeochemical Cycle of Soil Phosphorus in Natural Ecosystems. *Geoderma*, 64(3–4), 197–214. https://doi.org/10.1016/0016-7061(94)00023-4.

Cuni-Sanchez, A., White, L. J. T., Calders, K., Jeffery, K. J., Abernethy, K., Burt, A., Disney, M., Gilpin, M., Gomez-Dans, J. L., & Lewis, S. L. (2016). African Savanna-Forest Boundary Dynamics: A 20-Year Study. *PLOS ONE*, 11, e0156934. https://doi.org/10.1371/journal.pone.0156934

Darby, M. I., & Isaac, E. D. (1974). Magnetocrystalline Anisotropy of Ferro- and Ferrimagnetics. *IEEE Transactions on Magnetics*, 10, 259–304. https://doi.org/10.1109/TMAG.1974.1058331

da Silva, Y., Silva, A., Biondi, C., van Straaten, P., Souza J. V., & Ferreira, O. (2016). Weathering rates and carbon storage along a climosequence of soils developed from contrasting granites in northeast Brazil. *Geoderma*. 284, 1-12. 10.1016/j.geoderma.2016.08.009.

Deines, P. (1980). The isotopic composition of reduced organic carbon. In: Fritz P. andFontes J.C. (eds), The Terrestrial Environment. Elsevier, Amsterdam, 329-406. https://doi.org/10.1016/b978-0-444-41780-0.50015-8

Desjardins, T., Andreux, F., Volkoff, B., & Cerri, C. C. (1994). Organic carbon and 13C contents in soils and soil size-fractions, and their changes due to deforestation and pasture installation in eastern Amazonia. *Geoderma*, 61, 103–118. https://doi.org/10.1016/0016-7061(94)90013-2

Desjardins, T., Turcq, B., Nguetnkam, J.P., Achoundong, G., Mandeng-Yogo, M., Cetin, F., & Lézine, A.M. (2013). δ13C variation of soil organic matter as an indicator of vegetation change during the Holocene in central Cameroon. *Comptes Rendus – Geosciences*, 345, 266–271. https://doi.org/10.1016/j.crte.2013.06.001

de L. Dantas, V., Batalha, M.A., & Pausas, J.G. (2013). Fire drives functional thresholds on the savanna–forest transition. *Ecology*, 94, 2454–2463. https://doi.org/10.1890/12-1629.1

De Tapia, E., & Adriano-Morán, C. (2012). Stable Carbon Isotopes Applied to Vegetation Reconstruction in the Teotihuacan Valley, Mexico. *Boletín De La Sociedad Geológica Mexicana, 64*(2), 161-169. Retrieved August 25, 2021, from http://www.jstor.org/stable/24921053

Dezzeo, N., Chacón, N., Sanoja, E., & Picon Nava, G. (2004). Changes in soil properties and vegetation characteristics along a forest-savanna gradient in southern Venezuela. *Forest Ecology and Management*, 200, 183-193. 10.1016/j.foreco.2004.06.016.

do Nascimento, C. A., Pagliari, P. H., Schmitt, D., He, Z., & Waldrip, H. (2016). Phosphorus concentrations in sequentially fractionated soil samples as affected by digestion methods. *Science Reports*, 5:17967. doi: 10.1038/srep17967

Dunham, K.M. (1991). Comparative effects of Acacia albida and Kigelia africana trees on soil characteristics in Zambezi riverine woodlands. *Journal of Tropical Ecology*, 7, 215–220. https://doi.org/10.1017/S026646740000537X

Dupont, L. (2011). Orbital scale vegetation change in Africa. *Quaternary Science Reviews*, 30, 3589–3602. https://doi.org/10.1016/j.quascirev.2011.09.019

Durrer, A., Margenot, A. J., Silva, L. C. R., Bohannan, B. J. M., Nusslein, K., Meredith, L., Saleska, S., Tsai, S.M., Andreote, F., Parikh, S. J., & Rodrigues, J. (2021). Beyond total carbon: long-term effect of deforestation on Amazonian soils alters soil C cycling. *Biogeochemistry*, 152, 179-194. https://doi.org/10.1007/s10533-020-00743-x.

Dzombak, R. M., & Sheldon, N. D. (2020). Weathering Intensity and Presence of Vegetation Are Key Controls on Soil Phosphorus Concentrations: Implications for Past and Future Terrestrial Ecosystems. *Soil Systems*, 4, 73. https://doi.org/10.3390/soilsystems4040073

Essington, M. E., (2015). Soil and Water Chemistry: An Integrative Approach, in: Taylor & Francis Group, L. (Ed.), Soil and Water Chemistry - An Integrative Approach. p. 633.

Farquhar, G. D., O'Leary, M. H., & Berry, J. A. (1982). On the relationship between carbon isotope discrimination and the intercellular carbon dioxide concentration in leaves. *Australian Journal of Plant Physiology*, 9, 121–137. https://doi.org/10.1071/PP9820121

Favier, C., Chave, J., Fabing, A., Schwartz, D., & Dubois, M. A. (2004). Modelling forest–savanna mosaic dynamics in man-influenced environments: effects of fire, climate and soil heterogeneity. *Ecological Modelling*, 171, 85–102. https://doi.org/10.1016/j.ecolmodel.2003.07.003

Feng, J., Turner, B.L., Lü, X., Chen, Z., Wei, K., Tian, J., Wang, C., Luo, W., & Chen, L. (2016). Phosphorus transformations along a large-scale climosequence in arid and semiarid grasslands of northern China. *Global Biogeochemical Cycles,* 30, 1264-1275.

Fick, S.E., & Hijmans, R.J., 2017. Worldclim 2: new 1-km spatial resolution climate surfaces for global land areas. *International Journal of Climatology*, 37, 4302–4315.

Flügel, T. J., Eckhardt, F. D., & Cotterill, F. P. D. (2015). The present day drainage patterns of the Congo River system and their Neogene evolution. Chapter 15 in M.J. de Wit et al. (eds.) Geology and Resource Potential of the Congo Basin, Regional Geology Reviews. Pp. 315-337.

Fontes, M. P. F., & Weed, S.B. (1996). Phosphate adsorption by clays from Brazilian Oxisols: relationships with specific surface area and mineralogy. *Geoderma*, 72(1-2): 37-51.

Frossard, E., Stewart, J. W. B., & St. Arnaud, R. J. (1989). Distribution and mobility of phosphorus in grassland and forest soils of Saskatchewan. *Canadian Journal of Soil Science*, 69(2), 401-416. Https://doi.org/10.4141/cjss89-040

Fujii, K., Hayakawa, C., Panitkasate, T., Maskhao, I., Funakawa, S., Kosaki, T., & Nawata, E. (2017). Acidification and buffering mechanisms of tropical sandy soil in northeast Thailand. *Soil and Tillage Research*, 165, 80-87. 10.1016/j.still.2016.07.008.

Furley, P. (1997). Plant ecology, soil environments and dynamic change in tropical savannas. *Progress in Physical Geography Earth and Environment*, 21, 257–284. https://doi.org/10.1177/030913339702100205

Furley, P., & Ratter, J. A. (1990). I. Pedological and botanical variations across the forest-savanna transition on Maraca Island. *The Geographical Journal*, 156, 251-266.

Gehring, A. U., Fischer, H., Louvel, M., Kunze, K., & Weidler, P. G. (2009). High temperature stability of natural maghemite: A magnetic and spectroscopic study. *Geophysics Journal International*, 179, 1361–1371. https://doi.org/10.1111/j.1365-246X.2009.04348.x

Gibbon, A., Silman, M. R., Malhi, Y., Fisher, J. B., Meir, P., Zimmermann, M., Dargie, G. C., Farfan, W. R., & Garcia, K. C. (2010). Ecosystem Carbon Storage Across the Grassland–Forest Transition in the High Andes of Manu National Park, Peru. *Ecosystems*, 13, 1097–1111. https://doi.org/10.1007/s10021-010-9376-8

Ghosh, S., & Guchhait, S. K. (2020). Laterites of the Bengal Basin Characterization, Geochronology and Evolution. Springer Nature, Switzerland AG. https://doi.org/https://doi.org/10.1007/978-3-030-22937-5

González-Pérez J. A., González-Vila F. J., Almendros G., & Knicker H. (2004). The effect of fire on soil organic matter--a review. *Environment International*, 30(6), 855-70. doi: 10.1016/j.envint.2004.02.003.

Gray, E. F., & Bond, W. J. (2015). Soil nutrients in an African forest/savanna mosaic: Drivers or driven? *South African Journal of Botany*, 101, 66–72. https://doi.org/10.1016/j.sajb.2015.06.003

Gu, C., Margenot, A. J. Navigating limitations and opportunities of soil phosphorus fractionation. *Plant and Soil*, 459, 13–17 (2021). https://doi.org/10.1007/s11104-020-04552-x

Gu C., Dam T., Hart S. C., Turner, B. L., Chadwick, O. A., Berhe, A. A., Hu Y., Zhu M. (2020) Quantifying uncertainties in sequential chemical extraction of soil phosphorus using XANES spectroscopy. *Environmental Science and Technology*, 54, 2257–2267. https://doi. org/10.1021/acs.est.9b05278

Guede, I., Ortega, L. A., Zuluaga, M. C., Alonso-Olazabal, A., Murelaga, X., Pina, M., Gutierrez, F. J., Iacumin, P. (2017). Isotope analyses to explore diet and mobility in a medieval Muslim population at Tauste (NE Spain). *PLOS ONE*, 12(5), e0176572. https://doi.org/10.1371/journal.pone.0176572

Guillocheau, F., Chelalou, R., Linol, B., Dauteuil, O., Robin, C., Mvondo, F., Callec, Y., & Colin, J.-P. (2015). Cenozoic landscape evolution in and around the Congo basin: constraints from sediments and planation surfaces. Chapter 14 in M.J. de Wit et al. (eds.) Geology and Resource Potential of the Congo Basin, Regional Geology Reviews. Pp. 271-313.

Guo, F. & Yost, R. S. (1998). Partitioning soil phosphorus into three discrete pools of differing availability. *Soil Science*, 163(10), 822–33. https://journals.lww.com/soilsci/pages/articleviewer.aspx?year=1998&issue=10000&article=00006&type=abstract.

Guppy, C. Is soil phosphorus fractionation as valuable as we think? (2021). *Plant and Soil* 459, 19–21. https://doi.org/10.1007/s11104-020-04817-5

Guy, R. D., Reid, D. M., & Krouse, H. R. (1986). Factors affecting 13C/12C ratios of inland halophytes. II. Ecophysiological interpretations of patterns in the field. *Canadian Journal of Botany*, 64, 2700–2707. https://doi.org/10.1139/b86-356

Gypser S., Hirsch F., Schleicher A. M., & Freese D. (2018). Impact of crystalline and amorphous iron- and aluminum hydroxides on mechanisms of phosphate adsorption and desorption. *Journal of Environmental Science (China)*, 70, 175-189. doi: 10.1016/j.jes.2017.12.001. Epub 2017 Dec 12. PMID: 30037404.

Hall, S. J., McDowell, W. H., & Silver, W.L. (2013). When wet gets wetter: Decoupling of moisture, redox biogeochemistry, and greenhouse gas fluxes in a humid tropical forest soil. *Ecosystems*, 16, 576–589.

Hartemink, A.E., & Huting, J. (2005). Sandy soils in Southern and Eastern Africs: extent, properties and management. Proceedings of the Management of Tropical Sandy Soils for Sustainable Agriculture Conference, November 17-December 2, 2005, Khon Kaen, Thailand. UN-FAO, Volume 1: 54-59.

Hashimoto, Y., Kang, J., Matsuyama, N., & Saigusa, M. (2012). Path Analysis of Phosphorus Retention Capacity in Allophanic and Non-allophanic Andisols. *Soil Science Society of America Journal*, 76, 441-448. https://doi.org/10.2136/sssaj2011.0196

Hatch, M.D., & Slack, C.R. (1966). Photosynthesis by sugar-cane leaves. A new carboxylation reaction and the pathway of sugar formation. *Biochemical Journal*, 101, 103–111. https://doi.org/10.1042/bj1010103

Hedley, M. J., Stewart, J. W. B., Chauhan, B. S. (1982). Changes in Inorganic and Organic Soil Phosphorus Fractions Induced by Cultivation Practices and by Laboratory Incubations. *Soil Science Society of America Journal*, 46(5), 970–76. https://doi.org/10.2136/sssaj1982.03615995004600050017x.

Helfenstein, J., Pistocchi, C., Oberson, A., Tamburini, F., Goll, D. S., & Frossard, E. (2020). Estimates of mean residence times of phosphorus in commonly considered inorganic soil phosphorus pools, *Biogeosciences*, 17, 441–454, https://doi.org/10.5194/bg-17-441-2020, 2020.

Hengl T., Heuvelink G. B. M., Kempen B., Leenaars J. G. B., Walsh M. G., Shepherd K. D., Sila, A., MacMillan, R. A., de Jesus, J. M., Tamene, L., Tondoh, J. E. (2015) Mapping Soil Properties of Africa at 250 m Resolution: Random Forests Significantly Improve Current Predictions. *PLoS ONE*, 10(6), e0125814. https://doi.org/10.1371/journal.pone.0125814

Hengl T., Mendes de Jesus J., Heuvelink G. B. M., Ruiperez Gonzalez M., Kilibarda M., Blagotić A., et al. (2017) SoilGrids250m: Global gridded soil information based on machine learning. *PLoS ONE*, 12(2), e0169748. https://doi.org/10.1371/journal.pone.0169748

Herold, N., Schöning, I., Michalzik, B. Trumbore, S., & Schrumpf, M. (2014). Controls on soil carbon storage and turnover in German landscapes. *Biogeochemistry*, 119, 435–451. https://doi.org/10.1007/s10533-014-9978-x

Herrmann, S., & Mohr, K. A. (2011). A continental-scale classification of rainfall seasonality regimes in Africa based on gridded precipitation and land surface temperature products. *Journal of Applied Meteorology and Climatology*, 50, 2504–2513, doi:10.1175/ JAMC-D-11-024.1.

Hessler, I., Dupont, L., Bonnefille, R., Behling, H., González, C., Helmens, K.F., Hooghiemstra, H., Lebamba, J., Ledru, M.-P., Lézine, A.-M., Maley, J., Marret, F., & Vincens, A., 2010. Millennial-scale changes in vegetation records from tropical Africa and South America during the last glacial. *Quaternary Science Reviews*, 29, 2882–2899. https://doi.org/10.1016/j.quascirev.2009.11.029

Hirota M., Holmgren M., Van Nes E. H., & Scheffer, M. (2011). Global resilience of tropical forest and savanna to critical transitions. *Science*. 334(6053), 232-235. doi: 10.1126/science.1210657. PMID: 21998390.

Hoag, C., & Svenning, J.C. (2017). African Environmental Change from the Pleistocene to the Anthropocene. *Annual Review of Environment and Resources*, 42, 27–54. https://doi.org/10.1146/annurev-environ-102016-060653

Hou, E., Chen, C., Luo, Y., Kuang, Y., Zhang, Y., Heenan, M., Lu, X., & Wen, D. (2018a). Effects of climate on soil phosphorus cycle and availability in natural terrestrial ecosystems. *Global Change Biology*, 24, 3344– 3356. https://doi.org/10.1111/gcb.14093

Hou, E., Tan, X., Heenan, M., & Wen, D. (2018b). A global dataset of plant available and unavailable phosphorus in natural soils derived by Hedley method. *Scientific Data*, 5, 180166. https://doi.org/10.1038/sdata.2018.166

Hou, E., Tan, X., Heenan, M., Wen, D. (2018c). Data Descriptor: A Global Dataset of Plant Available and Unavailable Phosphorus in Natural Soils Derived by Hedley Method. *Scientific Data*, 5, 1–13. https://doi.org/10.1038/sdata.2018.166.

Hou, E., Lu, X., Jiang, L., Wen, D., & Luo, Y. (2019). Quantifying soil phosphorus dynamics: A data assimilation approach. *Journal of Geophysical Research: Biogeosciences*, 124, 2159– 2173. https://doi.org/10.1029/2018JG004903

Hou, E., Luo, Y., Kuang, Y., Chen, C., Lu, X., Jiang, L., Luo, X., Wen, D. (2020). Global meta-analysis shows pervasive phosphorus limitation of aboveground plant production in natural terrestrial ecosystems. *Nature Communications*, 11, 637. https://doi.org/10.1038/s41467-020-14492-w

Huang, W.-S., Jien, S.-H., Tsai, H., Hseu, Z.-Y., & Huang, S.-T. (2016). Soil evolution ina. Tropical climate: An example from a chronosequence on marine terraces in Taiwan. *Catena*, 139, 61-72.

Isichei, A.O., & Muoghalu, J. I., (1992). The effects of tree canopy cover on soil fertility in a Nigerian savanna. *Journal of Tropical Ecology*, 8, 329–338. https://doi.org/10.1017/S0266467400006623

Issaka, R.N., Masunaga, T., Kosaki, T., & Wakatsuki, T. (1996). Soils of inland valleys of West Africa: General fertility parameters. *Soil Science and Plant Nutrition*, 42, 71–80. https://doi.org/10.1080/00380768.1996.10414690

Jackson, M.L. (1969). Soil chemical analysis. Adv. 2nd ed. Univ. Wisconsin, Madison, WI.

Jackson, M.L., Lim, C. H., & Zelazny, L.W. (1986). Oxides, hydroxides, and aluminosilicates. In A. Klute (ed.) Methods of soil analysis. Part 1. Physical and mineralogical methods. 2nd ed. Pp 101–150.

Jackson, M.L., & Barak, P. W. (2005). Soil chemical analysis: Advanced course. Rev. 2nd ed. Univ. Wisconsin, Madison, WI.

Jackson. M.L. & Sherman, G.D. (1953). Chemical Weathering of Minerals in Soils. *Advances in Agronomy*, 5, 219–318. https://doi.org/https://doi.org/10.1016/S0065-2113(08)60231-X

Jeffery, S., Abalos, D., Prodana, M., Bastos, A., Van Groenigen, J. W., Hungate, B., & Verheijen, F. (2017). Biochar boosts tropical but not temperate crop yields. *Environmental Research Letters*, 12, 053001. 10.1088/1748-9326/aa67bd.

Jenkinson, D. S., & Rainer, J. H. (1977). The Turnover of Soil Organic Matter in some of the Rothamsted Classical Experiments. *Soil Science*, 171, S130–S137.

Jiang, Z., Liu, Q., Dekkers, M. J., Colombo, C., Yu, Y., Barron, V. & Torrent, J. (2014). Ferro and antiferromagnetism of ultrafine-grained hematite. *Geochemistry, Geophysics, Geosystems*, 15(6), 2699–2712. https://doi.org/10.1002/2014GC005377.

Jones, R. C., & Uehara, G. (1973). Amorphous Coatings on Mineral Surfaces. *Soil Science Society of America Journal*, 37(5), 792–98. https://doi.org/10.2136/sssaj1973.03615995003700050044x.

Kimbrough, D. E., & Wakakuwa, J. R. (1989). Acid digestion for sediments, sludges, soils, and solid wastes. A proposed alternative to EPA SW 846 Method 3050. *Environmental Science & Technology*, 23(7), 898-900.

Konhauser, K.O. (1997). Bacterial iron biomineralization in nature. *FEMS Microbiology Reviews*, 20, 315–326. https://doi.org/10.1016/S0168-6445(97)00014-4

Kooijman A. M., Lubbers I., & van Til M. (2009). Iron-rich dune grasslands: relations between soil organic matter and sorption of Fe and P. *Environmental Pollution*, 157(11), 3158-65. doi: 10.1016/j.envpol.2009.05.022. Epub 2009 Jul 16. PMID: 19608316.

Kottek, M. J. Grieser, C. Beck, B. Rudolf, & F. Rubel. 2006. World map of the Köppen-Geiger climate classification updated. *Meteorologische Zeitschrift*, 15(3), 259-263

Krull, E. S., Bestland, E. A., Gates, & W. P. (2002). Soil Organic Matter Decomposition and Turnover in a Tropical Ultisol: Evidence from δ13C, δ15N and Geochemistry. *Radiocarbon*, 44, 93–112. https://doi.org/10.1017/s0033822200064705

Kukla, G., Heller, F., Ming, L. X., Chun, X. T., Sheng, L. T., & Sheng, A. Z. (1988). Pleistocene climates in China dated by magnetic susceptibility. *Geology*, 16, 811–814. https://doi.org/10.1130/0091-7613

Lehmann, C. E. R., Archibald, S. A., Hoffmann, W. A., & Bond, W. J. (2011). Deciphering the distribution of the savanna biome. *New Phytologist*, 191, 197–209. https://doi.org/10.1111/j.1469-8137.2011.03689.x

Lekwa, G., & Whiteside, E.P. (1986). Coastal plain soils of southern Nigeria: I. Morphology, classification and genetic relationships. *Soil Science Society of America Journal*, 50, 154-160.

Linol, B., de Wit, M. J., Guillocheau, F., de Wit, M. C. J., Anka, Z., & Colin, J. P. (2015). Formation and collapse of the Kalahari duricrust ['African Surface'] across the Congo basin, with implications for changes in rates of Cenozoic off-shore sedimentation. Chapter 10 in M.J. de Wit et al. (eds.) Geology and Resource Potential of the Congo Basin, Regional Geology Reviews. Pp. 193-210.

Lloyd, J., Bird, M. I., Vellen, L., Miranda, A. C., Veenendaal, E. M., Djagbletey, G., Miranda, H. S., Cook, G., & Farquhar, G. D. (2008). Contributions of woody and herbaceous vegetation to tropical savanna ecosystem productivity: a quasi-global estimate. *Tree Physiology*, 28, 451–468. https://doi.org/10.1093/treephys/28.3.451

Lloyd, J., Domingues, T. F., Schrodt, F., Ishida, F. Y., Feldpausch, T. R., Saiz, G., Quesada, C. A., Schwarz, M., Torello-Raventos, M., Gilpin, M., Marimon, B. S., Marimon-Junior, B. H., Ratter, J. A., Grace, J., Nardoto, G. B., Veenendaal, E., Arroyo, L., Villarroel, D., Killeen, T. J., Steininger, M., & Phillips, O. L. (2015) Edaphic, structural and physiological contrasts across Amazon Basin forest–savanna ecotones suggest a role for potassium as a key modulator of tropical woody vegetation structure and function. *Biogeosciences*, 12, 6529–6571. https://doi.org/10.5194/bg-12-6529-2015

Long, X., Ji, J., & Balsam, W. (2011). Rainfall-dependent transformations of iron oxides in a tropical saprolite transect of Hainan Island, South China: Spectral and magnetic measurements. *Journal of Geophysical Research*, 116, F03015. https://doi.org/10.1029/2010JF001712

Long X. Y., Ji J. F., Barron V., & Torrent, J. (2016). Climatic thresholds for pedogenic iron oxides under aerobic conditions: Processes and their significance in paleoclimate reconstruction. *Quaternary Science Reviews*, 150, 264–277

Lovley, D. R., Stolzt, J. F., & Phillips, E. J. P. (1987). Anaerobic production of magnetite by a dissimilatory iron-reducing microorganism. *Nature* 330, 252–254.

Lynch, J. P. (2011). Root Phenes for Enhanced Soil Exploration and Phosphorus Acquisition: Tools for Future Crops. *Plant Physiology* 156(3), 1041–49. https://doi.org/10.1104/pp.111.175414.

Mahaney, W., Hancock, R., Somelar, P., & Milan, A. (2016). Iron and aluminum soil/paleosol extractions as age/environment indicators: Some examples from a catchment in southern Ontario, Canada. *Geomorphology*, 270, 159-171.

Maher, B. A., & Taylor, R. M. (1988). Formation of ultrafine-grained magnetite in soils. *Nature*, 336, 368–370. https://doi.org/10.1038/336368a0

Maher, B. A. (1991). Inorganic formation of ultrafine-grained magnetite, in: Frankel, R. B., Blakemore, R. P. (Eds.), Iron Biominerals. Plenum, Newyork, pp. 179–191.

Maher, B. A. (1998). Magnetic properties of modern soils and quaternary loessic paleosols: Paleoclimatic implications. *Palaeogeography, Palaeoclimatology, Palaeoecology*, 137, 25–54. https://doi.org/10.1016/S0031-0182(97)00103-X

Maher, B. & Thompson, R. (1995). Paleorainfall Reconstructions from Pedogenic Magnetic Susceptibility Variations in the Chinese Loess and Paleosols. *Quaternary Research (United States)*, 44, 383–391.

Malhi, Y., Adu-Bredu, S., Asare, R. A., Lewis, S. L., & Mayaux, P. (2013). African rainforests: Past, present and future. *Philosophical Transactions of the Royal Society B Biological Sciences*, 368, 1625. https://doi.org/10.1098/rstb.2012.0312

Maley, J. (1996). The African rainforest - main characteristics of changes in vegetation and climate from the Upper Cretaceous to the Quaternary. *Proceedings of the Royal Society of Edinburgh, Section B: Biological Sciences*, 104, 31–73.

Maley, J., Doumenge, C., Giresse, P., Mahé, G., Philippon, N., Hubau, W., M.O. Lokonda, J.M. Tshibamba, & Chepstow-Lusty, A. (2018). Late Holocene forest contraction and fragmentation in central Africa. *Quaternary Research*, 89(1), 43-59. doi:10.1017/qua.2017.97

Maranguit, D., Guillaume, T., & Kuzyakov, Y. (2017). Land-use change affects phosphorus fractions in highly weathered tropical soils. *Catena, 149*, 385-393.

Marfo, T., Datta, R., Pathan, S., & Vranová, V. (2019). Ecotone Dynamics and Stability from Soil Scientific Point of View. *Diversity*, 11, 53. https://doi.org/10.3390/d11040053

Margenot, A. J., Paul, B. K., Sommer, R. R., Pulleman, M. M., Parikh, S. J., Jackson, L. E., & Fonte, S. J. (2017). "Can Conservation Agriculture Improve Phosphorus (P)

Availability in Weathered Soils? Effects of Tillage and Residue Management on Soil P Status after 9 Years in a Kenyan Oxisol." *Soil and Tillage Research*, 166, 157–66. https://doi.org/10.1016/j.still.2016.09.003.

Markham, R. H., & Babbedge, A. J. (1979). Soil and Vegetation Catenas on the Forest-Savanna Boundary in Ghana. *Biotropica*, 11, 224. https://doi.org/10.2307/2388043

Maxbauer, D. P., Feinberg, J. M., & Fox, D. L. (2016). Magnetic mineral assemblages in soils and paleosols as the basis for paleoprecipitation proxies: A review of magnetic methods and challenges. *Earth-Science Reviews*, 155, 28–48. https://doi.org/10.1016/j.earscirev.2016.01.014

Maxbauer, D. P., Feinberg, J. M., Fox, D. L., Nater, E. A., 2017. Response of pedogenic magnetite to changing vegetation in soils developed under uniform climate, topography, and parent material. *Scientific Reports*, 7, 1–10. https://doi.org/10.1038/s41598-017-17722-2

McDowell, R. W., Cade-Menun, B., & Stewart, I. (2007). Organic Phosphorus Speciation and Pedogenesis: Analysis by Solution 31P Nuclear Magnetic Resonance Spectroscopy. *European Journal of Soil Science*, 58(6), 1348–57. https://doi.org/10.1111/j.1365-2389.2007.00933.x.

McFadden, L., & Hendricks, D. (1985). Changes in the Content and Composition of Pedogenic Iron Oxyhydroxides in a Chronosequence of Soils in Southern California. *Quaternary Research*, 23(2), 189-204. doi:10.1016/0033-5894(85)90028-6

Mcgill, W . B. & Cole, C. V. (1981). Comparative Aspects of Cycling of Organic C, N, S and P through Soil Organic Matter. *Geoderma*, 26, 267–86.

McLaren, T. I., Smernik, R. J., McLaughlin, M. J., McBeath, T. M., Kirby, J. K., Simpson, R. J., Guppy, C. N., Doolette, A. L., & Richardson, A. E. 2015. Complex Forms of Soil Organic Phosphorus-A Major Component of Soil Phosphorus. *Environmental Science and Technology*, 49(22), 13238–45. https://doi.org/10.1021/acs.est.5b02948.

Mills, A.J., Rogers, K.H., Stalmans, M., & Witkowski, E.T.F. (2006). A Framework for Exploring the Determinants of Savanna and Grassland Distribution. *BioScience*, 56, 579. https://doi.org/10.1641/0006-3568

Moir, J, & Tiessen, H. (2007). Characterization of Available P by Sequential Extraction. In *Soil Sampling and Methods of Analysis, Second Edition*. https://doi.org/10.1201/9781420005271.ch25.

Morley, R.J. (2000). Origin and evolution of tropical rain forests. John Wiley & Sons, Inc. Hoboken, NJ, USA. 384pp.

Morris, E. K., Caruso, T., Buscot, F., Fischer, M., Hancock, C., Maier, T. S., Meiners, T., Müller, C., Obermaier, E., Prati, D., Socher, S. A., Sonnemann, I., Wäschke, N., Wubet, T., Wurst, S., & Rillig, M. C. (2014). Choosing and using diversity indices: insights for ecological applications from the German Biodiversity Exploratories. *Ecology and Evolution*, 4(18), 3514-24. doi: 10.1002/ece3.1155.

Moskowitz, B. M., Frankel, R. B., Bazylinski, D. A., Jannasch, H. W., Lovley, D. R. (1989). A comparison of magnetite particles produced anaerobically by magnetotactic and dissimilatory iron-reducing bacteria. *Geophysical Research Letters*, 16, 665–668. https://doi.org/10.1029/GL016i007p00665

Mou, X. M., Wu, Y., Niu, Z., Jia, B., Guan, Z. H., Chen, J., Li, H., Cui, H., Kuzyakov, Y., & Li, X. G. (2020). Soil Phosphorus Accumulation Changes with Decreasing Temperature along a 2300 m Altitude Gradient. *Agriculture, Ecosystems and Environment*, 301, 107050. https://doi.org/10.1016/j.agee.2020.107050.

Mujuru, L., Mureva, A., Velthorst, E., & Hoosbeek, M. (2013). Land use and management effects on soil organic matter fractions in Rhodic Ferralsols and Haplic Arenosols in Bindura and Shamva districts of Zimbabwe. *Geoderma*, 209-210, 262-272. 10.1016/j.geoderma.2013.06.025.

Müldner, G. (2019). Investigating Medieval Diet and Society by Stable Isotope Analysis of Human Bone. *Medieval Archaeology*, 1957–2007, 327–346. https://doi.org/10.4324/9781315089034-17

Mullins, C. E. (1977). Magnetic Susceptibility of the Soil and Its Significance in Soil Science – a Review. *Journal of Soil Science*, 28, 223–246. https://doi.org/10.1111/j.1365-2389.1977.tb02232.x

Munroe, J. S., 2012. Physical, Chemical, and Thermal Properties of Soils across a Forest-Meadow Ecotone in the Uinta Mountains, Northeastern Utah, U.S.A. *Arctic, Antarctic, and Alpine Research*, 44, 95–106. https://doi.org/10.1657/1938-4246-44.1.95

Munzimi, Y.A., Hansen, M. C., Adusei, B., & Senay, G. B. (2015). Characterizing Congo Basin rainfall and climate using Tropical Rainfall Measuring Mission (TRMM) satellite data and limited rain gauge ground observations. *Journal of Applied Meteorology and Climatology*, 54(3): 541-555.

Murphy, B. P., Bowman, D. M. J. S. (2012). What controls the distribution of tropical forest and savanna?: Tropical forest and savanna distribution. *Ecology Letters*, 15, 748–758. https://doi.org/10.1111/j.1461-0248.2012.01771.x

Murphy, J. & Riley, J. P. (1962). A modified single solution method for the determination of phosphate in natural waters. *Analytica Chimica Acta*, 27: 31-36.

Myers, T. S., Tabor, N. J., & Jacobs, L. L. (2011). Late Jurassic paleoclimate of Central Africa. *Palaeogeography, Palaeoclimatology, Palaeoecology*, 311, 111–125. https://doi.org/10.1016/j.palaeo.2011.08.013

Nair, V. D., Portier, K. M., Graetz, D. A., & Walker, M. L. (2004). An environmental threshold for degree of phosphorus saturation in sandy soils. *Journal of Environmental Quality*, 33(1), 107-13. doi: 10.2134/jeq2004.1070. PMID: 14964364.

Naseem, S., Khan, S., Husain, S., & Khan, W. (2018). Exploring the Room-Temperature Ferromagnetism and Temperature-Dependent Dielectric Properties of Sr/Ni-Doped LaFeO3 Nanoparticles Synthesized by Reverse Micelle Method. *Journal of Electronic Materials*, 47, 1916–1923. https://doi.org/10.1007/s11664-017-5987-6

Nash, D. J., De Cort, G., Chase, B. M., Verschuren, D., Nicholson, S. E., Shanahan, T. M., Asrat, A., Lézine, A. M., & Grab, S. W. (2016). African hydroclimatic variability during the last 2000 years. *Quaternary Science Reviews*, 154, 1–22. https://doi.org/10.1016/j.quascirev.2016.10.012

Negassa, W., & Leinweber, P. (2009). How Does the Hedley Sequential Phosphorus Fractionation Reflect Impacts of Land Use and Management on Soil Phosphorus: A Review. *Journal of Plant Nutrition and Soil Science*, 172(3), 305–25. https://doi.org/10.1002/jpln.200800223.

O'Leary, M.H. (1988). Carbon Isotopes In Photosynthesis. *Bioscience*, 38, 328–336.

Oliveras, I., & Malhi, Y. (2016). Many shades of green: the dynamic tropical forest–savannah transition zones. *Philosophical Transactions of the Royal Society B Biological Sciences*, 371, 20150308. https://doi.org/10.1098/rstb.2015.0308

Onthong, J., Osaki, M., Nilnond, C., & Tadano, T. (1999) Phosphorus status of some highly weathered soils in peninsular Thailand and availability in relation to citrate and oxalate application. *Soil Science and Plant Nutrition*, 45:3, 627-637, DOI: 10.1080/00380768.1999.10415826

Parfitt, R. L., & Smart, R. S. C. 1978. The Mechanism of Sulfate Adsorption on Iron Oxides. *Soil Science Society of America Journal*, 42 (1): 48–50. https://doi.org/10.2136/sssaj1978.03615995004200010011x.

Peel, M. C., Finlayson, B. L., and McMahon, T. A. (2007). Updated world map of the Köppen-Geiger climate classification, Hydrol. *Earth Systems Science*, 11, 1633–1644, https://doi.org/10.5194/hess-11-1633-2007.

Pessenda, L., Aravena, R., Melfi, A., Telles, E., Boulet, R., Valencia, E., & Tomazello, M. (1996). The Use of Carbon Isotopes (13C,14C) in Soil to Evaluate Vegetation Changes During the Holocene in Central Brazil. *Radiocarbon, 38*(2), 191-201. doi:10.1017/S0033822200017562

Pessenda, L., Ribeiro, A., Gouveia, S., Aravena, R., Boulet, R., & Bendassolli, J. (2004). Vegetation dynamics during the late Pleistocene in the Barreirinhas region, Maranhão State, northeastern Brazil, based on carbon Isotopes in soil organic matter. *Quaternary Research, 62*(2), 183-193. doi:10.1016/j.yqres.2004.06.003

Pettapiece, W.W. (1969). The forest-grassland transition. In: S. Pawluk, (ed.), Pedology and Quaternary Research. University of Alberta, Edmonton, pp. 103-113.

Plana, V. (2004). Mechanisms and tempo of evolution in the African Guineo-Congolian rainforest. *Philosophical Transactions of the Royal Society B Biological Sciences*, 359, 1585–1594. https://doi.org/10.1098/rstb.2004.1535

Porder, S., & Ramachandran, S. (2013). The phosphorus concentration of common rocks—a potential driver of ecosystem P status. *Plant and Soil*, 367**,** 41–55. https://doi.org/10.1007/s11104-012-1490-2

Portes, R., Spinola, D., & Kühn, P. (2016). Pedogenesis across a climatic gradient in tropical high mountains, Cordillera Blanca - Peruvian Andes. *Catena*, 147, 441-452. 10.15496/publikation-14535.

Pronk, G. J., Heister, K. & Kögel-Knabner, I. (2011). Iron Oxides as Major Available Interface Component in Loamy Arable Topsoils. *Soil Science Society of America Journal*, 75, 2158-2168. https://doi.org/10.2136/sssaj2010.0455

Puttaso, A., Vityakon, P., Saenjan, P., Trelo-ges, V., & Cadisch, G. (2011). Relationship between residue quality, decomposition patterns, and soil organic matter accumulation in a tropical sandy soil after 13 years. *Nutrient Cycling in Agroecosystems*, 89, 159-174. 10.1007/s10705-010-9385-1.

R Core Team. 2019. R: A language and environment for statistical computing. R Foundation for Statistical Computing, Vienna, Austria. http://www.R-project.org/.

Reichard, P. U., Kraemer, S. M., Frazier, S. W., & Kretzschmar, R. (2005). Goethite Dissolution in the Presence of Phytosiderophores: Rates, Mechanisms, and the Synergistic Effect of Oxalate. *Plant and Soil*, 276, 115–132. https://doi.org/10.1007/s11104-005-3504-9

Rennert, T. (2019). Wet-chemical extractions to characterise pedogenic Al and Fe species – a critical review. *Soil Research*, 57, 1-16. 10.1071/SR18299.

Reynolds, R.L., & King, J.W. (1995). Magnetic records of climate change. *Reviews of Geophysics*, 33, 101–110. https://doi.org/10.1029/95RG00354

Roberts, E., Jelsma, H.A., & Hegna, T. (2015). Mesozoic sedimentary cover sequences of the Congo Basin in the Kasai region, Democratic Republic of Congo. In: de Wit, M. J.,

Guillocheau, F., & de Wit, M. C. J. Geology and Resources Potential of the Congo Basin. Springer-Verlag, Heidelberg, Germany. https://doi.org/10.1007/978-3-642-29482-2_9

Rounick, J.S., & Winterbourn, M.J. (1986). Stable Carbon Isotopes and Carbon Flow in Ecosystems. *Bioscienc*e, 36, 171–177. https://doi.org/10.2307/1310304

Sanchez, P. (2019). *Properties and Management of Soils in the Tropics* (1st ed.). Cambridge: Cambridge University Press. doi:10.1017/9781316809785

Scarseth, George D. (1935). The Mechanism of Phosphate Retention by Natural Alumino-Silicate Colloids. *Agronomy Journal*, 27(8), 596–616. https://doi.org/10.2134/agronj1935.00021962002700080002x.

Schaetzl, R. J. (2002). A Spodosol-Entisol Transition in Northern Michigan. *Soil Science Society of America Journal*, 66, 1272–1284. https://doi.org/10.2136/sssaj2002.1272

Schaetzl, R. J., & Thompson, M. L. (2015). Soils: Genesis and geomorphology (2nd Ed). Cambridge University Press, Cambridge, UK. 795 pp.

Schlesinger, W. H., Bruijnzeel, L. A., Bush, M. B., Klein, E. M., Mace, K. A., Raikes, J. A., & Whittaker, R. J. (1998). The biogeochemistry of phosphorus after the first century of soil development on Rakata Island, Krakatau, Indonesia. *Biogeochemistry*, 40: 37-55.

Schoeneberger, P. J., Wysocki, D. A., Benham, E. C., & Soil Survey Staff. (2012). Field book for describing and sampling soils, version 3.0. USDA– NRCS National Soil Survey Center, Lincoln, NE.

Schwartz, D., Mariotti, A., Lanfranchi, R., & Guillet, B. (1986). 13C/12C Ratios of soil organic matter as indicators of vegetation changes in the Congo. *Geoderma*, 39, 97–103. https://doi.org/10.1016/0016-7061(86)90069-8

Schwartz, D., Mariotti, A., Trouve, C., van der Borg, K., & Guillet, B. (1992). A study of 13C and 14C isotopic profiles in a sandy ferrallitic soil in the Congolese coastal area. Implications concerning soil organic matter dynamics and vegetation history[Etude des profils isotopiques 13C et 14C d'un sol ferrallitique sableux du littoral congolais. Implications sur la dynamique de la matiere organique et l'histoire de la vegetation]. *Comptes Rendus - Academie des Sciences, Serie II*, 315, 1411-1417

Schwartz, D,, de Foresta, H., Mariotti, A., Balesdent, J., Massimba, J. P., Girardin C. (1996). Present dynamics of the savanna-forest boundary in the Congolese Mayombe: a pedological, botanical and isotopic (^{13}C and ^{14}C) study. *Oecologia*, 106(4), 516-524. doi: 10.1007/BF00329710. PMID: 28307452.

Schwertmann, U. (1973). Use of oxalate for Fe extraction from soils. *Canadian Journal of Soil Science*, 53(2), 244-246. https://doi.org/10.4141/cjss73-037

Schwertmann, U. (1991). Solubility and dissolution of iron oxides. *Plant and Soil*, 130, 1–25. https://doi.org/10.1007/BF00011851

Schwertmann, U. (1993). Relations Between Iron Oxides Soil Color, and Soil Formation. Soil Science Society of America SSSA Special Publication no. 31. Pp 51–69.

Senut, B., Pickford, M., & Ségalen, L. (2009). Neogene desertification of Africa. C.R. *Geoscience*, 341, 591-602.

Severson, R. C., & Arneman, H. F. (1973). Soil Characteristics of the Forest-Prairie Ecotone in Northwestern Minnesota. *Soil Science Society of America Journal*, 37, 593–599. https://doi.org/10.2136/sssaj1973.03615995003700040035x

Shen, X.-H., Shen, Z.-Y., Yang, S.-J., & Fang, D.-J. (2001). Amorphous Matter in Kaolins and Its Geological Implications. *Journal of Zhejiang University SCIENCE* 2 (1): 84. https://doi.org/10.1631/jzus.2001.0084.

Shirato, Y., Paisancharoen, K., Sangtong, P., Nakviro, C., Yokozawa, M., & Matsumoto, N. (2005). Testing the Rothamsted Carbon Model against data from long-term experiments on upland soils in Thailand. *European Journal of Soil Science*, 56, 179-188. https://doi.org/10.1111/j.1365-2389.2004.00659.x

Silva, L. C. R., Hoffmann, W. A., Rossatto, D. R., Haridasan, M., Franco, A. C., & Horwath, W. R. (2013). Can savannas become forests? A coupled analysis of nutrient stocks and fire thresholds in central Brazil. *Plant and Soil*, 373, 829–842. https://doi.org/10.1007/s11104-013-1822-x

Sims, J. T., Maguire, R. O., Leytem, A. B., Gartley, K. L., & Paulter, M. C. (2002). Evaluation of Mehlich-3 as an agri-environmental soil phosphorus test for the Mid-Atlantic United States of America. *Soil Science Society of America Journal*, 66, 2016–2032.

Slessarev, E. W., Lin, Y., Bingham, N. L., Johnson, J. E., Dai, Y., Schimel, J. P., & Chadwick, O. A. (2016). Water balance creates a threshold in soil pH at the global scale. Nature, 540(7634), 567-569. doi: 10.1038/nature20139.

Smeck, E. N. (1973). Phosphorus: an indicator of pedogenetic weathering processes. *Soil Science*, 155, 199-206.

Smith, B. N., & Epstein, S. (1971). Two Categories of 13C/12C Ratios for Higher Plants. *Plant Physiology*, 47, 380–384. https://doi.org/10.1104/pp.47.3.380

Smith, S. E., Smith, F. A., & Jakobsen, I. (2003). Mycorrhizal Fungi Can Dominate Phosphate Supply to Plants Irrespective of Growth Responses. *Plant Physiology*, 133, 16–20. https://doi.org/www.plantphysiol.org/cgi/doi/10.1104/pp.103.024380.

Soil Survey Staff. 1997. Global soil moisture regimes. USDA-NRCS. Web Resource accessible at [https://www.nrcs.usda.gov/wps/portal/nrcs/detail/soils/use/worldsoils/?cid=nrcs142p2_054017, accessed 20AUG, 2021]

Soil Survey Staff. 2014a. Kellogg soil survey laboratory methods manual. R. Burt and Soil Survey Staff, editors, Soil survey investigations report no. 42, version 5.0. USDA–NRCS, Washington, DC.

Soil Survey Staff. 2014b. Keys to soil taxonomy, 12th ed. USDA–NRCS, Washington, DC.

Sokolova, T. A. 2013. The Destruction of Quartz, Amorphous Silica Minerals, and Feldspars in Model Experiments and in Soils: Possible Mechanisms, Rates, and Diagnostics (the Analysis of Literature). *Eurasian Soil Science*, 46(1), 91–105. https://doi.org/10.1134/S1064229313010080.

St. Arnaud, R.J., & Whiteside, E. P. (1964). Morphology and genesis ofa Chernozemic to Podzolic sequence of soil profiles in Saskatchewan. *Canadian Journal of Soil Science*, 44, 88-99.

Staal, A., & Flores, B. (2015). Sharp ecotones spark sharp ideas: comment on "Structural, physiognomic and above-ground biomass variation in savanna-forest transition zones on three continents - How different are co-occurring savanna and forest formations?" by Veenendaal et al. (2015). *Biogeosciences*, 12, 5563–5566. 10.5194/bg-12-5563-2015.

Stanjek, H. (1987). The formation of maghemite and hematite from lepidocrocite and goethite in a Cambisol from Corsica, France. *Zeitschrift für Pflanzenernährung und Bodenkunde*, 150, 314–318. https://doi.org/10.1002/jpln.19871500509

Stober, J.C., & Thompson, R. (1979). An Investigation into the Source of Magnetic Minerals in some Finnish Lake Sediments. *Earth and Planetary Science Letters*, 45(2), 464–474.

Sugihara, S., Shibata, M., Mvondo Ze, A. D., Araki, S., & Funakawa, S. (2014) Effect of vegetation on soil C, N, P and other minerals in Oxisols at the forest-savanna transition zone of central Africa, *Soil Science and Plant Nutrition*, 60:1, 45-59, DOI: 10.1080/00380768.2013.866523

Sugihara, S., Shibata, M., Ze, A., Araki, S., & Funakawa, S. (2015). Effects of vegetation on soil microbial C, N, and P dynamics in a tropical forest and savanna of Central Africa. *Applied Soil Ecology*, 87, 91-98. 10.1016/j.apsoil.2014.11.002.

Sugihara, S., Shibata, M., Mvondo Ze, A.D, Tanaka, H., Kosaki, T., & Funakawa, S. (2019). Forest understories controlled the soil organic carbon stock during the fallow

period in African tropical forest: a ^{13}C analysis. *Scientific Reports*, 9, 9835. https://doi.org/10.1038/s41598-019-46406-2

Syers, J. K., Williams, J. D. H., Campbell, A. S., & Walker, T. W. (1967). The Significance of Apatite Inclusions in Soil Phosphorus Studies. *Soil Science Society of America Journal*, 31(6), 752–56. https://doi.org/10.2136/sssaj1967.03615995003100060016x

Taboada, T., Ferro-Vázquez, C., Stoops, G., Martínez-Cortizas, A., Rodríguez-Flores, R., & Rodríguez-Lado, L. 2019. Secondary aluminium, iron and silica phases across a volcanic soil climosequence, Galápagos Islands. *Eurasian Journal of Soil Science*, 70: 540– 549. https://doi.org/10.1111/ejss.12788

Takamoto, A., Hashimtot, Y, Asano, M., Noguchi, K., & Wagai, R. (2021). Distribution and chemical species of phosphorus across density fractions in Andisols of contrasting mineralogy. *Geoderma*, 395, 115080. https://doi.org/10.1016/j.geoderma.2021.115080

Tamaura, Y., Ito, K., & Katsura, T. (1983). Transformation of y-FeO(0H) to Fe304 by adsorption of iron (II) ion and FeO(OH). *Journal of the Chemical Society, Dalton Transactions*, 2, 189–194.

Tauxe, L., Banerjee, S. K., Butler, R. L., & Voo, R. V. D. (2008). Essentials of Rock and Paleomagnetism 496.

Taylor, R. M., Maher, B. A., & Self, P.G. (1987). Magnetite in soils: I. The synthesis of single -domain and superparamagnetic magnetite. *Clay Mineralogy*, 22, 411–422.

Thompson, J.A., & Bell, J.C. (1996). Color Index for Identifying Hydric Conditions for Seasonally Saturated Mollisols in Minnesota. *Soil Science Society of America Journal*, 60, 1979-1988. https://doi.org/10.2136/sssaj1996.03615995006000060051x

Tiessen, H., & Moir, J.O. (2006). Characterization of Available P by Sequential Extraction. In *Soil Sampling and Methods of Analysis, Second Edition*, edited by E.G. Carter, M.R. & Gregorich, 2nd ed., 321–34. Boka Raton, FL: Taylor & Francis Group, LLC.

Tiessen, H., Stewart, J. W. B., & Cole, C. V. (1984). Pathways of Phosphorus Transformations in Soils of Differing Pedogenesis. *Soil Science Society of America Journal*, 48(4), 853–58. https://doi.org/10.2136/sssaj1984.03615995004800040031x.

Tiessen, H., Chacon, P., Cuevas, E. (1994). Phosphorus and Nitrogen Status in Soils and Vegetation along a Toposequence of Dystrophic Rainforests on the Upper Rio Negro" *Oecologia*, 99, 145–50.

Turner, B. L. & Condron, L. M. (2013). Pedogenesis, Nutrient Dynamics, and Ecosystem Development: The Legacy of T.W. Walker and J.K. Syers. *Plant and Soil*, 367, 1–10. https://doi.org/10.1007/s11104-013-1750-9.

Turner, B. L., Condron, L. M., Richardson, S. J., Peltzer, D. A., & Allison, V. A. (2007). Soil Organic Phosphorus Transformations during Pedogenesis. *Ecosystems*, 10(7), 1166–81. https://doi.org/10.1007/s10021-007-9086-z.

Uygur, V., Durgun, B., & Senol, H. (2017) Chemical Fractions of Phosphorus: The Effect of Soil Orders, Soil Properties, and Land Use. *Communications in Soil Science and Plant Analysis*, 48:11, 1319-1335, DOI: 10.1080/00103624.2017.1341919

Vågen, T. G, Winowiecki, L. A., Walsh, M. G., Desta, L. T., & Tondoh, J. E. (2010). Land Degradation Surveillance Framework (LSDF): Field Guide. International Center for Tropical Agriculture, World Agroforestry Centre, and the Earth Institute at Columbia University.

Vågen, T.G., Winowiecki, L.A., Abegaz, A., & Hadgu, K.M. (2013). Landsat-based approaches for mapping of land degradation prevalence and soil functional properties in Ethiopia. *Remote Sensing of the Environment*, 134, 266–275. https://doi.org/10.1016/j.rse.2013.03.006

Van Hees, P. A. W., Lundström, U. S., & Giesler, R. (2000). Low molecular weight organic acids and their Al-complexes in soil solution - Composition, distribution and seasonal variation in three podzolized soils. *Geoderma*, 94, 173–200. https://doi.org/10.1016/S0016-7061(98)00140-2

Veenendaal, E. M., Torello-Raventos, M., Miranda, H. S., Sato, N. M., Oliveras, I., van Langevelde, F., Asner, G. P., & Lloyd, J. (2018). On the relationship between fire regime and vegetation structure in the tropics. *New Phytologist*, 218, 153–166. https://doi.org/10.1111/nph.14940

Verosub, K. L., Fine, P., Singer, M. J., & Tenpas, J. (1993). Pedogenesis and paleoclimate: interpretation of the magnetic susceptibility record of Chinese loess-paleosol sequences. *Geology*, 21, 1011–1014. https://doi.org/10.1130/0091-7613

Vitousek, P.M., & Chadwick, O.A. (2013). Pedogenic Thresholds and Soil Process Domains in Basalt-Derived Soils. *Ecosystems*, 16, 1379–1395. https://doi.org/10.1007/s10021-013-9690-z

Vogel, J.C. (1980). Fractionation of the Carbon Isotopes During Photosynthesis. Sitzungsberichte der Heidelberger Akademie der Wissenschaften book series (HD AKAD, volume 1980 / 3. https://doi.org/10.1007/978-3-642-46428-7 e-ISBN-13:

Wada, K. (1989). Allophane and imogolite. In J.B. Dixon and S.B. Weed (eds.) Minerals in soil environment. 2nd ed. Soil Science Society of America Publication 1, pp 1051–1087.

Wade, J., Waterhouse, H., Roche, L., & Horwath, W. (2018). Structural equation modeling reveals iron (hydr)oxides as a strong mediator of N mineralization in California agricultural soils. *Geoderma*, 315, 120-129. 10.1016/j.geoderma.2017.11.039.

Wagai, R., Mayer, L. M., Kitayama, K., & Shirato, Y. (2013). Association of organic matter with iron and aluminum across a range of soils determined via selective dissolution techniques coupled with dissolved nitrogen analysis. *Biogeochemistry*, 112, 95–109.

Walker, T.W. & Adams, A. F. R. (1957). Studies on soil organic matter I: Influence of Phosphourus Content of Parent Materials on Accumulations of Carbon, Nitrogen, Sulphur and Organic Phosphorus in Grassland Soils. *Soil Science*, 85, 307-318.

Walker, T. W. & Syers, J. K. 1976. The fate of phosphorus during pedogenesis. *Geoderma*, 15, 1–19, https://doi.org/10.1016/0016-7061(76)90066-5, 1976.

Wang, Y., Jiang, J., Xu, R. K., & Tiwari, D. (2009). Phosphate Adsorption at Variable Charge Soil/Water Interfaces as Influenced by Ionic Strength. *Australian Journal of Soil Research*, 47(5), 529–36. https://doi.org/10.1071/SR08181.

Wardle, D. A., Walker, L. R., & Bardgett, R. D. 2004. Ecosystem Properties and Forest Decline in Contrasting Long-Term Chronosequences. *Science*, 305(5683), 509–13. https://doi.org/10.1126/science.1098778.

Warman, L., Bradford, M. G., & Moles, A.T. (2013) A Broad Approach to Abrupt Boundaries: Looking Beyond the Boundary at Soil Attributes within and Across Tropical Vegetation Types. *PLoS ONE*, 8(4), e60789. doi:10.1371/journal.pone.0060789

Watson, M., & Mullen, R. (2007). Understanding Soil Tests for Plant-Available Phosphorus. *School of Environment and Natural Resources Fact Sheet*, 1–3. http://citeseerx.ist.psu.edu/viewdoc/download?rep=rep1&type=pdf&doi=10.1.1.190.3527

Weijers, J. W. H., Schefuß, E., Schouten, S., Damsté, J. S. S. (2007). Coupled thermal and hydrological evolution of tropical Africa over the last deglaciation. *Science*, 315 (5819), 1701–1704. https://doi.org/10.1126/science.1138131

Winowiecki, L. A., Vågen, T. G., Boeckx, P., & Dungait, J. A. J. (2017). Landscape-scale assessments of stable carbon isotopes in soil under diverse vegetation classes in East Africa: application of near-infrared spectroscopy. *Plant and Soil*, 421, 259–272. https://doi.org/10.1007/s11104-017-3418-3

Wittmer, M., Auerswald, K., Bai, Y., Schäufele, R., & Schnyder, H. (2009). Changes in the abundance of C3/C4 species of Inner Mongolia grassland: evidence from isotopic composition of soil and vegetation. *Global Change Biology*, 16, 605-616.

Xu, R. K., Qafoku, N. P., Van Ranst, E., Li, J. Y., & Jiang, J. (2016). Adsorption Properties of Subtropical and Tropical Variable Charge Soils: Implications from Climate Change and

Biochar Amendment. *Advances in Agronomy*. Vol. 135. Elsevier Inc. https://doi.org/10.1016/bs.agron.2015.09.001.

Yang, X., & Post, W. M. (2011). Phosphorus transformations as a function of pedogenesis: A synthesis of soil phosphorus data using Hedley fractionation method, *Biogeosciences*, 8, 2907-2916, doi:10.5194/bg-8-2907-2011.

Yang, X., Post, W. M., Thornton, P. R., & Jain, A. (2013). The distribution of soil phosphorus for global biogeochemical modeling. *Biogeosciences*, 10, 2525-2537, doi:10.5194/bg-10-2525-213.

Yang, X., Post, W. M., Thornton, P. E., & Jain, A. 2014. Global Gridded Soil Phosphorus Distribution Maps at 0.5-degree Resolution. Data set. Available on-line [http://daac.ornl.gov] from Oak Ridge National Laboratory Distributed Active Archive Center, Oak Ridge, Tennessee, USA. http://dx.doi.org/10.3334/ORNLDAAC/1223

Yang, L., Yang, Z., Xiaojian, Z., Xu, C., Lin, Y., Fan, Y., Wang, M., Chen, G., & Yang, Y. (2021). Decreases in soil P availability are associated with soil organic P declines following forest conversion in subtropical China. *Catena*, 205, 105459. 10.1016/j.catena.2021.105459

Zachos, J., Pagani, M., Sloan, L., Thomas, E., & Billups, K. (2001). Trends, rhythms, and aberrations in global climate 65 Ma to present. *Science*, 292(5517), 686-93. doi: 10.1126/science.1059412. PMID: 11326091.

Zhao, Q., Zeng, D., Fan, Z., Yu, Z., Hu, Y., & Zhang, J. (2009). Seasonal variations in phosphorus fractions in semiarid sandy soils under different vegetation types. *Forest Ecology and Management*, 258(7): 1376-1382

Zhou, L., Tian, Y., Myneni, R.B., Ciais, P., Saatchi, S., Liu, Y.Y., Piao, S., Chen, H., Vermote, E.F., Song, C., & Hwang, T. (2014). Widespread decline of Congo rainforest greenness in the past decade. *Nature*, 508, 86–90. https://doi.org/10.1038/nature13265

Zhu, Y. G., Cavagnaro, T. R., Smith, S. E., & Dickson, S. (2001). Backseat Driving? Accessing Phosphate beyond the Rhizosphere-Depletion Zone. *Trends in Plant Science* 6 (5), 194–95. https://doi.org/10.1016/S1360-1385(01)01957-4.